28TH ANNUAL CONDENSED MATTER AND MATERIALS MEETING

WAGGA WAGGA

3 – 6 FEBRUARY 2004

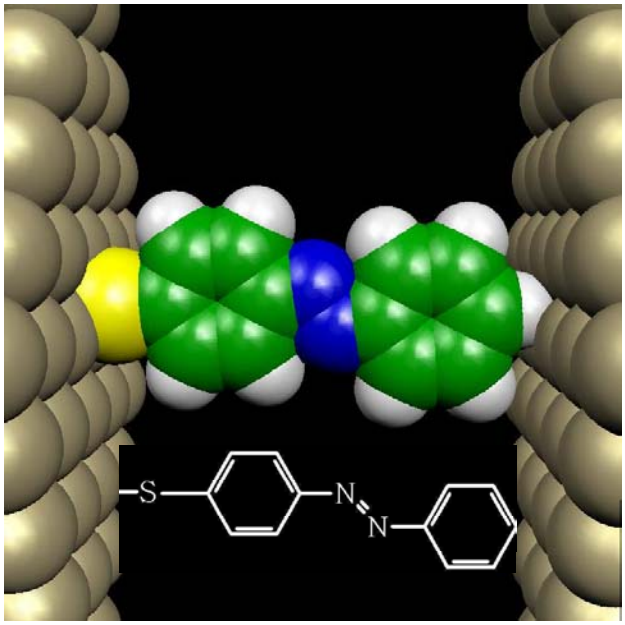

CONDENSED MATTER PHYSICS, ELECTRONIC MATERIALS
MATERIALS SCIENCE ENGINEERING, EARTH SCIENCES
NANOSCIENCE AND NANOTECHNOLOGY, PHOTONICS
NEUTRON PHYSICS, SOLID STATE THEORY, MAGNETISM
SYNCHROTRON PHYSICS AND SPECTROSCOPY

Australian and New Zealand Institutes of Physics

28TH ANNUAL CONDENSED MATTER AND MATERIALS MEETING

Charles Sturt University,

Wagga Wagga, NSW

3 February – 6 February 2004

CONFERENCE HANDBOOK

ISSN-1037-1214

Organised by: Stephen Collocott, John Dunlop, Paul Gwan, Don Price, Nick Savvides

CSIRO Telecommunications & Industrial Physics

The Organising Committee wishes to thank
Dr Gerry Haddad, Chief, CSIRO Telecommunications
& Industrial Physics for his and the Division's support,
Mrs Khuen Wong for her administrative support, and
Peter Saunders for the Wagga 2004 web site.

CONTENTS

Location Map

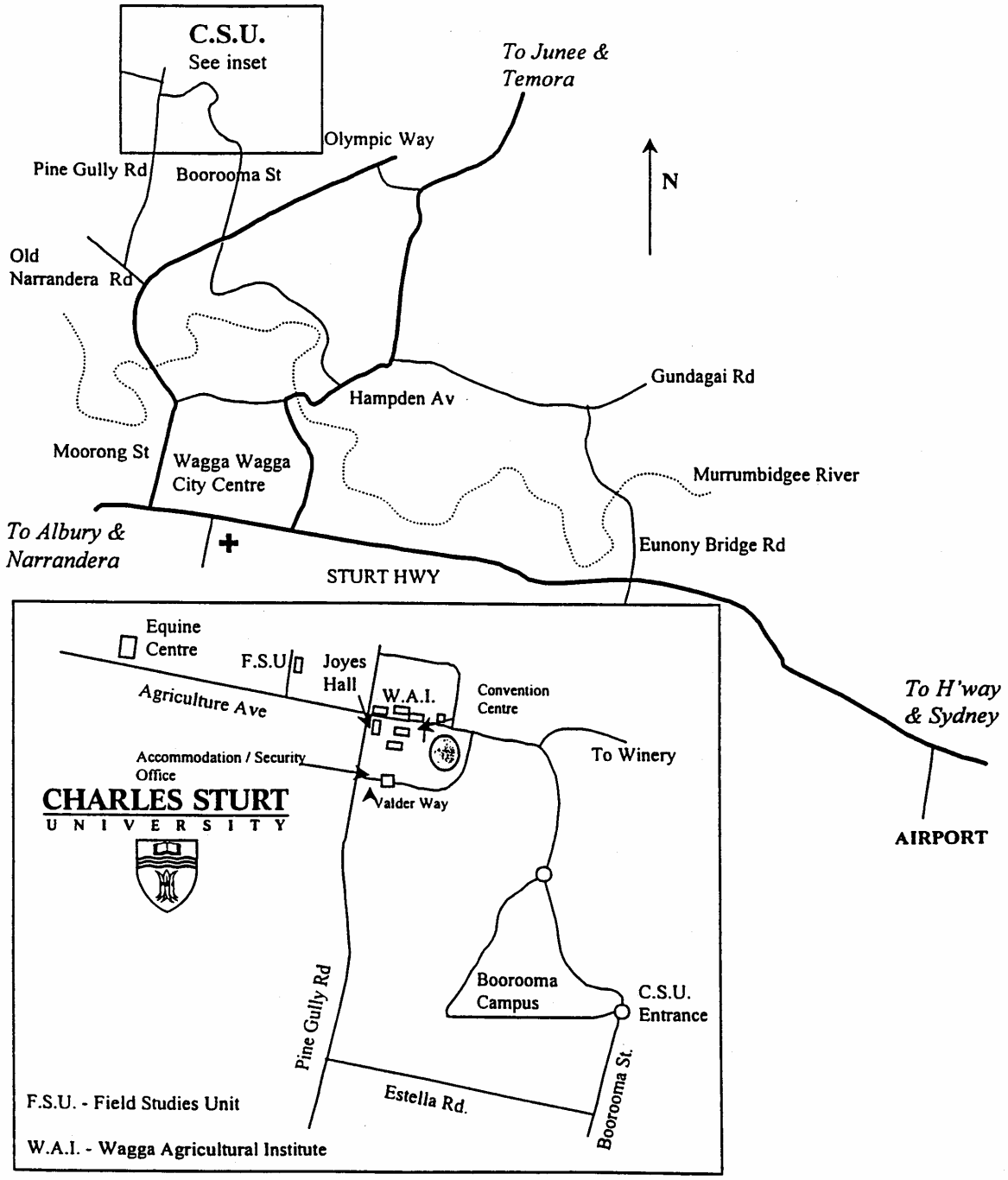

Campus Map

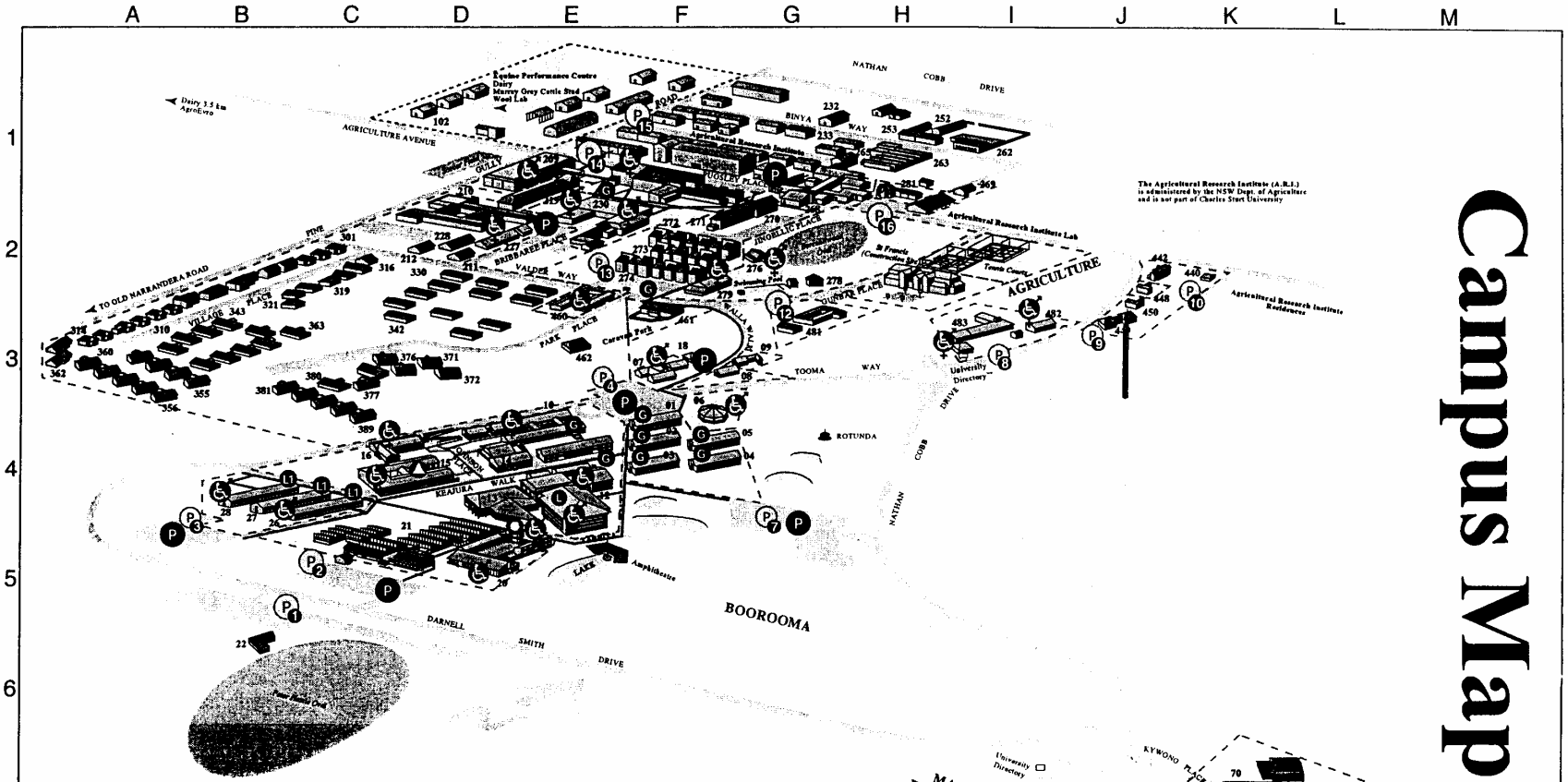

Convention Centre	Site 230
Conference accommodation	Grid C2 - C3
After hours security and accommodation office	Site 460
Swimming pool	Site 279
Squash courts	Site 278

- Unisex toilet
- Female toilet
- Male toilet
- Designated parking for people with disabilities
- Disabled access
- Lift to all levels
- Ground floor access only
- Level 1 access
- Buzzer at door
- Kick pad

Revision date: August 1998

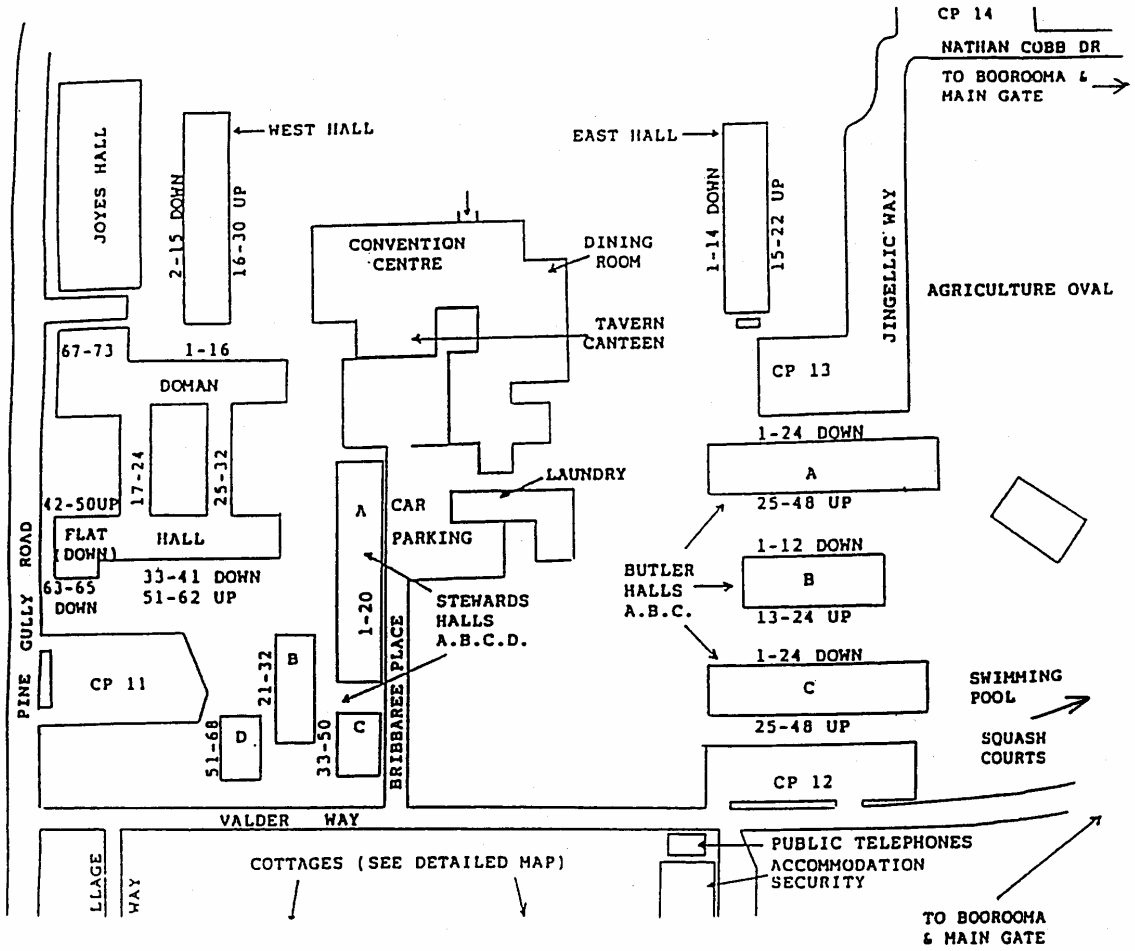
CP 14
NATHAN COBB DR
TO BOOROOMA & MAIN GATE
JOYES HALL
WEST HALL
2-15 DOWN
16-30 UP
EAST HALL
1-14 DOWN
15-22 UP
JINGELLIC WAY
AGRICULTURE OVAL
CONVENTION CENTRE
DINING ROOM
TAVERN CANTEEN
67-73
1-16
DOMAN
CP 13
1-24 DOWN
A
25-48 UP
17-24
25-32
42-50UP
FLAT (DOWN)
HALL
LAUNDRY
A
CAR PARKING
1-12 DOWN
B
13-24 UP
BUTLER HALLS A.B.C.
63-65 DOWN
33-41 DOWN
51-62 UP
STEWARDS HALLS A.B.C.D.
1-20
PINE GULLY ROAD
CP 11
B
21-32
BRIBBAREE PLACE
1-24 DOWN
C
25-48 UP
SWIMMING POOL
SQUASH COURTS
D
51-68
C
33-50
CP 12
VALDER WAY
PUBLIC TELEPHONES
ACCOMMODATION SECURITY
COTTAGES (SEE DETAILED MAP)
LLAGE
WAY
TO BOOROOMA & MAIN GATE

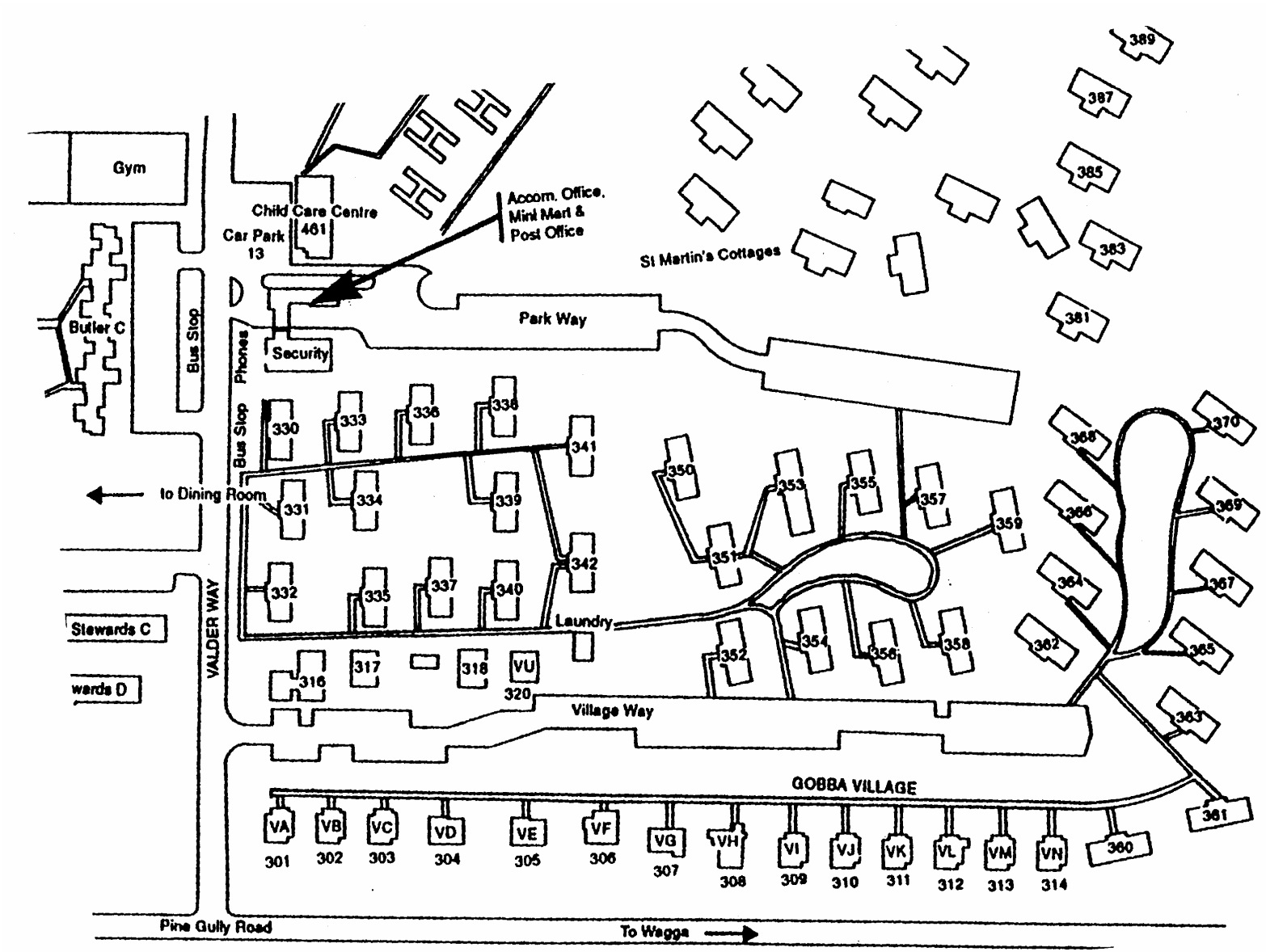
Gym
Child Care Centre
461
Car Park
13
Accom. Office,
Mini Mart &
Post Office
St Martin's Cottages
Butler C
Bus Stop
Phones
Bus Stop
Security
Park Way
to Dining Room
VALDER WAY
Stewards C
wards D
Laundry
Village Way
GOBBA VILLAGE
Pine Gully Road
To Wagga
330
331
332
333
334
335
336
337
338
339
340
341
342
316
317
318
VU
320
350
351
352
353
354
355
356
357
358
359
362
363
364
365
366
367
368
369
370
381
383
385
387
389
VA
VB
VC
VD
VE
VF
VG
VH
VI
VJ
VK
VL
VM
VN
301
302
303
304
305
306
307
308
309
310
311
312
313
314
360
361

GENERAL INFORMATION

Scientific Program

All poster sessions and lectures will be held at the Convention Centre. Chairpersons and speakers must keep to the lecture program schedule. An overhead projector and microphone are available. If slides are to be used, please arrange these at least 10 minutes before the relevant session. Oversee their mounting and, preferably, test one or two prior to the session. If you intend to make a *PowerPoint* presentation, please check that it is compatible with the facilities provided as soon as possible. Posters must be mounted and removed at the times specified in the timetable.

Administration

Please wear your name tag at all times. Registration and all other administrative matters should be addressed to the registration desk or a committee member. For lost keys or if locked out of your room from 0900 to 1700, contact Ray Farnham at the Convention Centre Office for assistance; after hours, contact the Accommodation and Security Office near the corner of Valder Way and Park Way or phone them at 69332288.

Convention Centre Contact Numbers

Registration Desk Phone	(02) 6933 4989
Convention Centre Office Phone	(02) 6933 4974, Fax (02) 6933 4977
After hours Emergencies, Accommodation and Security Office Phone	(02) 6933 2288

Meals, Coffee & tea, Bar Facilities

All meals will be served in the dining room, except the Conference Dinner on Wednesday 4 February, which will be held in the Convention Centre. You will receive a dining room pass on registration and a ticket to the Conference Dinner. The dining room pass must be produced at every meal. It may also be required as identification for use of all other campus facilities, which are at your disposal. Morning and afternoon tea will be served each day, as indicated in the timetable. Coffee and tea-making facilities are also available in the Common Room of each building. In addition, at the time for author attendance at posters on Wednesday and Thursday, the Conference Bar will be open. The Union Bar at the rear of the Convention Centre opens in the afternoon and remains open until late in the evening.

Sport and Recreational Facilities

The swimming pool is open from 0730 until 2200, as are the adjacent squash courts. Tennis courts opposite the oval are also available. A wide range of facilities such as exercise bikes, weight training, table tennis and basketball are available in the gymnasium. All of the facilities are free, i.e., covered by your registration fee.

SPONSORS

The organisers gratefully acknowledge support from:

The MacDiarmid Institute
for Advanced Materials and Nanotechnology

and the following industrial and commercial sponsors:

Stanton Scientific

AVT Services Pty Ltd

Scitek Australia Pty. Ltd.

Some of these companies are exhibiting their products and we encourage you to visit them during the course of the conference. Their sponsorship has helped with the costs of running the conference and their contribution is much appreciated.

We acknowledge the support of the AIP, through the local Branch Committees, in assisting students to attend the conference.

TIMETABLE

Tuesday 3 February

1600 onwards	Registration
1600 – 1800	*Conference Bar Open*
1800 – 1930	*Dinner*
1900 onwards	Posters WP may be mounted

Wednesday 4 February

0730 – 0830	*Breakfast*
0850 – 0900	**Conference Opening**
0900 – 1030	Oral Session: Papers WM1 – WM4
1030 – 1100	*Morning Tea*
1100 – 1230	Oral Session: Papers WM5 – WM9
1230 – 1330	*Lunch*
1400 – 1530	Oral Session: Papers WA1 – WA6
1530 – 1600	*Afternoon Tea*
1545	Author attendance at Posters WP1 – WP22 (until 1645)
1600	*Conference Bar opens*
1645	Author attendance at Posters WP23 – WP43 (until 1745)
1800	*Conference Bar closes*
1900 – 2100	***Conference Dinner and After Dinner Talk***
	From Fibres to Cosmology: The Square Kilometre Array
	Ray Norris, ATNF
2100	Removal of WP Posters and mounting of TP Posters

Thursday 5 February

0730 – 0830	*Breakfast*
0730 – 0900	Mounting of TP Posters
0900 – 1030	Oral Session: Papers TM1 – TM4
1030 – 1100	*Morning Tea*
1100 – 1230	Oral Session: Papers TM5 – TM9
1230 –1330	*Lunch*
1400 – 1530	Oral Session: Papers TA1 – TA6
1530 – 1600	*Afternoon Tea*
1545	Author attendance at Posters TP1 – TP20 (until 1645)
1600	*Conference Bar opens*
1645	Author attendance at Posters TP21 – TP40 (until 1745)
1800	*Conference Bar closes*
1800 – 1900	*Dinner*
2000	*Trivia Quiz: Union Bar (Lindsay Davis Cup)*

Friday 6 February

0730 – 0830	*Breakfast*
0900 – 1030	Oral Session: Papers FM1 – FM5
1030 – 1100	*Morning Tea*
1100 – 1215	Oral Session: Papers FM6 – FM9
1215 – 1230	*Prizes and Closing*
1230 –1330	*Lunch*

Wednesday Morning, 4 February

0850 – 0900		**Opening: Stephen Collocott**
Session WM-I		**Chairperson: Don Price**
0900 – 0930	WM1	Towards Molecular Electronics: Electron Transport through Single Molecules *Karl-Heinz Müller* ***INVITED***
0930 – 1000	WM2	Coupling Molecules to Electronic Materials *David Cahen* ***INVITED***
1000 – 1015	WM3	Controlled Assembly of Sb and Ag Clusters on Insulating Substrates *J. G. Partridge, S. A. Brown, A. D. F. Dunbar, R. Reichel, M. Kaufmann, M. Schulze, S. Scott, C. Siegert and R. J. Blaikie*
1015 – 1030	WM4	Structure of Gold Clusters (Au_n, n = 3…38) *Benjamin Soulé de Bas, Michael J. Ford, Michael B. Cortie*
Session WM-II		**Chairperson: Robert Robinson**
1100 – 1130	WM5	Neutron scattering and material function: the example of viscous flow *F. Mezei* ***INVITED***
1130 – 1145	WM6	Measuring diffuse scattering *D. J. Goossens, T. R. Welberry and A. P. Heerdegen*
1145 – 1200	WM7	Modulated Structures in the Ta_2O_5-WO_3 System *S. A. Schmid and A. Binder*
1200 – 1215	WM8	Evidence for an orbital Peierls state in YVO_3 *J. Sirker and G. Khaliullin*
1215 – 1230	WM9	Spin Polarised Quantum-well States in Layered Magnetic Nanostructures of Cu/Co/Cu(100) *D. H. Yu and M. Donath*

Wednesday Afternoon, 4 February

Session WA **Chairperson: Tam Greaves**

1400 – 1415	WA1	Development of a superconducting absolute tensor gradiometer *D. L. Tilbrook, K. E. Leslie, M. Bick, C. P. Foley, R. A. Binks, J. Du, R. Gnanarajan, S. K. H. Lam, B, Thorn, P. Sullivan*
1415 – 1430	WA2	Nanoscale magnetite/maghemite particle-based ferrofluids: the effect of local particle arrangement on magnetic properties *H. Pardoe, W. Chua-anusorn and T. St. Pierre*
1430 – 1445	WA3	The Antiferromagnetic Structure of $BaPrO_3$ *R. A. Robinson, D. J. Goossens and M. F. Telling*
1445 – 1500	WA4	Theoretical Studies of a Mixed-Spin Antiferromagnetic Model for the Rare Earth Nickelates R_2BaNiO_5 *A. M. A. von Brasch and J. Oitmaa*
1500 – 1515	WA5	XRD characterisation of nanoparticle size and shape distributions *N. Armstrong, W. Kalceff, J. P. Cline and J. Bonevich*
1515 – 1530	WA6	The eigenvalue distribution of the time-evolution operator of a non-equilibrium system *Yuichi Nakamura and Naomichi Hatano*

Poster Session WP

Author Attendance:

1545 - 1645 WP1 – WP22

1645 - 1745 WP23 – WP43

Conference Dinner and After Dinner Talk

1900 - 2100 *From Fibres to Cosmology: The Square Kilometre Array*

Ray Norris, ATNF

Thursday Morning, 5 February

Session TM-I **Chairperson: Nick Savvides**

0900 – 0930	TM1	Microphotonic and photonic bandgap devices: Towards all-optical technology *Benjamin Eggleton* ***INVITED***
0930 – 0945	TM2	2D photonic crystal-based optical microcomponents on Indium Phosphide (InP) membrane for integrated optics *C. Grillet, X. Letartre, C. Seassal, P. R. Romeo and P. Viktorovitch*
0945 – 1015	TM3	Left-handed materials: recent progress and perspectives *I. V. Shadrivov, A. A. Zharov, A. A. Sukhorukov and Yu. S. Kivshar* ***INVITED***
1015 – 1030	TM4	The effects of GaN capping layer thickness on electrical properties of two-dimensional electron gas in GaN/AlGaN/GaN heterostructures *A. Asgari and L. Faraone*

Session TM-II **Chairperson: Nicole Gorham**

1100 – 1130	TM5	Calcite Microcrystals in the Pineal Gland of the Human Brain: Second Harmonic Generators and Possible Piezoelectric Transducers *Sidney B. Lang* ***INVITED***
1130 – 1145	TM6	Magnetic Materials for Hyperthermic Cancer Treatment *K. M. Spiers, J. D. Cashion, K. A. Gross and S. J. Harker*
1145 – 1200	TM7	Nanoparticulate Cobalt/polymer Complexes for Biomedical Applications *M. A. Zalich, T. G. St. Pierre, V. V. Baranauskas and J. S. Riffle*
1200 – 1215	TM8	Computer simulation studies of the rheology of soft condensed matter *P. J. Daivis, I. K. Snook, M. L. Matin, T. Kairn and M. McPhie*
1215 – 1230	TM9	A Novel In-Line Micro-Fourier Rheometer *Julie Glasscock and Robin Smith*

Thursday Afternoon, 5 February

Session TA **Chairperson: Kathryn Spiers**

1400 – 1415	TA1	Synchrotron based Measurements of the Electronic Structure of the Organic Semiconductor Copper Phthalocyanine *J. E. Downes*
1415 - 1430	TA2	New approaches to fitting the Mössbauer spectra of Prussian Blue *T. L. Greaves and J. D. Cashion*
1430 – 1445	TA3	Light Scattering from Spin Wave Excitations in Non-Collinear Thin Film Magnetisation Structures *D. C. Crew and R .L. Stamps*
1445 – 1500	TA4	Experimental determination of Lévy flight distributions of the energy barriers in spin glasses *N. T. Gorham, R. C. Woodward, T .G. St Pierre, R. L. Stamps, M .J. Walker, D. Greig, and J. A. D. Matthew*
1500 – 1515	TA5	Inductive Measurements of Ferromagnetic Resonance *R. C. Woodward, K. Kennewell, D. C. Crew and R. L. Stamps*
1515 – 1530	TA6	Magnetic Properties, Curie Temperature and Microstructures of PrFeB and NdFeB-based Magnets With Additives by Blending *A. Ahmad and I. R. Harris*

Poster Session TP

Author Attendence

1545 – 1645	TP1 – TP20
1645 – 1745	TP21 – TP40

Friday Morning, 6 February

Session FM-I **Chairperson: Trevor Finlayson**

0900 – 0930	FM1	The Fabrication of Nano-Scale Devices in Silicon *F. J. Ruess, M. Y. Simmons, L. Oberbeck, K. E. J. Goh, A. R. Hamilton, T. Hallam, N. J. Curson and R. G. Clark* ***INVITED***
0930 – 0945	FM2	Fabrication of a Novel Silicon Single Electron Transistor for Si:P Quantum Computer Devices *S. J. Angus, C. E. A. Smith, G. L. Snider, E. Gauja, A. S. Dzurak and R. G. Clark*
0945 – 1000	FM3	The Dependence of the Critical Thickness of an InGaAs/GaAs Multilayer on Quantum Well Thickness, Barrier Thickness and Number of Periods *M. Madebo, B. F. Usher and J Riley*
1000 – 1015	FM4	X-ray Absorption and Emission Study of Amorphous and Nanocrystalline GaN Films Containing Buried N_2 *B. J. Ruck, A. Koo, F. Budde, S. Granville, A. Bittar and H. J. Trodahl*
1015 – 1030	FM5	Molybdenum disulphide (MoS_2) – gallium arsenide (GaAs) heterostructures for solar cell applications *Ian M. Jamieson and G. Jakovidis*

Session FM-II **Chairperson: Jan Oitmaa**

1100 – 1130	FM6	Nature of the Peierls- to Mott-insulator transition in one dimension *H. Fehske, G. Wellein, A. Weiße, G. Hager, A. P. Kampf, M. Sekania and A. R. Bishop* ***INVITED***
1130 – 1145	FM7	Minority-Spin Band Gap of Half-Metallic NiMnSb *H. J. Trodahl, C. E. A. Grigorescu, N. Strickland and A. Bittar*
1145 – 1200	FM8	Transport in Layered Materials: Polarons and Angular Magneto-Resistance *U. Lundin and R. H. McKenzie*
1200 – 1215	FM9	Density Functional Theory calculations of Band-gaps in Diamond Nanowires. *S. P. Russo, A. S. Barnard and I. K. Snook*
1215 – 1230	**Closing Remarks and Prizes**	

POSTER SESSION: Wednesday, 4 February

WP1	The Effects of Multiple Scattering on the Analysis of USANS Data	*W. K. Bertram*
WP2	Crystallization in polydisperse colloidal suspensions	*Stephen Martin, Gary Bryant and William van Megen*
WP3	Studies of Magnetic Structure of $La_{1-x}Sr_xMnO_3$ Colossal Magnetoresistive Perovskites	*T. R. Finlayson, X. Wu, T. Ersez and J. C. Schulz*
WP4	Taipan - A Spectrometer for Inelastic Neutron Scattering At The Replacement Research Reactor	*M. E. Hagen, G. Horton, R. Moore, G. Braoudakis and L. D. Cussen*
WP5	High Intensity and High Resolution Neutron Powder Diffraction at the Replacement Research Reactor	*M. E. Hagen, B. A. Hunter and T. J. Noakes*
WP6	A polarised neutron study of crystal field transitions in $CeCu_6$	*S. J. Harker, T. J. Hicks, D. J. Goossens, A. M. Mulders, Y. Fei, D. Yu and S. J. Kennedy.*
WP7	Effects of Solutes on Membrane Phase Transitions	*Thomas Lenné and Gary Bryant*
WP8	Dynamics associated with domain walls	*R. L. Stamps, P. Falloon, R. Jalabert, D. Weinmann and A. Mougin*
WP9	Electron Transport in Disordered Films of Metal Nanoparticles Linked by Organic Molecules	*K.-H. Müller, G. Wei, J. Herrmann, B. Raguse and G. Baxter*
WP10	Finite Hydrogenated Silicon Nanotubes And Toroids	*O. Ponomarenko, M. W. Radny and P. V. Smith*
WP11	Carbon- based toroidal nanostructures	*O. Ponomarenko, M. W. Radny and P. V. Smith*
WP12	Nanocrystalline diamond grown by chemical vapour deposition using He and Ar diluted H_2/CH_4 gas mixtures	*J. R. Rabeau, P. John and J. I. B. Wilson*
WP13	Nucleation and Optical Properties of Gold Nano-Hemispheres on Plate Glass	*X. Xu, M. B. Cortie and M. Stevens*
WP14	Electrochemical Capacitors based on Self-Assembled Gold Nanoparticle Films Cross-Linked with Thiols	*Burkhard Raguse, Wenrong Yang and G. Stockton*
WP15	Synthesis and Characterization of RF Magnetron Sputtered Carbon Nanostructures	*D. M. Zhu, S. Goh, G. Jakovidis and L. Bourgeois*
WP16	Muon spin relaxation in spin-Peierls phase of NaV_2O_5	*M. Aïn, J. Lord, J. Jegoudez and A. Revcolevschi*

WP17	Magnetic properties of $Dy_{1-x}Sr_xCoO_{3-\delta}$ (x = 0.67 to 0.95)	*D. J. Goossens, K. F. Wilson and M. James*
WP18	Magnetic Structures and Valence States of $YbMn_2Si_xGe_{2-x}$	*D. Grimm, M. Hoffman, S. J. Campbell, A. V. J. Edge and A. Studer*
WP19	Soft Magnetic Properties of Nanocrystalline $Fe_{89-x}Zr_7B_3Cu_1Co_x$ (x = 0 to 70) Alloys	*N. Ito*
WP20	The Magnetic Properties of $GdNiAl_4$	*G. A. Stewart, W. D. Hutchison, A. V. J. Edge, K. Rupprecht, G. Wortmann, K. Nishimura and Y. Ishikawa*
WP21	Magnetic and Crystal Field Properties of Thulium Calcium Manganite	*G. A. Stewart, A. V. J. Edge, A. Studer, M. Elcombe, J. Horvat and R. Lewis*
WP22	Structural and Magnetic Properties of $DyFe_{12-x}Nb_x$ Compounds	*J. L. Wang, S. J. Campbell, S. James, A. V. J. Edge and D. Grimm*
WP23	Exchange bias in a model system	*R. L. Stamps, W. Pang and Z. Celinski*
WP24	Analysis of an Ideal Amorphous Solid	*L. Th. To and Z. H. Stachurski*
WP25	A Comparison of the Influence of Different Dopants on the Radar-absorbing Properties of Barium Hexaferrite	*M. Jones, M. M. Suder, A. Amiet, A. V. J. Edge, G. A. Stewart, W. D. Hutchinson and P. Jewsbury*
WP26	Analysis of hydrogenated amorphous carbon films deposited using an open plasma generator under various bias voltage	*M. Rybachuk and J. M. Bell*
WP27	The Electric Field Gradient of $FePS_3$: a comparison between calculated and measured values	*A. E. Smith, K.C. Rule, J.D. Cashion and T.J. Hicks*
WP28	Mapping Disorder-Order Induced Changes To The Fermi Surface Of Cu_3Au Using A New Toroidal Electron Energy Analyser	*A. Tadich, L. Broekman, J. Riley, R. Leckey, T.Seyller, K.Emtsev and L. Ley*
WP29	High Resolution Angle Resolving Toroidal Electron Spectrometer	*A. Tadich, L. Broekman, E. Huwald, R. Leckey, J. Riley, T. Seyller and L. Ley*
WP30	Whiskies: further EPR and Antioxidant Efficiency Studies	*Irwin Cheah, Steven J. Langford, Jim Kelly and Gordon Troup*
WP31	An EPR and Antioxidant Efficiency Study of the Two Pinebark Phenolic Extracts Pycnogenol (R) and Endogenol	*Irwin Cheah, Steven J. Langford and Gordon Troup*
WP32	Bilirubin photoisomer variable quantum yield – end of a chapter	*G. Agati, Marina Mazzoni, R. Pratesi and Gordon Troup*
WP33	High-Power Ultrasonic Treatment of Contaminated Soils and Sediments	*A. F. Collings, P. B. Gwan and A. P. Sosa Pintos*

WP34	Phase Transformations in the $Ca_{1-x}Sr_xTiO_3$ Perovskite System	*J. E. Daniels, M. M. Elcombe, T. R. Finlayson and E. R. Vance*
WP35	High-temperature viscoelastic relaxation: in search of the creep function	*Ian Jackson and Ulrich Faul*
WP36	Proximity effect in low resistivity yttria-stabilized-zirconia thin films	*S. K. H. Lam and S. Gnanarajan*
WP37	A new thin film deposition process by cathodic plasma electrolysis	*Thierry Paulmier, Emad Kiriakos, John Bell and Peter Fredericks*
WP38	The Storage of Nuclear Waste in Concrete	*T. M. Sabine*
WP39	Fermi Surface Comparisons For Materials Susceptible To Phase Transitions	*A. E. Smith, T.R. Finlayson, Robert Leckey and J. Riley*
WP40	Formation of Ion Tracks in Single-Crystal Indium Phosphide Irradiated by Swift Heavy Ions	*A. S. Khalil, A. M. Stewart, M. C. Ridgway, L. T. Chadderton, D. J. Llewellyn and A. P. Byrne*
WP41	Fe and Mg solubility in the Ca site of zirconolite, $CaZrTi_2O_7$	*E. R. Vance, J G. Cashion, J .V. Hanna, Z. Garrett and M. Bhati*
WP42	Thermal Expansion Studies of Ni_2MnGa Shape-Memory Material	*X. D. Wu and T. R. Finlayson*
WP43	Characterization of microstructural evolution in Fe-C(-Mn) alloys during early stages of ageing using atom probe	*X. Y. Xiong, P. Tran, S. P. Ringer and E. Pereloma*

POSTER SESSION: Thursday, 5 February

TP1	Surface Electron Structure of Short-Period Semiconductor Superlattice	*I. Bartos, T. Strasser, W. Schattke*
TP2	Quantum pumping and geometric phases in nanoscale electronic devices	*Huan-Qiang Zhou, Sam Young Cho, Urban Lundin, and Ross H. McKenzie*
TP3	High Resolution Lithography of PMMA with a Scanning Probe Microscope	*A. Cimmino, D. Gassull, S. Prawer, D. Jamieson*
TP4	Towards a Quantum-Limited Charge Detector	*N. A. Court, D. J. Reilly, T. M. Buehler, R. P. Starrett, R. G. Clark and A. R. Hamilton*
TP5	Influence of N_2 Background Pressure on the Incorporation of Arsenic during MBE Growth of GaAs	*T. Dieing and B. F. Usher*
TP6	Comparison of hydrogen resist removal techniques for STM-fabricated nanoscale devices	*T. Hallam, L. Oberbeck, F. J. Ruess, N. J. Curson, M. Y. Simmons and R. G. Clark*
TP7	Measurement and Simulation of the effects of ion induced defects on ion beam induced charge (IBIC) measurements in Si Schottky diodes	*S. M. Hearne, M. D. H. Lay and D. N. Jamieson*
TP8	Magnetic Resonance and P:Si Qubits	*W. D. Hutchison, D. Tempelaars, R. Bramley, A. R. Hamilton, E. Gauja and R .G. Clark*
TP9	Electron transport in multi-layer thermionic cooling structures	*S. P. Lee, B. C. C. Lough, X. Z. Shang, Q. Wang, R. A. Lewis and C. Zhang*
TP10	Characterization of Si-SiO_2 Trap Density Due to Ion Implantation	*D. R. McCamey, M. J. Francis, J. C. McCallum, A. R. Hamilton, A. D. Greentree and R .G. Clark*
TP11	Nanofabrication of Charge-based Si:P Quantum Computer Devices using Single-ion Implantation	*M. Mitic, T. M. Buehler, A. J. Ferguson, V. Chan, E. Gauja, F. E. Stanley, S. J. Angus, K. H. Lee, A. D. Greentree, D. J. Reilly, A. R. Hamilton, A. S. Dzurak, R. G. Clark, C. I. Pakes, C. Yang, D. N. Jamieson and S. Prawer*
TP12	The diffusion mechanism of Mn in GaAs.	*D. James, J. Riley, R. Leckey, Yvegen Biltosky and Kathryn Prince*
TP13	Atomic structure of the hydrogen saturated a-planes of 4H-SiC	*Th. Seyller, N. Sieber, A. Taddich, D. James, J. D. Riley, R. G. C. Leckey and L. Ley*
TP14	Spin structure of small quantum dots	*C. Sloggett and O. P. Sushkov*

TP15	Local bonding environment of low temperature silicon nitride thin films produced by plasma-enhanced chemical vapour deposition	*M. T. K. Soh, N. Savvides, C. A. Musca and L. Faraone*
TP16	Variations in the Apparent Optical Band-gap of RPE-CVD Grown Indium Nitride Thin Films	*K. S. A. Butcher[a], M. Wintrebert-Fouquet[a], P. P.-T. Chen[a], T. L. Tansley[a] and K. E. Prince[b]*
TP17		
TP18		
TP19	Electronic Structure of Single Crystal Copper Measured by Electron Momentum Spectroscopy	*C. Bowles, C. Chen, A. Kheifets, M. Vos and E. Weigold*
TP20	Fast Simulation of a Quantum Phase Transition in an Ion-Trap Realisable Unitary Map	*J. P. Barjaktarevic, G. Milburn and R. H. McKenzie*
TP21	Magnetic Materials for Hyperthermic Cancer Treatment	*K. M. Spiers, J. D. Cashion, K. A. Gross and S. J. Harker*
TP22	Mixed-Spin S=(½,1) Quantum Ferrimagnet at Zero Temperature	*Weihong Zheng and J. Oitmaa*
TP23	Phase Diagram of the BCC S=½ Heisenberg Antiferromagnet with First and Second Neighbour Exchange	*J. Oitmaa and Weihong Zheng*
TP24	Comparative numerical study of localization in disordered electron systems	*G. Schubert, A. Weisse and H. Fehske*
TP25	Structure factors for the alternating Heisenberg chain	*C. J. Hamer, Weihong Zheng and R. R. P. Singh*
TP26	Superconducting Correlations and Model System Design	*Y. Hancock and D. M. Paganin*
TP27	Low-lying excitations in odd-legged spin-½ tubes with strong rung coupling	*A. Lüscher, R. Noack, G. Misguich, V. Kotov and F. Mila*
TP28	Photoconductivity in Disordered GaN	*A. Koo, B. J. Ruck, H. J. Trodahl, F. Budde and A. Bittar*
TP29		
TP30	Quantum Interference with Heisenberg Spin Chains	*D. J. Miller*
TP31	Schockley and Rydberg Surface States and Quantum Wells on the Cu(111) Surface	*M. N. Read*

TP32	Searches for the electron electric dipole moment and nuclear anapole moments in solids	*T. N. Mukhamedjanov, O. P Sushkov, J. M Cadogan and V. A. Dzuba*
TP33	Apparent Sizes of Solute Atoms and Vacancies in Aluminium from First Principles	*A. E. Smith and S. Homolya*
TP34	Superconducting Spiral Phases in the two-dimensional t-J model	*Oleg P. Sushkov and Valeri N. Kotov*
TP35	Corrosion Resistance of Organic Layers on GaAs via X-ray Reflectometry Characterization	*J. D. Smith, T. R. Finlayson, C. Kirchner and U. Klemradt*
TP36	New tools for the numerical calculation of dynamical correlation functions at finite temperature	*Alexander Weisse*
TP37	Does the probability density imply the equation of motion?	*Rotha P. Yu, David M. Paganin and Michael J. Morgan*
TP38	Reactive Ion Etching of Microphotonic Structures	*J. Du, J. Glasscock, J. Vanajek and N. Savvides*
TP39	An Apparent Shift in Optical Constants in Nanostructured Metal Films Overcoated with Insulator: a New class of Multilayer Thin Film Systems	*A. I. Maaroof and G. B. Smith*
TP40	Silicon Microphotonic Waveguides	*V. Ta'eed, M. J. Steel, C. Grillet, B. Eggleton, J. Du, J. Glasscock and N. Savvides*

Oral Sessions
Abstracts

Wednesday
4 February

WM1

Towards Molecular Electronics: Electron Transport through Single Molecules

Karl-Heinz Müller

CSIRO Telecommunications and Industrial Physics, Sydney 2070, Australia.

Molecular electronics, a new emerging science area in the field of nanotechnology, is seen as a potential replacement for silicon device-technology in the next decade. To enable such a technology, an essential initial requirement is a detailed understanding of the electrical conduction properties of molecules placed between metal electrodes. We recently investigated the electrical conduction of single molecules using first-principle quantum mechanical calculations based on the density functional theory and non-equilibrium Green's function techniques. We demonstrate that each molecule has its own distinct current-voltage characteristic, determined by the positions of the molecular energy levels and the degree of electrode-molecule coupling. We show that the calculated attenuation factors of molecular wires made of polyenedithiol, polyphenyldithiol and alkanedithiol agree with experimental data. Furthermore we reveal that photoisomerization of azobenzene can be utilized as an electrical molecular switch and that bipyridinedithiol, in the presence of a gate electrode, can function as a single-molecule field-effect transistor. Different experimental techniques that help to elucidate the conduction properties of single molecules will be discussed.

WM2

Coupling Molecules to Electronic Materials

D. Cahen

Department of Materials & Interfaces, Weizmann Institute of Science, Israel

If we would know how to place molecules at metal-semiconductor interfaces, even if only as poorly organized, partial, rather than ideal monolayers, this could give a significant degree of electronic control over these interfaces and, thus, over the simplest of electronic devices.[1] This is primarily because electron energetics at interfaces determine the electronic behaviour of semiconductor & metal contacts.[2] Two types of control are distinguished, electro-static and -dynamic. For the former, requirements for (near-)ideally structured monolayers can be relaxed because the molecules can act as "gatekeepers", leading to devices with no current flow through molecules.[1] In systems with near-ideal molecular films, electronic transport through molecules is often by "through bond" tunneling.[3]

To make device structures reproducibly, soft contacting methods are needed.[3] Results obtained with such methods show how intimate contact between molecules and metal can polarize the contacts.[1,4] Experimental evidence is accumulating that in most devices with molecules, the nature of the molecule/electrode contact is crucial for the resulting junction.[3,5]

1. A.Vilan et al. *Nature* **404** (2000) 166; *J. Phys. Chem B*, **107** (2003) 6360;
G. Ashkenasy et al. *Acc. Chem. Res*. **35** (2002) 121
2. D. Cahen, A. Kahn, *Adv. Mater*., **14** (2003) 271
3. Y. Selzer et al*., J. Phys. Chem. B* **106** (2002) 10432;
D. Cahen, G. Hodes, *Adv. Mater*. **14** (2002) 789;
A. Salomon, D. Cahen, S. Lindsay, C. Frisbie et al, *Adv. Mater*., **15** (2003) 1881.
4. A. Vilan, D. Cahen, *Adv. Funct. Mater.* **12** (2002) 795; H. Haick et al., to be published
5. Y. Selzer et al., *Angew. Chem. Int. Ed*., **41** (2002) 827.

WM3

Controlled Assembly of Sb and Ag Clusters on Insulating Substrates

J.G. Partridge[a,b], S.A. Brown[a,b], A.D.F. Dunbar[a,b], R. Reichel[a,b], M. Kaufmann[a,b], M. Schulze[a,b], S. Scott[a,b], C. Siegert[a,b] and R. J. Blaikie[a,c]

[a] *Nanostructure Engineering Science and Technology (NEST) Group and the MacDiarmid Institute of Advanced Materials and Nanotechnology*

[b] *Department of Physics and Astronomy, University of Canterbury, New Zealand*

[c] *Department of Electrical and Computer Engineering , University of Canterbury, New Zealand*

Atomic clusters exhibit a range of useful electronic, chemical and magnetic properties, and show great potential as building blocks for nanoscale electronic and photonic devices. To date, self-assembly of cluster structures has relied on surface diffusion of clusters, or of atoms which aggregate to form clusters. Chains resembling wires can be achieved through diffusion to the naturally occurring step-edges on graphite, but since the position of these surface defects is random, the placement of the wires cannot be controlled. Electrical characterization is impossible unless the wires are transplanted onto an insulating surface and contacts are introduced.

The cluster assembly methods reported here occur on passivated silicon substrates. In the first method, clusters are deposited over interdigitated conducting fingers with separations equal to >10 cluster diameters. A percolating conduction path forms at a critical coverage value and the deposition can be stopped at this value. In the second method, V-grooves are employed as template elements; the momentum of the deposited clusters causes them to bounce or slide to the apex of the V-groove, where they assemble into a wire. Since diffusion is not an important factor, the assembly process is insensitive to defects and preformed lithographically defined electrical contacts ensure that the wire is self-contacting and that onset of conduction can be observed. Control of the flow rate of argon gas into the inert gas aggregation source allows control over the cluster velocity and hence the morphology and width of the wires formed. Wires have been fabricated with widths down to ~100nm and lengths exceeding 150μm.

WM4

Structure of Gold Clusters (Au_n, n = 3…38)

Benjamin Soulé de Bas, Michael J. Ford, Michael B. Cortie

Institute for Nanoscale Technology

University of Technology, Sydney, PO Box 123, Broadway, NSW 2007, Australia

We have investigated small gold clusters using Density Functional Theory (DFT) as implemented in the SIESTA package [1]. Simulated Annealing (SA) with a Lennard-Jones (LJ) pair potential and a Gupta n-body potential was used as a first stage geometry optimisation to locate the global minima. Low energy candidates from the SA were then used as starting points for the full *ab initio* structure optimisation. We have already reported geometries for clusters of 3 to 20 atoms [2]. DFT calculations predicted disordered structures for Au_n with n > 9, and a transition from planar to 3-dimensional structures between Au_6 to Au_7. The LJ potential predicted high symmetry structures up to 20 atoms. Here we extend this work to the clusters Au_{21} to Au_{38}. The LJ potential favours ordered structures, whereas the Gupta potential predicts equally ordered and disordered structures. For the magic cluster Au_{38}, one of the low energy structures predicted by the Gupta potential is the truncated octahedron. Disordered structures are predicted by DFT for Au_{21} to Au_{38}. For each of these clusters DFT also predicts a number of disordered structures lying close in energy. This was also the case for clusters in the size range 3 to 20 atoms. It is reasonable to conclude from these results that experimentally prepared gold clusters will contain a distribution of structures even if the clusters are monodisperse in size. We are now in the process of pushing these calculations towards larger sizes and are performing *ab initio* calculations for clusters in the range of 400 atoms. Such calculations are approaching clusters sizes that are experimentally more relevant.

[1] J M Soler, E Artacho, J D Gale, A Garcia, J Junquera, P Ordejon, and D Sanchez-Portal, *J. Phys.: Condens. Matter* **14**, 2745 (2002).

[2] B Soulé de Bas, M J Ford, M B Cortie, Gold 2003 New Industrial Applications for Gold, Sept 2003, Vancouver, Canada.

WM5

Neutron Scattering and Material Function: the Example of Viscous Flow

F. Mezei

Hahn-Meitner-Institut, Berlin and Los Alamos National Laboratory, Los Alamos

Neutron scattering is the one direct probe at our disposal to explore materials in space and time on the atomic scale. Indeed, in crystalline matter it proved itself to be an extremely effective tool to provide detailed information atom by atom on the microscopic structure and motion – at least when sizable single crystals can be made. Many materials of primary interest in nature, however, are not available in the form of large single crystals or they are not even crystalline. Neutron scattering has been used with great success to study non-crystalline matter too, nevertheless in more complex substances we are far from an atom-by-atom exploration of structure and dynamics. Increasing sensitivity to be provided by advanced neutron sources and instruments combined with more powerful model calculations will offer unprecedented opportunities in this field. As a rather modest illustration the case of the exploration of supercooled liquids near the glass transition will be discussed in more detail. In such systems an unexpected dynamic process has been discovered more than a decade ago, whose nature remained a subject of guesswork for a long time. More recent evidence suggests that the flow in highly viscous media is a dynamically heterogeneous process, combining a fast and a slow component on nanoscopic length scale.

WM6

Measuring Diffuse Scattering

D.J. Goossens, T.R. Welberry and A.P. Heerdegen

Research School of Chemistry, Australian National University, Canberra Australia.

Diffuse scattering – electron, neutron, X-ray -- is a valuable probe of the short range order in a crystal [1]. Because typical diffuse scattering intensities are ~10^3 – 10^4 orders of magnitude smaller than those of Bragg peaks, in order to record diffuse scattering over substantial regions of reciprocal space, multidetectors, low noise and if possible a bright source are all desirable. Even then, the need to measure the weak diffuse in the presence of the Bragg peaks, to reduce air scattering and other sources of noise and to perform the experiments in a reasonable length of time makes the data collection demanding.

Methods for the collection of diffuse scattering in the laboratory, at a synchrotron and using time-of-flight Laue neutron diffraction (at ISIS) are outlined, including the scattering geometries used. The advantages and disadvantages of these various techniques are discussed and the types of data which can be collected are illustrated using a single family of samples – benzil ($C_{14}H_{10}O_2$) and its derivatives [2].

We conclude that the ability to collect diffuse scattering data is improving all the time, but that a strong interaction between the user and the instrumentation is needed to get the best results.

1. T.R. Welberry and B.D. Butler, *Chem. Rev.* **95** 2369-2403 (1995)
2. T.R. Welberry, D.J. Goossens, A.J.Edwards and W.I.F. David, *Acta Crystallographica A*. **A57** 101-109 (2001).

WM7

Modulated Structures in the Ta_2O_5-WO_3 System

S. A. Schmid[a] and A. Binder[b]

[a] *School of Chemistry, The University of Sydney, NSW 2006, Australia.*

[b] *Institute for Inorganic Chemistry, University of Tübingen, Germany.*

Systems that form modulated structures are a fascinating class of materials, which lack lattice periodicity but may still be perfectly long-range ordered. Such systems exist across the whole range of chemical disciplines from organic conductors to high-Tc superconductors and minerals. Consequently the importance of modulated structures has been recognised, but there have been few systematic studies across composition ranges of solid solutions that form modulated structures. Such a systematic investigation is expected to further our understanding of crystal chemical and structural aspects of modulated structures as well as the reasons for their existence.

One example for a modulated structure, the wide-range, non-stoichiometric solid solution $(1-x)Ta_2O_5 \cdot xWO_3$, $0 \leq x \leq 0.267$, has been subject to intensive investigation over many years [2]. Owing to the phase transition at 1360°C, large single-crystals of L-Ta_2O_5 were impossible to grow. Thus, attempts were made to stabilise the phase by the addition of other oxides. For WO_3, a series of anion-deficient α-UO_3-related 'line phases' with basic structure dimensions very similar to those of L-Ta_2O_5 was found within the composition range $(1-x)Ta_2O_5 \cdot xWO_3$, $0 \leq x \leq 0.267$.

X-ray and neutron powder diffraction data for a number of compositions were collected at the ANBF and at Lucas Heights, respectively. The results of the structure refinements using JANA [3] will be presented.

1. Withers, R. L., Schmid, S. & Thompson, J. G. (1998). Prog. Solid State Chem. **26,** 1.
2. Schmid, S., Fütterer, K. & Thompson, J. G. (1996). Acta Cryst. **B52,** 223.
3. Petrícek, V. & Dušek, M. (2000). JANA2000, Programs for Modulated and Composite Crystals, Institute of Physics, Praha, Czech Republic.

WM8

Evidence for an Orbital Peierls State in YVO_3

J. Sirker[a], G. Khaliullin[b]

[a] *UNSW, School of Physics, Sydney 2052, Australia.*

[b] *Max-Planck-Institut für Festkörperforschung, 70569 Stuttgart, Germany.*

Neutron spectroscopy has revealed a highly unusual magnetic structure and dynamics in YVO_3, an insulating pseudocubic perovskite that undergoes a series of temperature induced phase transitions between states with different spin and orbital ordering patterns. A good description of the neutron data is obtained by a theoretical analysis of the spin and orbital correlations of a quasi-one-dimensional model with spins S=1. At small Hund's coupling J_H we discover dimerization in a pure electronic system solely due to a dynamical spin-orbital coupling. Above a critical value J_H, a uniform ferromagnetic state is stabilized at zero temperature. More surprisingly, we observe a temperature driven dimerization of the ferrochain, which occurs due to a large entropy released by dimer states. This leads to the tentative identification of one of the phases of YVO_3 with the "orbital Peierls state", a theoretically proposed many-body state comprised of orbital singlet bonds.

[1] J. Sirker and G. Khaliullin, *J. Phys. B* **67**, 100408(R) (2003).

[2] C. Ulrich, G. Khaliullin, J. Sirker, M. Reehuis, M.~Ohl, S. Miyasaka, Y.Tokura, and B. Keimer, *Phys. Rev. Lett.* (in print, 2003)

WM9

Spin Polarised Quantum-Well States in Layered Magnetic Nanostructures of Cu/Co/Cu(100)

D. H. Yu[a] and M. Donath[b]

[a] *Bragg Institute, Australian Nuclear Science and Technology Organisation, Lucas Heights, NSW 2234, Australia.*

[b] *Physics Institute, University of Muenster, D-48149, Muenster, Germany.*

The unoccupied electronic structures of bilayer Co/Cu(100) and trilayer Cu/Co/Cu(100) structures have been investigated by spin-resolved inverse photoemission. For the first time, the spin-polarised unoccupied quantum-well states have been observed for both systems. The exchange splitting of the quantum-well states and the bulk-like sp band of Co (100) have been determined. A simple phase accumulation model simulated the electron confinement in the ultra-thin Co(100) film very well. The offset between the Co and Cu $X_{4'}$ point provides the confinement potential for electrons in the Co film. For the sandwich structure of Cu/Co/Cu(100), in addition to the spin-polarised quantum-well states, surface states and a surface resonant state at the copper/vacuum interface, and bulk-like minority d contributions from the underlying ferromagnetic Co layer have also been identified. The quantum-well states are shown to develop into a surface resonant state as a function of the electron momentum, as evidenced by the loss of the exchange splitting. The quantum-well states in Cu/Co structure are formed by resonance due to high reflectivity, because there is no absolute confinement potential for this structure. The experiment has shown that the spin resolution provides a possible access to the penetration depth of the wave function of the surface state and surface resonant state.

Acknowledgments: D H Yu would like to acknowledge the hospitality of the University of Muenster and support by the Alexander von Humboldt foundation in Germany.

WA1

Development of a Superconducting Absolute Tensor Gradiometer

D.L. Tilbrook, K.E. Leslie, M. Bick, C.P. Foley, R.A. Binks, J. Du, R. Gnanarajan,

S. K. H. Lam, B. Thorn, P. Sullivan.

CSIRO Telecommunications and Industrial Physics,

PO Box 218, Lindfield, NSW, 2070, Australia.

Although the use of high-temperature superconducting (HTSC) materials for the fabrication of SQUID-based magnetometers and gradiometers is now well established [1] these materials remain more difficult to use than the alternative low-temperature superconducting materials. In particular, the lack of HTSC wires and the difficulty of forming superconducting connections means that the standard low-T_c design practice of forming gradiometer coils from superconducting wires, is not applicable in high-T_c materials. Designs for HTSC axial gradiometers [2] have been implemented only by means of electronic or software subtraction of the outputs of a pair of SQUID magnetometers, and generally have insufficient dynamic range to be rotated in the earth's magnetic field.

In this work we describe the development of a new concept axial gradiometer [3] which is implemented through the use of a flux transformer pick-up loop structure patterned on flexible superconducting tape that is inductively coupled to a SQUID-based magnetometer. This is the first example of a series axial gradiometer in HTSC materials and offers significant advantages over the two-SQUID systems mentioned above. The design provides sufficient dynamic range and intrinsic noise immunity to operate while rotated in the full earth's field. Data analysis facilitates the measurement of the absolute value of all five independent components of the magnetic gradient tensor using a set of three such gradiometers, each of which is rotated about its axis. Initial results are presented showing the measurement by a prototype instrument of the tensor gradient of a small bar magnet.

1. For example, W. Eidelloth et. al., Appl. Phys. Lett., **59**, 3473 (1991); S. Knappe et. al., Cryogenics **32**, 881, (1992); M. N. Keene et. al., Appl. Phys. Lett. **64**, 366 (1994); G. M. Daalmans, Appl. Supercond., **3**, 399, (1995); M. I. Faley, et. al., IEEE Trans. Appl. Supercond., **7**, 3702 (1997).

2. For example, R. H. Koch et. al., Appl. Phys. Lett., **63**, 403, (1993); H. J. M. ter Brake et. al., IEEE Trans. Appl. Supercond., **7**, 2545, (1997); J. Borgmann et. al., Rev. Sci. Instrum., **68**, 2730, (1997).

3. D.L. Tilbrook, "The design of a new concept HTSC axial gradiometer", Submitted to Physica C.

WA2

Nanoscale Magnetite/Maghemite Particle-based Ferrofluids: the Effect of Local Particle Arrangement on Magnetic Properties

H. Pardoe, W. Chua-anusorn and T. St. Pierre

School of Physics, The University Of Western Australia, Nedlands W.A. 6009, Australia.

Many biological systems possess the ability to synthesise ferrimagnetic iron oxide particles as magnetite (Fe_3O_4). These biogenic magnetite particles have individual particle sizes of less than 100 nm, a range that limits them to single magnetic domains. The development of aqueous based ferrofluids containing ferrimagnetic particles within this size range has provided a model that can be used to study the properties of such systems. There are also a number of new biomedical and diagnostic applications that utilise ferrofluids and whose effectiveness depends on the magnetic properties of the ferrofluid.

Nanoscale magnetite/maghemite-based ferrofluids were chemically synthesised by coprecipitation of Fe(III) and Fe(II) in alkaline conditions in the presence of dextran or polyvinyl alcohol. Characterisation by magnetometry, Mössbauer spectroscopy and electron microscopy and diffraction indicate that the presence of the dextran and polyvinyl alcohol affects both the particle size and the local distribution of the ferrimagnetic particles with respect to one another.

We show that the arrangement of these particles, as determined by the presence of dextran or polyvinyl alcohol, plays a major role in determining the magnetic properties of the ferrofluid. The fact that the presence of dextran or polyvinyl alcohol during magnetite synthesis exerts some control over the arrangement of the particles may prove useful for applications in which specific magnetic properties are desirable, both when modelling biological systems, and utilising the magnetic properties of ferrofluids for biomedical applications.

WA3

The Antiferromagnetic Structure of $BaPrO_3$

R. A. Robinson[a], D. J. Goossens[a,b] and M. F. Telling[c]

[a] *Bragg Institute, ANSTO, PMB-1, Menai, NSW 2234*

[b] *Research School of Chemistry, ANU, Canberra, ACT 0200.*

[c] *ISIS, Rutherford Appleton Laboratory, Chilton, Oxon. OX11 0QX, UK*

In this study, we report the magnetic space group and moment direction in the canted antiferromagnetic system $BaPrO_3$. While previous work had shown that perovskite-based $BaPrO_3$, which is orthorhombic crystallographically, orders antiferromagnetically below 11.7K, and that it also exhibits weak ferromagnetism at the same temperatures, the exact magnetic symmetry and moment directions were previously undetermined. In this report, we show, by means of cold-neutron high-resolution powder diffraction, that the magnetic (Shubnikov) group is in fact Pb'n'm, and that the antiferromagnetism lies along the a-axis, with $\mu_x = 0.37 \pm 0.03\ \mu_B$. This is qualitatively and quantitatively consistent with previous neutron diffraction results reporting the configurational symmetry of the antiferromagnetism. Our model explicitly allows for ferromagnetism, and necessarily implies that the ferromagnetism previously observed in bulk magnetisation measurements must lie along the z-axis. We discuss ways in which this prediction might be tested, even in the absence of single crystals of $BaPrO_3$.

WA4

Theoretical Studies of a Mixed-Spin Antiferromagnetic Model for the Rare Earth Nickelates R_2BaNiO_5

A.M.A. von Brasch and J. Oitmaa

School of Physics, University of New South Wales, Sydney 2052, Australia.

An interesting class of magnetic materials was recently discovered, the rare earth nickelates R_2BaNiO_5, where R is a rare earth ion [1]. When the rare earth species is non-magnetic, the system is a very good experimental realisation of a Haldane-gap S = 1 antiferromagnet [2], with a gap in the excitation spectrum and the absence of long-range order [3]. If the rare earth ions are magnetic, long-range antiferromagnetic order is observed, with the associated gapless order parameter excitations. However, the Haldane excitations are also seen to co-exist in these compounds, even in the ordered phase.

It has been proposed that the magnetic behaviour of these compounds could be modeled with two dimensional layers, consisting of alternating rows of S = 1 and S = ½ spins, interacting antiferromagetically [4]. We will present our preliminary studies of such a mixed-spin antiferromagnetic model, performed using cluster series expansion techniques and analytical spin-wave theory.

1. Zheludev, J.M. Tranquada, T. Vogt and D.J. Buttrey, *Phys. Rev. B* **54**, 6437 (1996).
2. J. Darriet and L.P. Regnault, *Solid State Commun.* **86**, 409 (1993).
3. F.D.M. Haldane, *Phys. Rev. Lett.* **50**, 1153 (1983).
4. Y. Takushima, A. Koga, and N. Kawakami, *Phys. Rev. B* **61**, 15189 (2000).

WA5

XRD Characterisation of Nanoparticle Size and Shape Distributions

N. Armstrong[a], W. Kalceff[a], J. P. Cline[b] & J. Bonevich[c]

[a] *Department of Applied Physics, University of Technology Sydney, NSW 2007, Australia*

[b] *Ceramics &* [c] *Metallurgy Divisions, National Institute of Standards and Technology, Gaithersburg, MD 20899-8523, USA*

The form of XRD lines and the extent of their broadening provide useful structural information about the shape, size distribution, and modal characteristics of the nanoparticles comprising the specimen. Also, the defect content of the nanoparticles can be determined, including the type, dislocation density, and stacking faults/twinning. This information is convoluted together and can be grouped into "*size*'' and "*defect*'' broadening contributions. Modern X-ray diffraction analysis techniques have concentrated on quantifying the broadening arising from the size and defect contributions, while accounting for overlapping of profiles, instrumental broadening, background scattering and noise components [1-4].

We report on a combined Bayesian/Maximum Entropy (MaxEnt) technique developed for use in the certification of a NIST Standard Reference Material (SRM) for size-broadened line profiles [1]. The approach used was chosen because of its generality in removing instrumental broadening from the observed line profiles, and its ability to determine not only the average crystallite size, but also the distribution of sizes and the average shape of crystallites. Moverover, this Bayesian/MaxEnt technique is fully quantitative, in that it also determines uncertainties in the crystallite-size distribution and other parameters.

Both experimental and numerical simulations of size broadened line-profiles modelled on a range of specimens with spherical and non-spherical morphologies are presented to demonstrate how this information can be retrieved from the line profile data. The sensitivity of the Bayesian/MaxEnt method to determining the size distribution using varying *a priori* information are emphasised and discussed.

[1] N. Armstrong, W. Kalceff, J. P. Cline & J. Bonevich, J. NIST Res., **108**, (2003) *In press*

[2] J. I. Langford, D. Louër & P. Scardi, *J. Appl. Cyst.*, **33**, 964-974, (2000).

[3] P. Scardi, M Leoni & Y. H. Dong, *Eur. Phys. J. B***, 18,** 23-30 (2000).

[4] P. Scardi & M Leoni, *Acta Cryst.*, **A58**, 190-200, (2002).

WA6

The Eigenvalue Distribution of the Time-Evolution Operator of a Non-Equilibrium System

Yuichi Nakamura [a] and Naomichi Hatano [b]

[a] *Department of Physics, University of Tokyo, 4-6-1 Komaba, Meguro, Tokyo 153-8505, Japan*

[b] *Institute of Industrial Science, University of Tokyo, Tokyo, Japan*

We study a one-dimensional cellular automaton as a discrete traffic-flow model. We investigate the eigenvalue distribution of the time-evolution operator of the model. We show that the eigenvalue distribution can indicate stationary flows in the non-equilibrium system with interaction. We incorporate the flux operator into the time-evolution operator; we generalize the matrix elements of the flow of a specific car from unity to e^{g} [1]. Figure 1 shows the eigenvalue distribution for ten sites. All the eigenvalues are on the unit circle for $g = 0$. By increasing g, we notice in Fig.1 a remarkable difference between the free phase (the number of the cars is from one to five) and the congested phase (the number of the cars is from six to nine). We can thus regard the congested phase as a localized state and the free phase as an extended state. In the present study, we used a recently introduced algorithm of computing the eigenvalue distribution of huge non-Hermite matrices [2].

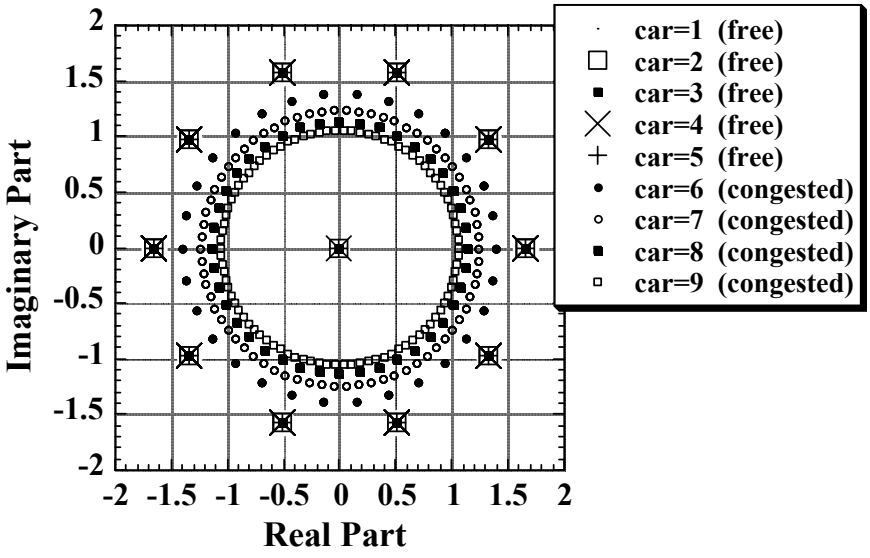

Fig.1: The eigenvalue distribution for g =0.5 (ten sites). In the free phase, the eigenvalues do not depend on the number of the cars and are located on the circle of radius e^{g}. In the congested phase, the eigenvalues are located closer to the unit circle. Note that zero eigenvalues exist when the number of the cars is from two to eight.

[1] N. Hatano and D. R. Nelson, Phys. Rev. Lett. **77**, 570 (1996); Phys. Rev. B **56**, 8651 (1997)

[2] N. Hatano and J. Yamasaki, in preparation.

Oral Sessions
Abstracts

Thursday
5 February

TM1

Microphotonic and Photonic Bandgap Devices: Towards All-Optical Technology

Benjamin J. Eggleton

ARC Centre of Excellence for Ultra-high-bandwidth Devices for Optical Systems (CUDOS)
School of Physics, University of Sydney. NSW 2006

The Centre for Ultrahigh bandwidth Devices for Optical Systems (CUDOS) was created under the Australian Research Council's Centres of Excellence program. Of the eight centres that were funded, three (including CUDOS) are heavily based around leading-edge research in optics. CUDOS' research is aimed at the study and potential applications of linear and nonlinear optical behavior in micro-structured materials. Examples of such materials include photonic crystals and micro-structured optical fibres. The CUDOS team aims to investigate phenomena driven by high intensity optical fields propagating through these materials. This presentation will overview the CUDOS research program with particular emphasis on microstructured materials and novel microfabrication techniques.

TM2

2D Photonic Crystal-based Optical Microcomponents on Indium Phosphide (InP) Membrane for Integrated Optics

C. Grillet[a], X. Letartre[b], C. Seassal[b], P. R. Romeo[b] and P. Viktorovitch[b]

[a] *Centre for Ultra-high-bandwidth Devices for Optical Systems*
School of Physics, University of Sydney.
[b] *Laboratoire Electronique Optoelectronique Microsystemes*
Ecole Centrale de Lyon, France

Realization of optical devices containing photonic crystals [1] seems a very promising way to fulfill the requirements of miniaturization of integrated optics [2]. Photonic Crystals (PC) are periodic dielectric structures conceived so as to modify the behavior of the photons in the same way that a semi conductor crystalline affects electrons properties. They thus provide an effective control of light on a wavelength scale. Moreover insertion of defects in the periodic lattice allows the realization of microcavities which can be exploited either to reinforce the interaction matter-radiation (light emission and detection), or to filter and redirect the light on very short distances.

We first describe concepts and general characteristics related to two-dimensional (2D) planar (finite height) photonic crystal and their fabrication.

Then, we focus on 2D PC waveguides realized on InP membrane. Original experimental studies [3], carried out by a diffracted photoluminescence technique, allow us to release, as well the modal properties of the guide, as the access to the propagation losses.

1. E. Yablonovitch, *Phys. Rev. Lett.* **58**, 2059 (1987).
2. R. D. Meade, A. Devenyi, J. D. Joannopoulos, O. L. Alerhand, D. A. Smith, and K. Kash, *J. Appl. Phys.* **75**, 4753 (1994).
3. X. Letartre, C. Grillet, P. R. Romeo, C. Seassal, P. Viktorovitch, M. Le Vassor d'Yerville, D. Cassagne, and C. Jouanin, *Appl. Phys. Lett*. **79**, 2312 (2001)

TM3

Left-Handed Materials: Recent Progress and Perspectives

I. V. Shadrivov[a], A. A. Zharov[a,b], A. A. Sukhorukov[a], and Yu. S. Kivshar[a]

[a]*Nonlinear Physics Group, Research School of Physical Sciences and Engineering, Australian National University, Canberra ACT 0200, Australia*

[b]*Institute for Physics of Microstructures, GSP-105 Nizhny Novgorod, Russia*

Left-handed materials (LHM) or materials with negative refraction received much attention due to many recent experimental demonstrations, even though they were predicted theoretically almost 40 years ago [1]. LHMs are artificially created structures with simultaneously negative dielectric permittivity and magnetic permeability. In such media electromagnetic waves have the electric field, the magnetic field, and the wave vector forming a left set of vectors in contrast with conventional materials, where these vectors form a right set. As a result, in LHM all waves are backward, i.e. the wave front propagates in the direction opposite to that of the energy flow. The most famous properties of LHMs are negative refraction, reversed Doppler effect, and reversed Vavilov-Cherenkov effect.

In this talk, we overview the basic properties of LHMs and recent experimental results as well as discuss possible applications. All types of LHMs do not exist in nature, but they are artificial composite structures containing arrays of metallic resonators with the negative parameters in a microwave frequency range. We underline requirements to the composite structures which make these composites left-handed.

Also, we present our recent results demonstrating a number of novel phenomena in LHMs, such as nonlinear switching of material properties between left- and right-handed types, effective second-harmonic generation in novel geometries, nonlinear lenses, and photonic crystals based on LHMs with a novel type of the bandgap. We show that nonlinear magnetic phenomena are strongly enhanced in LHM composites.

1. V. G. Veselago, Usp. Fiz. Nauk **92**, 517 (1967) [Sov. Phys. Usp. **10**, 509 (1968)].

TM4

The Effects of GaN Capping Layer Thickness on Electrical Properties of Two-dimensional Electron Gas in GaN/AlGaN/GaN Heterostructures

A. Asgari[♣], L. Faraone

School of Electrical, Electronic and Computer Engineering, The University of Western Australia, Crawley, WA 6009, Australia

In this article we present a study of the effect of GaN capping layer thickness on the two-dimensional electron gas (2DEG) electrical properties. This study is undertaken using a fully numerical calculation for unintentionally doped GaN/$Al_xGa_{1-x}N$/GaN heterostructures with different Al mole fraction in the $Al_xGa_{1-x}N$ barrier, and for various values of barrier layer thickness [1,2,3]. The results of our analysis clearly indicate that increasing the GaN capping layer thickness leads to a decrease in the 2DEG density. Furthermore, it is found that the room temperature 2D-electronmobility reaches a maximum value of approximately $1.8x10^3$ cm^2/Vs for GaN capping layer thickness grater than 500 Å with an $Al_{0.32}Ga_{0.68}N$ barrier layer of 200 Å thick. In contrast, for same structure, the 2DEG density decreases monotonically with GaN capping layer thickness, and eventually saturates at approximately $6x10^{12}$ cm^{-2} for capping layer thickness greater than 500 Å. A comparison between our calculated results with published experimental data is shown to be in good agreement for GaN capping layers up to 500 Å thick.

PACS: 72. 10. –d; 73. 20. –r; **Keywords:** mobility; AlGaN/GaN; capping layer; HFET.

1 A. Asgari, M. Kalafi, and L. Faraone, J. Appl. Phys. (in press)

2 M. Kalafi and A. Asgari, Physica E **19**, 321 (2003).

3 I. P. Smorchkova, L. Chen and T. Mates, L. Shen and S. Heikman, B. Moran, S. Keller, S. P. DenBaars and J. S. Speck, and U. K. Mishra, J. Appl. Phys. **90**, 5196 (2001).

♣ asgari@ee.uwa.edu.au

TM5

Calcite Microcrystals in the Pineal Gland of the Human Brain: Second Harmonic Generators and Possible Piezoelectric Transducers

Sidney B. Lang

Department of Chemical Engineering, Ben-Gurion University of the Negev, Beer Sheva, Israel

A new form of biomineralization in the pineal gland of the human brain has been studied. It consists of small crystals that are less than 20 μm in length and that are completely distinct from the often-observed mulberry-type hydroxyapatite concretions. Cubic, hexagonal and cylindrical morphologies have been identified using scanning electron microscopy. Energy dispersive spectroscopy, selected-area electron diffraction and near infrared Raman spectroscopy established that the crystals were calcite. Experiments at the European Synchrotron Radiation Facility (ESRF) to study the biomineralization showed the presence of sulfur originating from both sugars and proteins. Other studies at the ESRF furnished information on the complex texture crystallization of the calcite. With the exception of the otoconia structure of the inner ear, this is the only known non-pathological occurrence of calcite in the human body. The calcite microcrystals are believed to be responsible for the previously observed second harmonic generation (SHG) in pineal tissue sections. There is a strong possibility that the complex twinned structure of the crystals may lower their symmetry and permit the existence of a piezoelectric effect.

TM6

Magnetic Materials for Hyperthermic Cancer Treatment

K.M. Spiers, J.D. Cashion, K.A. Gross and S.J. Harker

School of Physics and Materials Engineering, Monash University, Victoria 3800, Australia.

One method of hyperthermic treatment of tumours is by hysteresis heating of a magnetic implant. This project aims at developing a suitable combination of magnetic material and AC magnetic field which could provide a means of treating deep-seated cancers such as liver cancer. The first part is the production of a smooth-shelled magnetic powder, of micrometre dimensions, which can be introduced by injection into a suitable artery. Magnetite, Fe_3O_4, and maghemite, γ-Fe_2O_3, are the prime candidates. Since the heating power is proportional to the frequency, the second part is to develop an AC magnet with sufficient strength and which is capable of operating at suitable frequencies. Most work to date has used air-cored solenoids, but we are trialling a pole-piece electromagnet system which will provide a more focussed magnetic field and hence reduce the resistive heating of nearby tissue.

Samples of magnetite were produced from a solution of $FeSO_4.7H_2O$ by adding KOH/KNO_3. The washed and dried precipitate was heated in flowing air to convert the magnetite to maghemite. XRD analysis confirmed the structures. Squid measurements were taken at 40^{o}C in fields of ±24 kA/m (±300 Oe) to determine the hysteresis loop area. Maghemite produced the larger hysteresis area. Mössbauer spectra of the maghemite showed a quite symmetrical sextet structure for which a left and right sextet gave a better fit than did an inner and outer sextet. However, some other workers [e.g. 1,2] have obtained distinctively asymmetrical sextets. There is disagreement in the literature regarding the extent to which ordering of the iron vacancies occurs and it probably preparation dependent. Further fitting and modelling of the spectra are being undertaken to try and determine how much information can be obtained about vacancy ordering in the maghemite structure.

[1] R.J. Pollard, Hyperfine Interact. **41**, 509 (1988)

[2] G.M. da Costa, E. De Grave, L.H. Bowen, R.E. Vandenberghe and P.M.A. de Bakker, Clays and Clay Min. **42** 628 (1994).

TM7

Nanoparticulate Cobalt/Polymer Complexes for Biomedical Applications

M. A. Zalich[a, b], T. G. St. Pierre[a], V. V. Baranauskas[b] and J. S. Riffle[b]

[a] *School of Physics, The University of Western Australia, Western Australia 6009, Australia.*

[b] *Department of Chemistry, Virginia Polytechnic Institute and State University, Blacksburg, Virginia, USA*

The preparation of cobalt nanoparticles is of great interest for biomedical applications owing to their high magnetic susceptibility. Of the transition metals, cobalt (bulk) has one of the largest magnetic susceptibilities per gram of material (1400 emu cm^{-3}); however, cobalt readily oxidizes to form an antiferromagnetic oxide. The presence of antiferromagnetic cobalt oxide on the surface of cobalt metal detracts from the magnetic response of the material. Protecting cobalt nanoparticles against oxidation would be advantageous in preparing highly responsive core elements for developing technologies to address retinal detachment disorders, targeted drug delivery and toxin removal from biological fluids.

Cobalt nanoparticles (~10 nm) were prepared by the thermal decomposition of dicobalt octacarbonyl in poly(styrene-*b*-4-vinylphenoxyphthalonitrile) nanoreactors. A portion of the sample was subsequently pyrolyzed at 700 ^{o}C for 4 hours. The magnetic properties of the pre- (sample 1) and post-pyrolyzed (sample 2) materials were investigated using SQUID magnetometry. Transmission electron microscopy (TEM) was used to probe the structure and chemistry of the materials while small angle x-ray scattering (SAXS) was used to investigate particle size and distribution.

Magnetic measurements indicated that each sample contained both magnetically blocked and unblocked particles. Zero-field-cooled/field-cooled hysteresis loops at 5K indicated the presence of a cobalt oxide layer in sample 1, whereas sample 2 contained little or no cobalt oxide. In addition, the pyrolyzed sample was found to have a high saturation magnetization of 71 emu/g sample (sample 2).

In conclusion, the data show that pyrolysis of polymer coatings around metallic cobalt nanoparticles can produce coatings that protect the nanoparticles from oxidation while retaining a high magnetic susceptibility.

TM8

Computer Simulation Studies of the Rheology of Soft Condensed Matter

P. J. Daivis, I. K. Snook, M. L. Matin, T. Kairn and M. McPhie

Department of Applied Physics, RMIT University, GPO Box 2476V, Melbourne, Victoria 3001, Australia.

The rheology of soft condensed matter systems, such as polymer melts, polymer solutions and colloidal dispersions, is a subject of enduring interest - not only because of its importance in materials processing technology, but also because of the fascinating theoretical challenges it presents. Many of the rheological features possessed by these systems, such as normal stress differences, non-Newtonian viscosity and elasticity, are spectacularly evident on the macroscopic scale, but these properties are also crucial to emerging modern technologies such as micro- and nano-fluidics. Over the last seven years, we have studied many different aspects of the rheology of soft condensed matter systems using non-equilibrium molecular dynamics computer simulation techniques. Of particular importance, has been our development of a new algorithm for studying elongational flow [1], a comparison of the planar elongational and shear flow rheology of molecular fluids [2], our examination of the approach to the Brownian limit in colloidal fluids [3], and our detailed investigation of the concentration dependence of the viscosity and normal stress differences in short-chain polymer solutions [4]. In this paper, we review the results of these investigations, discuss the current capabilities and limitations of non-equilibrium molecular dynamics simulations, and discuss our current work and future directions.

1. B. D. Todd and P. J. Daivis, *Comp.Phys. Commun.* **117**, 191 (1999).
2. P. J. Daivis, M. L. Matin and B. D. Todd, *J. Non-Newtonian Fluid Mech.* **111**, 1 (2003).
3. I. Snook, B. O'Malley, M. McPhie and P. Daivis, *J. Molec. Liq.* **103-104**, 405 (2003).
4. T. Kairn, P. J. Daivis, M. L. Matin and I. K. Snook, accepted, *Polymer* (2004).

TM9

A Novel In-Line Micro-Fourier Rheometer

J.A. Glasscock and R.S. Smith

CSIRO Telecommunications and Industrial Physics
PO Box 218 Lindfield, NSW 2070, Australia.

A new rheometer has been designed which is capable of being used in industrial process flows. This instrument is able to measure the rheological parameters of a process fluid in a very short time across a frequency range of at least two orders of magnitude in situ. Product quality can be monitored and maintained through rapid manipulation of process variables in response to product fluctuations that are visible as changes in the measured rheological properties of the fluid. The rheometer is constructed such that no process fluid can be trapped in the measurement volume which would lead to errors in subsequent measurements due to fouling or contamination. All parts of the rheometer in contact with the process stream are stainless steel, allowing for the rigorous cleaning procedures commonly required in industry.

The operation of this rheometer is described and results from measurements of flowing sunflower oil are presented [1]. The instrument shows an excellent level of reproducibility and its ability to capture and release discrete samples is demonstrated. Static (no flow) measurements have been undertaken on the viscoelastic standard SRM 2490 supplied by NIST [2] in order to compare the results obtained by the in-line micro-Fourier rheometer with those obtained by NIST using a common controlled strain rheometer. The rheological data was compared using a correlation analogous to the Cox-Merz rule [3] using an “effective shear rate". The rheological properties as determined by both instruments were in good agreement showing a similar trend and magnitude.

[1] J. Glasscock, R. Smith, J. Vanajek, and J. Winter, Review of Scientific Instruments **74**, 4925 (2003).

[2] C. Schultheisz and S. Leigh, Tech. Rep. 260143, National Institute of Standards and Technology (2002).

[3] D. Doraiswamy, A. Mujumdar, I. Tsao, and A. Beris, Journal of Rheology **35**, 647 (1991).

TA1

Synchrotron-based Measurements of the Electronic Structure of the Organic Semiconductor Copper Phthalocyanine

J. E. Downes

MacDiarmid Institute, Victoria University, Wellington, New Zealand.

Copper phthalocyanine (CuPc) is a prototypical molecular organic semiconductor that is currently used in the construction of many organic electronic devices such as organic light emitting diodes (OLEDs) [1]. Although the material is currently being used, and despite many experimental [2,3] and theoretical [4] studies, it's detailed electronic structure is still not completely understood. This is likely due to two key factors. Firstly, the interaction of the Cu *3d* and phthalocyanine ligand *2p* electrons leads to the formation of a complex arrangement of localized and delocalized states near the Fermi level. Secondly, thin films of the material are subject to damage by the photon beam used to make measurements of their electronic structure.

Using the synchrotron-based techniques of soft x-ray emission spectroscopy (XES) and x-ray photoemission spectroscopy (XPS), we have measured the detailed electronic structure of *in-situ* grown thin film samples of CuPc. Beam damage was minimized by continuous translation of the sample during data acquisition. The results obtained differ significantly from previous XES and ultraviolet photoemission measurements, but are in excellent agreement with recent density functional calculations. The reasons for these discrepancies will be explained, and their implications for future measurements on similar materials will be explored.

[1] S.R. Forrest, *Chemical Reviews* **97**, 1793 (1997)

[2] I.G. Hill, A. Kahn, Z.G. Soos*, et al.*, *Chemical Physics Letters* **327**, 181 (2000)

[3] E.Z. Kurmaev, S.N. Shamin, V.R. Galakhov*, et al.*, *Physical Review B (Condensed Matter and Materials Physics)* **64**, 045211/1 (2001)

[4] M.-S. Liao and S. Scheiner, *Journal of Chemical Physics* **114**, 9780 (2001)

TA2

New Approaches to Fitting the Mössbauer Spectra of Prussian Blue

T. L. Greaves and J. D. Cashion

School of Physics and Materials Engineering, Monash University, Victoria 3800, Australia.

The Mössbauer spectra of Prussian Blue have traditionally been fitted using one singlet and one doublet, to fit the ferrocyanide and ferric iron sites. However, it is widely accepted in the literature that there are several possible configurations for the ferric site, and each of these should be fitted individually to obtain a meaningful fit.

According to the literature, there are two possible Prussian Blue structures, Insoluble Prussian Blue (IPB), $Fe^{3+}{}_4[Fe^{II}(CN)_6]_3.14H_2O$, and Soluble Prussian Blue (SPB) $KFe^{3+}[Fe^{II}(CN)_6]$. In IPB there are ten uniquely different coordinations for the ferric site due to many different arrangements of cyanide and water ligands. In SPB there is a more continuous range of ferric sites, due to the presence of potassium ions in voids throughout the cubic lattice. A variety of samples have been prepared which, according to the literature, should have produced three IPB and three SPB samples. However, all the samples appear to be best represented by the IPB structure.

A number of different methods have been used to fit the Mössbauer spectra of Prussian Blue, using both Gaussian and Voigtian line shapes. The point charge model has been used to calculate the quadrupole splitting for each ferric site, and the corresponding isomer shifts have been estimated from the partial isomer shifts for each ligand. These theoretical parameters have been used to obtain excellent fits to a range of Prussian Blue samples.

Details will be given of improvements in our knowledge of the structure of these well known, but crystallographically complex compounds.

TA3

Light Scattering from Spin Wave Excitations in Non-Collinear Thin Film Magnetisation Structures

D.C. Crew[a] and R.L. Stamps[a]

[a] *School of Physics M013, The University of Western Australia, Nedlands WA 6009*

We present a theory of Brillouin Light Scattering (BLS) for spectra obtained by scattering from spin wave excitations in highly non-collinear magnetisation structures. As an application we present calculated results for BLS spectra from the spiral state found in exchange coupled hard/soft bilayers during reversal. Effects observable in Stokes/Anti-Stokes ratio asymmetry are described in relation to recent experimental measurements [1].

The thin film structure is modelled as a system of coupled atomic layers in which the material parameters can vary from layer to layer. First, the ground state of the system is found, then a spin spectral density is calculated using a semi-classical Heisenberg model. The cross section for inelastic light scattering spectra is calculated using this spin spectral density together with classical electromagnetic Green's functions appropriate for a multilayer geometry.

This model allows the calculation of spin wave excitations in non-uniform magnetisation structures, which are becoming increasingly common in magnetic nanotechnology where two different magnetic materials are exchange coupled across an interface. The layer by layer model can also be applied to the problem of scattering of excitations at disordered interfaces, which is a topic of particular practical as well as basic interest.

As an application of the model we consider a recently measured exchange spring system[1]. The exchange spring system has been found to display characteristic structure in the magnetic hysteresis, which allows important information on interface exchange and the effects of magnetic anisotropies to be obtained. Spin wave frequencies can also be used [2] to provide measures of interlayer exchange and anisotropy energies. Here we show the application of the model to data taken from an exchange spring bilayer, Co/CoPt, using BLS.

1. D.C. Crew, R.L Stamps, H.Y Liu, Z.K. Wang, M.H. Kuok, S.C. Ng, K. Barmak, J. Kim, L.H. Lewis, ICM 2003, Rome Italy (2003) Paper 1-ppm14 in press
2. D.C. Crew and R.L. Stamps, J. Appl. Phys. **93** 6483 (2003)

TA4

Experimental Determination of Lévy Flight Distributions of the Energy Barriers in Spin Glasses

N.T. Gorham [a], R.C. Woodward [a], T.G. St Pierre [a], R.L. Stamps [a], M.J. Walker [b], D. Greig [b], and J.A.D. Matthew [c]

[a] *School of Physics, The University of Western Australia, Perth WA, 6009, Australia*

[b] *Department of Physics and Astronomy, University of Leeds, Leeds, LS2 9JT, UK*

[c] *Department of Physics, University of York, York, YO10 5DD, UK*

"Spin glass" was a term originally developed to describe certain magnetic alloys in which there was observed a freezing transition to a low temperature phase where the magnetic moments (or spins) are aligned in fixed but random directions. Although the study of spin glasses is at least three decades old, our current understanding of some very basic issues is still quite limited. Observable characteristics associated with spin glasses are thought to result from the complex dynamics associated with a large number of metastable magnetic states separated by a broad distribution of energy barriers to magnetic reversal. To date, a number of models have been developed which produce this type of energy landscape including the random energy model and the hierarchical energy model.

In this study we use a technique previously developed for the study of magnetic nanoparticles [1,2] to characterise the apparent magnetic energy barrier distribution that results from this complex energy landscape for a series of $Pd_{40}Ni_{40-x}Fe_xP_{20}$ (x=10-20) alloys. The distributions observed are best described by a stretched exponential in the form of a truncated Lévy flight distribution. This form would appear to suggest a hierarchical landscape of apparent energy barriers arising from interactions between randomly oriented magnetic clusters of spins within the material. The degree of stretching of the exponential form of the energy barrier distributions is found to increase with decreasing iron concentration.

1. T.G. St Pierre et al., Phys. Rev. B, **65** (2002) 024436
2. N.T. Gorham et al., J. Magn. Magn. Mat., (in press)

TA5

Inductive Measurements of Ferromagnetic Resonance

R. C. Woodward*, K. Kennewell, D. C. Crew and R. L. Stamps

School of Physics, The University of Western Australia, M013, 35 Stirling Hwy Crawley WA 6009 Australia.

The rapid advance in magnetic data storage has driven groundbreaking work in the science that underpins the properties of ferromagnetic materials at high frequencies. Recent work in this area has included the use of precession in order to produce ultra-high speed switching of magnetic elements [1], the generation of excited dynamical structures by application of inhomogeneous field pulses [2], and examination of the propagation of localized spin waves [3]. This paper describes explorations of ultra-fast magnetization dynamics being undertaken at The University of Western Australia.

We have studied the differences in magnetization dynamics in simple permalloy films when a sample is excited with sharp pulse compared to the to the dynamics generated by the application of a small amplitude continuous wave signal. We have observed a difference in the resonant frequency determined from these two excitations and will propose reasons for the different resonance responses of the system. Using the ultra-fast techniques described above we have measured dynamical properties that are significantly different to the static properties. These results are explained by the dynamical measurements being made on time scales smaller than the characteristic relaxation time.

Future applications of these devices will be to examine broadening of line widths and frequency shifts associated with the excitation of magnetostatic modes, factors limiting quasiballistic reversal and differences between the dynamic and static properties of magnetic materials.

1. H.W. Schumacher, C. Chappert, R.C. Sousa, P.P. Freitas and J. Milat, Phys. Rev. Lett. **90**, 017204, (2003)
2. M. Covington, T.M. Crawford and G.J. Parker, Phys. Rev Lett., **89**, 237202, (2002)
3. M. Bailleul, D. Olligs and C Fermon, Phys. Rev Lett., **91**, 137204, (2002)

* corresponding author: woodward@physics.uwa.edu.au

TA6

Magnetic Properties, Curie Temperature and Microstructures of PrFeB and NdFeB-based Magnets with Additives by Blending

A.Ahmad[a] and I.R.Harris[b]

[a] *Department of Metallurgical and Materials Engineering, University of Engineering and Technology, Lahore, Pakistan*

[b] *School of Metallurgy and Materials, The University of Birmingham, UK*

Since the invention of rare earth based magnets a great deal of research activity has been devoted to improve their magnetic properties by adding alloying elements. In the present study PrFeB and NdFeB-based magnets were made with the additives Co, Al, V, Co-Al (combined addition) and Co-Cu (combined additions) by conventional powder metallurgical process. However the additions of these elements were made by powder blending technique. By blending powders prior to sintering a wide range of compositions can be assessed rapidly using only a small number of starting alloys. The properties of the blended magnets produced have been compared with the magnets produced from alloys modified at a pre-casting stage.

The paper describes the microstructure, domains structure, magnetic properties and Curie temperature of the sintered magnets. It has been found that blending is an effective way of adding elements to RFeB alloys. The magnetic properties and Curie temperature of blended magnets have been improved by Co, Co-Al and Co-Cu additions. The coercivity of as-sintered Pr-based magnets after these additions has been found to be better than those of the corresponding Nd-based magnets.

Oral Sessions
Abstracts

Friday
6 February

FM1

The Fabrication of Nano-Scale Devices in Silicon

F.J. Ruess, M.Y. Simmons, L. Oberbeck, K.E.J. Goh, A.R. Hamilton,
T. Hallam, N. J. Curson and R.G. Clark
Centre for Quantum Computer Technology, School of Physics,
University of New South Wales, Sydney 2052, Australia

Over the last three years our group has solved several key issues in the fabrication of nano-scale devices in silicon [1] using an ultra-high vacuum (UHV) scanning tunneling microscope (STM) and silicon molecular beam epitaxy (MBE). These steps include: the placement of single phosphine (PH_3) molecules at predefined locations on a silicon surface using STM lithography [2], the controlled phosphorus incorporation from the PH_3 molecules into the top layer of the silicon surface with ~ 1 nm accuracy [3] and the encapsulation of P δ-doped layers with minimal segregation using MBE [4,5].

In this talk we present our results for arguably one of the most critical steps of device fabrication using a scanning tunneling microscope – that of connecting the STM patterned buried phosphorus devices outside the vacuum environment to perform electrical measurements. We have achieved this by etching registration markers into the Si surface that allow us to align and contact the nano-scale device fabricated in the UHV system using conventional optical lithography. We present electrical transport data showing a cross over from two-dimensional to one-dimensional behaviour by confining dopants to a 90nm wide quantum wire using STM based lithography. Our results highlight the potential of this fabrication approach for the creation of electronic nano-scale devices in Si down to the atomic level [6] including the realisation of atomically ordered transistors, quantum cellular automata, single atom memory devices and a solid-state quantum computer.

1. J.R. Tucker, T.-C. Shen, Solid State Electronics **42,** 1061 (1998).
2. J.L. O'Brien *et al*., Phys. Rev. B **64,** 161401 (2001).
3. S.R. Schofield *et al*., Phys. Rev. Lett. **91,** 136104 (2003).
4. L. Oberbeck *et al*., Appl. Phys. Lett. **81,** 3197 (2002).
5. T.-C.Shen *et al*., Appl. Phys. Lett. **80** (2002) 1580.
6. F.J. Ruess *et al.,* manuscript in preparation.

FM2

Fabrication of a Novel Silicon Single Electron Transistor for Si:P Quantum Computer Devices

S.J. Angus[a], C.E.A. Smith[a], G.L. Snider[b], E. Gauja[a], A.S. Dzurak[a] and R.G. Clark[a]

[a] *Centre for Quantum Computer Technology, University of New South Wales, Sydney, NSW 2052, Australia.*

[b] *Department of Electrical Engineering, University of Notre Dame, IN, USA.*

Quantum computation relies on the successful measurement of quantum states. Single electron transistors (SETs) are known to be able to perform fast and sensitive charge measurements [1] of solid state qubits. However, due to their sensitivity, SETs are also very susceptible to random charge fluctuations in a solid-state materials environment. In previous dc transport measurements [2], silicon-based SETs have demonstrated greater charge stability than Al/Al_2O_3 SETs. We have designed and fabricated a novel silicon SET architecture for a comparison of the noise characteristics of silicon and aluminium based devices.

The silicon SET described here is designed for controllable and reproducible low temperature operation. It is fabricated using a novel dual gate structure on a silicon-on-insulator substrate. A silicon quantum wire is formed in a 100nm thick high-resistivity superficial silicon layer using reactive ion etching. Carriers are induced in the silicon wire by a back gate in the silicon substrate. The tunnel barriers are created electrostatically, using lithographically defined metallic electrodes (~40nm width). These tunnel barriers surround the surface of the quantum wire, thus producing excellent electrostatic confinement. This architecture provides independent control of tunnel barrier height and island occupancy, thus promising better control of Coulomb blockade oscillations than in previously investigated silicon SETs. The use of a near intrinsic silicon substrate offers compatibility with Si:P qubits in the longer term.

1. M.H. Devoret and R.J. Schoelkopf, *Nature* **406**, 1039 (2000).
2. N.M. Zimmerman, W.H. Huber, A. Fujiwara and Y. Takahashi, *Appl. Phys. Lett.* **79**, 3188 (2001).

FM3

The Dependence of the Critical Thickness of an InGaAs/GaAs Multi-layer on Quantum Well and Barrier Thicknesses and Number of Periods

M. Madebo, B.F. Usher and J. Riley[a]

Department of Electronic Engineering, La Trobe University, Victoria, 3086, Australia.

[a]*Department of Physics, La Trobe University.*

Strained-layer superlatices (SLS's) and multiple-quantum-wells (MQW's), in which multilayer structures are grown lattice mismatched to a substrate, but with individual layer thicknesses smaller than their critical thicknesses, have become increasingly important in electronic and optoelectronic device applications. Despite the widespread application of SLS's and MQW's, there have been serious shortcomings in previous attempts [1,2] to predict the stability criteria for multi-layered structures. In view of this, Madebo et al [3] have developed a Threading Dislocation Configuration (TDC) model that can be applied to any strained layer structure to predict its critical thickness. This paper uses the TDC model to predict the number of MQW periods and the corresponding GaAs barrier thickness required for a given InGaAs layer thickness if the formation of misfit dislocations is to be avoided. This approach follows the evolution of the threading dislocation's configuration as each monolayer is added to the structure. It is observed that in MQW structures with strained layer thicknesses less than half the critical thickness, there are ranges of quantum well periods for which the barrier thickness required to forbid the formation of a misfit dislocation is the same. But for thicker strained layers (greater than half the critical thickness) the relationship between the minimum barrier thickness required for a given number of quantum well periods is logarithmic in form.

[1] G. Allen Vawter and D. R. Myers, *J. Appl. Phys*., **65**, 4769 (1989).

[2] R. Hull, J. C. Bean, F. Cerdeira, A. T. Fiory, and J. M. Gibson, *Appl. Phys. Lett*., **48**, 56 (1986).

[3] M. Madebo, B.F. Usher and J.D. Riley, *Conference on Optoelectronic and Microelectronic Materials and Devices*," UNSW Sydney, Australia, pp 209, IEEE, Piscataway NJ (2003).

FM4

X-ray Absorption and Emission Study of Amorphous and Nanocrystalline GaN Films Containing Buried N_2

B.J. Ruck[a], A. Koo[a], F. Budde[a], S. Granville[a], A. Bittar[b], H.J. Trodahl[a]

[a] *School of Chemical and Physical Sciences, Victoria University of Wellington, Wellington, New Zealand.*
[b] *Industrial Research Ltd, P.O. Box 31-310, Lower Hutt, New Zealand.*

It has been predicted that amorphous gallium nitride (a-GaN) may possess a well-defined wide band gap, and is thus a potential substitute for the more expensive crystalline form used in short wavelength optoelectronic devices [1]. Experimental investigations of disordered GaN have lent support to this prediction, but the picture is complicated because the properties of the amorphous state are not unique, and instead depend on the exact nature of the disordered structure. We have pioneered a novel ion-assisted growth technique that produces GaN films with a microstructure that ranges from nanocrystalline, with crystallite size of order 3 nm, to fully amorphous, depending on the exact growth conditions. This presentation will give an overview of our research into the properties of disordered GaN, including characterization of the physical structure of the films and their electronic energy levels, and also their photoconductive response. In particular I will focus on synchrotron radiation studies of samples with a range of different microstructures.

X-ray absorption spectroscopy (XAS) and x-ray emission spectroscopy (XES) provide particularly powerful tools for examining a sample's empty and filled electronic energy levels, respectively. The details of the absorption and emission processes make it possible to obtain atom-specific information and to investigate the symmetry of the electronic levels. An example of the information obtained is shown in Figure 1. The thin solid curve shows XAS data, which is a measure of the nitrogen *p*-projected density of unfilled electronic states in this nanocrystalline GaN sample. The thick solid curve shows XES data from the same sample, which provides complementary information about the occupied valence band states. Although the spectral features are broader in fully amorphous films than in nanocrystalline samples, a well-defined band gap exists in both cases with magnitude similar to that of crystalline GaN.
There are additional feature present in both spectra that have no analogue in crystalline GaN. The strong absorption peak near 402 eV and the narrow emission line near 393 eV are related to nitrogen atoms trapped within our disordered films in the form of N_2 molecules embedded during growth. The coupling between the trapped N_2 and the GaN matrix appears to be weak, although there is some evidence for interaction between the two.

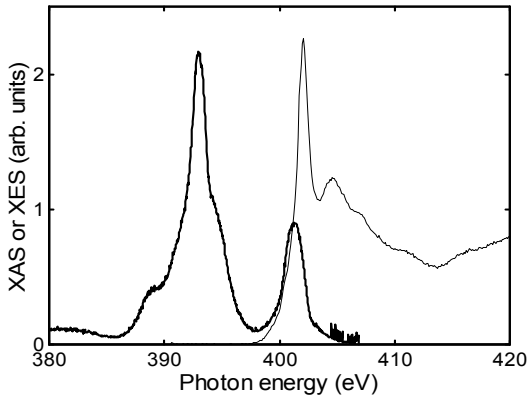

Figure 1: XAS (thin line) and XES (thick line) spectra of a nanocrystalline GaN film. The large peak in the absorption at 402 eV and the peaks in the emission at 393 eV and just over 400 eV are the signatures of molecular nitrogen trapped within the films. The rest of the spectral features represent the valence (XES) and conduction (XAS) band density of states in the GaN.

1. P. Stumm and D.A. Drabold, *Phys. Rev. Lett.* **79**(4), 677 (1997).

FM5

Molybdenum Disulphide (MoS_2) – Gallium Arsenide (GaAs) Heterostructures for Solar Cell Applications

I.M. Jamieson and G. Jakovidis

School of Physics and Materials Engineering, Monash University, Victoria 3800, Australia

Heterostructures provide a means of absorbing a greater range of the broad solar spectrum in photovoltaic cells compared with single band gap materials. Several layered transition metal dichalcogenides are potential candidates since they have near ideal top layer band gap energy, high absorption coefficients, long minority carrier lifetimes, and large diffusion lengths [1]. One major problem with heterostructures has been the lattice parameter mismatch leading to misfit dislocations. Such defects act as recombination centres that are detrimental to cell performance. Two dimensional layered materials overcome this difficulty because a weak Van der Waals interaction exists at the interface instead of the usual epitaxial growth, with crystallographic texture an important film structural property.

If the layered compounds are to be useful as solar cells then they must be grown in a highly textured manner with the c-axis perpendicular to the substrate. Much effort has been devoted to such growth [2–4], to date there is no method which does not rely on metal particles [5] or substrates that promote precursor phases [6] to achieve this aim.

In this study, thin films of a model material from this class, molybdenum disulphide, MoS_2, (band gap E_g = 1.8 eV), has been deposited by radio frequency magnetron sputtering and pulsed laser deposition techniques on a gallium arsenide substrate (E_g =1.4 eV). Thin film structures are characterised mainly by angle dispersive x-ray diffraction, scanning electron microscopy, atomic force microscopy, and transmission electron microscopy. These techniques reveal that there exists a region of parameter space where substantial desired bulk texturing of MoS_2 takes place without the need for metal or precursor phases. It was found that higher substrate temperatures, lower power density and higher sputtering gas pressures favoured the desired texture.

[1] A. Aruchamy, (Ed.), *Photoelectrochemistry and photovoltaics of Layered Semiconductors*, (Kluwer Academic Publishers, Dordrecht, 1992).
[2] P.A. Bertrand, *J. Mater. Res.* **4**, 180-4, (1989).
[3] J. Moser and F. Levy, *J. Mater. Res.* **7**, 734-40, (1992).
[4] E. Gourmelon, J.C. Bernede, J. Pouzet and S.Marsillac, *Journal of Applied Physics* **87**, 1182-6, (2000).
[5] J.C. Bernede, J.Pouzet, E. Gourmelon and H. Hadouda, *Synthetic Metals* **99**, 45-52, (1999).
[6] N. Barreau, J.C. Bernede, J. Pouzet, M. Guilloux-Viry and A. Perrin, *Physica Status Solidi A* **187**, 427-37, (2001).

FM6

Nature of the Peierls- to Mott-Insulator Transition in One Dimension

H. Fehske[a], G. Wellein[b], A. Weisse[c], G. Hager[b], A. P. Kampf[d], M. Sekania[d], A. R. Bishop[e]

[a]*Institut für Physik, Ernst-Moritz-Arndt Universität Greifswald, Greifswald, Germany.*

[b]*Regionales Rechenzentrum, Friedrich-Alexander-Universität Erlangen, Erlangen, Germany.*

[c]*School of Physics, The University of New South Wales, Sydney, Australia.*

[d]*Institut für Physik, Universität Augsburg, Augsburg, Germany.*

[e]*Los Alamos National Laboratory, Los Alamos, New Mexico, U.S.A.*

In order to clarify the physics of the crossover from a Peierls insulator to a correlated Mott-Hubbard insulator, we analyze ground-state and spectral properties of the one-dimensional half-filled Holstein-Hubbard model using quasi-exact numerical techniques. In particular the spin and charge excitation gaps are determined by a density-matrix renormalization group finite-size scaling analysis. Moreover we calculate the spin- and charge structure factors, the optical conductivity as well as the photoemission and inverse photoemission spectra and use these quantities to establish the phase diagram of the model. While polaronic features emerge only at strong electron-phonon couplings, pronounced phonon signatures, such as multi-quanta band states, can be found in the Mott insulating regime as well. In the adiabatic limit the Peierls-Mott transition is connected to the band to Mott insulator transition of the ionic Hubbard model. Depending on the strengths of the electron-phonon coupling and the Hubbard interaction this transition is either first order or evolves continuously across an intermediate phase with finite spin, charge, and optical excitation gaps.

H. Fehske, A. P. Kampf, M. Sekania, and G. Wellein, Eur. Phys. Jour. B **31**, 11 (2003).

H. Fehske, G. Weillein, G. Hager, A. Weiße and A. R. Bishop, submitted to Phys. Rev. Lett.

FM7

Minority-Spin Band Gap of Half-Metallic NiMnSb

H.J. Trodahl[a], C.E.A. Grigorescu[b], N. Strickland[c] and A. Bittar[c]

[a] *MacDiarmid Institute for Advanced Materials and Nanotechnology, Victoria University, Wellington, New Zealand.*

[b] *Institute for Research and Development of Optoelectronics, Bucharest, Romania .*

[c] *Industrial Research Ltd., Lower Hutt, New Zealand*

NiMnSb is expected to be a ferromagnetic half metal, an expectation that is based in part on band structure calculations. We report optical conductivity studies of the band structure for a film prepared by pulsed laser deposition onto a Si substrate held at a relatively low temperature required for some device applications, films which are susceptible to site disorder associated with the vacant site in this half-Heusler compound. We demonstrate that the direct interband transitions are essentially unshifted in comparison with bulk material, though they are somewhat broadened. Below the direct-transition absorption edge we report the presence of *indirect* transitions between the Fermi energy (E_f) and the extrema of the minority-spin valence and conduction bands, providing a measure of the band edge energies. Both of these edges appear closer to E_f than is seen in well-ordered bulk NiMnSb, with the conduction band minimum showing weight at only 200 cm^{-1} above E_f, close enough to have substantial occupation at ambient temperature.

FM8

Transport in Layered Materials: Polarons and Angular Magneto-Resistance

Urban Lundin[a] and Ross H. McKenzie[a]

[a] *Department of Physics, University of Queensland, Brisbane Qld 4072, Australia.*

Many of the most interesting strongly correlated materials have a layered crystal structure and highly anisotropic electronic properties. This talk will address two striking properties of this class of materials: The difference in temperature dependence of interlayer and intralayer transport, and the appearance of so called "Magic Angles" (MA) in quasi-one-dimensional organic conductors. We have developed a model, based on coherence of quasi-particles, that is capable of explaining many aspects of the different temperature dependence. The quasi-particles within each layer has two contributions, one from coherent states (dominant at low temperatures) and another from incoherent states (dominant at higher temperatures). The temperature dependence comes from scattering of the quasi-particles on phonons (in a polaron model). At low temperatures the polarons are coherent and occasionally scatters off phonons in the layers, but at higher temperatures bound, incoherent, polarons exist on each site. We extract information about the resistivity, spectral function, optical conductivity, and thermopower, quantities which can be directly measured in experiments [1]. For the quasi-one-dimensional materials we will show how incoherent transport between the conducting chains gives rise to the MA seen in many organic quasi-one-dimensional materials when a magnetic field is applied [2].

1. Urban Lundin, Ross H. McKenzie and V. White, *Phys. Rev. B* **68**, 81101(R) (2003).
2. Urban Lundin and Ross H. McKenzie, (*in manuscript*)

FM9

Density Functional Theory Calculation of Band-gaps in Diamond Nanowires

S.P. Russo, A.S. Barnard and I.K. Snook

Department of Applied Physics, RMIT University,
Melbourne, Australia.

Diamond has been found to possess remarkable electronic and chemical properties, and development of diamond nanowires are now considered feasible [1,2]. In an attempt to predict the electronic properties of diamond nanowires, we have used ab initio (plane wave-DFT) techniques [3] to calculate the T=0^{o}K band-gaps of structurally stable hydrogenated and dehydrogenated diamond nanowires, with cubic, cylindrical and dodecahedral morphology. Our results indicate the nanowire band-gap dependence on structural parameters such as the nanowire diameter, surface morphology and surface hydrogenation.

[1] A.S. Barnard, S.P.Russo, and I.K.Snook , Nano Letters **3** (2003) 1323

[2] A.S. Barnard, S.P.Russo, and I.K.Snook, Physical Review B **68** (2003) 073406

[3] G. Kresse and J. Hafner, Phys. Rev. B **54** (1996) 11 169

Poster Session
Abstracts

Wednesday
4 February

WP1

The Effects of Multiple Scattering on the Analysis of USANS Data

W. K. Bertram

Materials Division, Australian Nuclear Science and Technology Organisation, Menai, NSW 2234, Australia

Small-angle neutron scattering (SANS) and ultra-small-angle neutron scattering (USANS) are widely used to investigate the micro- and nano-structure of condensed matter. However, measurements on materials such as cements, clays etc. are often affected by multiple scattering.

If a substantial number of neutrons experience more than one scattering event within a sample, the result is broadening of the angular distribution profile. Often samples cannot be made thin enough to guarantee single scattering and even in cases where it is possible to make thin samples, surface effects can sometimes lead to results that are not representative of the bulk material. In addition, for many SANS and USANS measurements there is no reliable method for determining whether or not a sample is thin enough to produce predominantly single scattering.

Here we present a new method for extracting singly-scattered data from data affected by multiple scattering. One of the main advantages over our previously published method [1] is that this method is much easier to apply as it requires no initial modeling and fitting of the data.

[1] Sabine T. M. and Bertram W. K., Acta Cryst. A **55** (1999), 500-507

WP2

Crystallization in Polydisperse Colloidal Suspensions

Stephen Martin[a], Gary Bryant[a] and William van Megen[a]

[a] *Department of Applied Physics, RMIT University, Melbourne 3001, Australia.*

Crystallization and glass formation in colloidal hard spheres has been a very active area of research over the last 15-20 years. For most of this time particle polydispersity has been considered to be a minor concern in these studies. However, over the last few years an increasing number of simulations, theoretical work and experiments have shown that consideration of the polydispersity is critical in understanding these phenomena [1-4].

In this paper we provide an overview of recent crystallization studies [5-6] on particles with two very different particle size distributions. These particles exhibit very different equilibrium crystal structures and crystallization kinetics. Based on these measurements and time lapse photographs, we propose a growth mechanism whereby crystallization occurs in conjunction with a local fractionation process near the crystal-fluid interface, which significantly alters the kinetics of crystallite nucleation and growth. This fractionation effect becomes more significant as polydispersity or skewness increases. The unusual crystal structures observed are explained using a schematic model that explains the structure in terms of stacks of planes, which are unregistered due to a high incidence of stacking faults caused by the incorporation of a large number of small particles.

[1] D.A. Kofke and P.G. Bolhuis, *Phys. Rev. E* **59**, 618, 1999.

[2] P. Bartlett, *J. Phys.: Condens. Matter* **12**, A275, 2000.

[3] S. Auer and D. Frenkel, *Nature*, London, **413**, 711, 2001.

[4] S.R. Williams, I.K. Snook, and W. van Megen, *Phys. Rev. E*, **64**, 021506, 2001.

[5] S. Martin, G. Bryant and W. van Megen, *Phys. Rev. E.* **67**, 061405, 2003.

[6] S. Martin, G. Bryant and W. van Megen, *Phys. Rev. Lett.* **90**, 255702, 2003.

WP3

Studies of Magnetic Structure of $La_{1-x}Sr_xMnO_3$ Colossal Magnetoresistive Perovskites

T.R. Finlayson [a], X. Wu[a], T. Ersez [b] and J.C. Schulz[c]

[a] *School of Physics and Materials Engineering, Monash University, Victoria 3800, Australia.*

[b] *Nuclear Technology, ANSTO, Lucas Heights, NSW 2234, Australia.*

[c] *Bragg Institute, ANSTO, Lucas Heights, NSW 2234, Australia.*

This class of materials, based on the compound $LaMnO_3$, continues to be the focus of attention because they exhibit colossal magnetoresistance (CMR) [1] which could lead to possible applications in magnetic recording and field sensors. In addition to the technological applications, the materials are important from a fundamental point of view due to the strong correlations between transport, structural and magnetic behaviour. The origin of the CMR effect has been attributed to the presence of magnetic polarons above the ferromagnetic ordering temperature, T_c.

From recent research, using a combination of powder neutron diffraction, polarisation analysis and small-angle neutron scattering together with magnetic measurements, we present diffuse scattering, spin dynamics and lattice and magnetic correlations results for the $La_{1-x}Sr_xMnO_3$ (x=0.125 and 0.175) compounds. The diffuse scattering in the neutron diffraction patterns increases as the temperature approaches T_c from low temperature and continues to increase above T_c. The scattering peak in the forward direction above T_c ($T_c<T<1.6T_c$) showed a Lorentzian-type *q* dependence. In the $La_{0.875}Sr_{0.125}MnO_3$ sample the forward scattering peak has neutron spin-flip and non-spin-flip components indicating the presence of both lattice and magnetic type polarons above T_c.

1 A.P. Ramirez, *J. Phys.: Condens. Matter* **9**, 8171 (1997).

WP4

TAIPAN – A Spectrometer for Inelastic Neutron Scattering at the Replacement Research Reactor

M.E. Hagen[a], G. Horton[a], R. Moore[a], G. Braoudakis[a] and L.D. Cussen[a]

[a] Bragg Institute, ANSTO, PMB 1, Menai, New South Wales 2234, Australia.

Inelastic neutron scattering is widely used to study the lattice vibrational (phonon) and magnetic (spin wave and crystal field) excitations in condensed matter. In order to characterise such excitations comprehensively measurements on single crystal specimens are required and the most appropriate instrument for doing this at a steady state (reactor) neutron source is a three-axis spectrometer (TAS). We will describe the characteristics of the three-axis spectrometer TAIPAN, which is currently under construction at the replacement research reactor, ANSTO and which will be available to the Australian scientific community in 2006.

WP5

High Intensity and High Resolution Neutron Powder Diffraction at the Replacement Research Reactor

M.E. Hagen[a], B.A. Hunter[a] and T.J. Noakes[a]

[a] Bragg Institute, ANSTO, PMB 1, Menai, New South Wales 2234, Australia.

Neutron powder diffraction is an established technique for studying the structures of crystalline materials. In any diffraction experiment the two most basic quantities which characterise the quality of the measured spectra are resolution and intensity. High-resolution measurements are used to determine precise and intricate details of the crystal structure, while high intensity measurements are used to characterise changes driven in real time by in-situ measurements. In both cases recent developments in the instrumentation have focussed on the use of position sensitive and area detectors to increase the effective count rate in high resolution and high intensity measurements respectively. We will describe the characteristics of the High Intensity Powder Diffractometer (Wombat) and the High Resolution Powder Diffractometer (Echidna), which are currently under construction at the replacement research reactor, ANSTO and which will be available to the Australian scientific community in 2006.

WP6

A Polarised Neutron Study of Crystal Field Transitions in $CeCu_6$

S J Harker[a], T J Hicks[a], D J Goossens[b],
A M Mulders[c], Y Feid, D Yu[d] and S J Kennedy[d]

[a]*School of Physics and Materials Engineering, PO Box 27, Monash University Vic 3800, Australia*
[b]*Research School of Chemistry, Australian National University, ACT 0200, Australia*

[c]*Department of Physics, Uppsala University, Box 530, S-75121 Uppsala, Sweden*

[d]*Bragg Institute, Australian Nuclear Science and Technology Organisation, Menai NSW 2234, Australia*

$CeCu_6$ is a heavy Fermion compound in which the Ce magnetic moment is suppressed by the Kondo effect resulting from the admixture of the local 4*f* electrons with the conduction electrons. Crystal field transitions between the low-lying states of the Ce ion have been observed using inelastic neutron scattering [1–3]. The transitions were contaminated by phonon scattering which can be corrected using a complex scaling function using a complementary spectrum of $LaCu_6$. Neutron time of flight spectroscopy with neutron polarisation analysis permits the *in situ* separation of magnetic and lattice vibrational energy spectra. Preliminary experiments on LONGPOL allow an indicative separation of a broadened crystal field transition and features due to lattice vibrations [4]. The preliminary analysis indicated an inelastic spin-flip feature at -12 meV which is due to the crystal field while an inelastic non-spin-flip feature at -6 meV is predominantly due to phonon scattering. A more complete polarisation analysis study has been performed using a magnetic coil to switch the polarisation at the sample position between perpendicular and parallel to the scattering vector. These results and their interpretation are reported here.

[1] U. Walter, D. Wohlleben and Z. Fisk, *Z. Phys. B* **62**, 325 (1986).

[2] B. Stroka, A. Schroder, T. Trappmann, H. v. Lohneysen, M. Loewenhaupt and A. Severing, *Z. Phys. B* **90**, 155 (1993).

[3] E. A. Goremychkin and R. Osborn, *Phys. Rev. B* **47**, 14580 (1993).

[4] T. J. Hicks, D. J. Goossens, S. J. Harker, A. M. Mulders and S. J. Kennedy, *Physica B*, Proceedings of the Polarised Neutrons and Synchrotrons X-rays for Magnetism (2003), accepted.

WP7

Effects of Solutes on Membrane Phase Transitions

Thomas Lenné[a] and Gary Bryant[a]

[a] *Department of Applied Physics, RMIT University, Melbourne 3001, Australia.*

Severe dehydration is lethal for most biological species. However, there are a number of organisms or organelles which have evolved mechanisms to avoid damage during dehydration. One of these mechanisms is the accumulation of small solutes (such as sugars), which has been shown to preserve membranes by inhibiting deleterious phase changes at low hydration [1].

The aim of this project is to use small angle x-ray scattering (SAXS) to investigate the effects of small solutes on the phase behaviour and packing parameters of multilamellar membranes as a function of hydration. In the experiment a synthetic phospholipid 1,2-dipalmitoyl-*sn*-glycero-3-phosphatidylcholine (DPPC) will be used as a model system, as it is the most well characterized phospholipid. Hence the repeat spacings (distance between consecutive bilayers ~50Å) and the intra-lipid spacing (distance between a lipid and its neighbor ~5Å) are well documented.

An appropriate solute, and solute concentration range will be chosen, and its effect on the freezing temperature of DPPC will be observed. Experiments will be conducted at a number of hydrations to accurately model the phase behavior for DPPC over the entire range of hydrations and solute concentrations. Although SAXS has been performed extensively on synthetic phospholipids [2], experiments with solutes over a range of hydrations, particularly low hydrations, have not yet been attempted.

In this poster we will outline the background to the project, and discuss the applications of this research.

[1] J. Wolfe and G. Bryant, *Cryobiology* **39,** 103-129 (1999).

[2] B. Demé, M. Dubois and T. Zemb, *Biophysical Journal* **82,** 215-225 (2002).

WP8

Dynamics Associated with Domain Walls

R. L. Stamps[a], P. Falloon[a], R. Jalabert[b], D. Weinmann[b], A. Mougin[c]

[a] *School of Physics, University of Western Australia, Australia.*

[b] *IPCMS-CNRS and University of Louis Pasteur, Strasbourg, France.*

[c] *LPS-CNRS, Orsay, France.*

Recent experimental and theoretical results from our groups are highlighted that illustrate some of the interesting phenomena associated with magnetic domain boundary walls. Two problems will be discussed: dynamics associated with domain wall propagation, and effects related to spin transport through domain walls. For the first problem, an example of wall interaction and motion through a random potential will be discussed with reference to the general problem of roughening transitions. Images of domain dynamics in thin films of ion irradiated Co reveal a possible de-roughening transition associated with long range magnetostatic interactions between pairs of domain walls. A scaling theory of this transition is described in which a curious type of dynamic hysteresis can occur. For the second problem, results from calculations of ballistic charge and spin transport through domain boundary walls will be presented in which we show how channel blocking controls magnetoresistance in nanowires. An effective circuit model is proposed, and the problem of coherent elastic scattering is discussed. Finally, a new mechanism for non-local dissipation in conducting magnets is described which has important consequences on domain wall propagation and non-uniform switching in magnetic nanostructures.

WP9

Electron Transport in Disordered Films of Metal Nanoparticles Linked by Organic Molecules

K.-H. Müller, G. Wei, J. Herrmann, B. Raguse and G. Baxter

CSIRO Telecommunications and Industrial Physics, Sydney 2070, Australia.

We have investigated theoretically and experimentally the mechanism of electron transport in films made of ~10 nm sized gold nanoparticles linked by alkanedithiol molecules. Conduction in these films is due to linker-molecule assisted single-electron tunnelling between neighbouring nanoparticles where electrons have to overcome the Coulomb blockade energy. Strong disorder in our films in the form of separation gap fluctuations between adjacent nanoparticles and variations in Coulomb blockade energies cause electron current percolation. We have found that the dependence of the conduction on the length of the alkanedithiol molecules is affected by the degree of disorder. In addition, we have observed that percolation leads to a non-Arrhenius-like temperature dependence of the conduction and to a film-thickness dependent conductivity. I-V characteristics at low temperatures reveal Coulomb blockade effects. The strong dependence of the electrical conduction on the separation gaps between adjacent nanoparticles can be utilized in strain gauge and gas sensor applications.

1. K.-H. Müller, J. Herrmann, B. Raguse, G. Baxter and T. Reda, *Phys. Rev. B* **66**, 075417 (2002).
2. K.-H. Müller, G. Wei, B. Raguse, G. Baxter and J. Myers, *Phys. Rev. B* **68**, 155407 (2003).

WP10

Finite Hydrogenated Silicon Nanotubes and Toroids

O. Ponomarenko, M. W. Radny, P. V. Smith

School of Mathematical and Physical Sciences, The University of Newcastle, Australia 2308

Recent reports of the preparation of silicon nanotubes (SiNTs) using porous alumina templates by molecular beam epitaxy [1] or chemical vapor deposition process [2] still have to be more rigorously supported. Nevertheless, it has been shown using the DFT-TB method that certain classes of silicon-based nanotubular structures (such as SiH nanotubes) are stable and energetically viable [3]. Using the extended empirical Brenner potential [4], we have conducted a systematic study [5] of the influence of different types of hydrogenation on the energetics and stability of Si-based finite, open-ended, nanotubes considered as silicon clusters.

In this paper we present the results of MD simulations of finite open-ended silicon nanotubes with hydrogen chemisorbed on the outer surface (SiH-sf). We have found that the frustration energy of the dangling bonds has a profound effect on the geometry of such tubes, leading to the appearance of new, topologically different structures –hydrogenated silicon tori. We have also found a new way of forming small diameter and narrow (in tubular cross-section) tori by rolling the open edges of the short open-ended nanotubes inside the generating tube and forming bonds on the equator of the resulting torus. The resulting reduction in the chemical (frustration) energy leads to stability of the final toroidal structures. We also present the atomic structure, and discuss the relationships between the helicity and radius of the generic nanotube, and stability of the resulting SiH-sf nano-toroids.

1. S. Y. Jeong *et al*, *Advanced Materials* **15**, 1172 (2003).
2. J. Sha *et al*, *Advanced Materials* **14***,* 1219 (2003)
3. G. Seifert et al, Physical Review B **63**, art –No 193409 (2001)
4. A. J. Dyson and P. V. Smith, Molecular Physics **96** 1491 (1999)
5. O. Ponomarenko, M. W. Radny, P. V. Smith (to be published)

WP11

Carbon-based Toroidal Nanostructures

O. Ponomarenko, M. W. Radny and P. V. Smith

School of Mathematical and Physical Sciences, The University of Newcastle, Australia 2308

Rings of bundles of single-walled carbon nanotubes (SWCNTs) formed in the products of the laser vaporisation method have been shown to be true toroidal structures [1]. Toroidal carbon nanostructures were predicted to possess exciting electronic and magnetic properties [2]. While the diameter of the circular ropes was always larger than 300 nm [1], some calculations demonstrate a considerable stability of small defect-free tori [3]. From the elastic model [4], the thinner a generic tube is, the smaller can be the outer diameter of the corresponding torus. Chemical modification (functionalization) of toroidal shells could lead to stabilization of small toroidal structures by changing the strain effects on the shell. Our calculations using the Brenner potential show that in some cases the most stable form of finite silicon nanotubes with hydrogen atoms chemisorbed on the outer surface (SiH-sf) is a toroid [5]. In this paper we explore the energetics and stability of clean and hydrogenated carbon toroidal structures using the extended Brenner potential. We propose a new way of forming small hydrogenated tori which involves eliminating the excess chemical energy by rolling the edges of the open ends of short wide nanotubes inside the tube and bonding the opposite edges on the equator of the formed torus. The resulting small, narrow "clean" and hydrogenated carbon tori (CH-sf tori) appear to be stable. The calculations also show that the total energy of "clean" carbon toroidal structures is comparable with the total energy of the corresponding "clean" carbon finite, open-ended, single-walled nanotubes.

1 J. Lui *et al*, Nature **385**, 780 (1997).

2 A. Latge *et al*, Physical Review B **67**, art. no. –155413 (2003)

3 M. Huhtala, A. Kuronen and K. Kaski, Computer Physics Communications **147**, 91 (2002)

4 V. Meunier, P. Lambin and A. A. Lucas, Physical Review B **57**, 14886 (1998)

5 O. Ponomarenko, M. W. Radny and P. V. Smith (to be published)

WP12

Nanocrystalline Diamond Grown by Chemical Vapour Deposition using He and Ar Diluted H_2/CH_4 Gas Mixtures

J.R. Rabeau[a,*], P. John[a] and J.I.B. Wilson[a]

[a] *School of Engineering and Physical Sciences, Heriot-Watt University, Edinburgh, Scotland*

In order to fully exploit the potential of nanocrystalline diamond (NCD) in tribology, MEMS and field emission applications, a greater understanding of the growth process is essential. This can be accomplished by spectral interrogation of the reaction environment and characterisation of the resulting deposited material.

We have grown NCD in a coaxial blade microwave CVD reactor using either argon or helium diluted H_2/CH_4 gas mixtures. Under these conditions, similar material was deposited as characterised by AFM, SEM and Raman spectroscopy. The Raman spectra verified the presence of sp^3 bonded carbon, indicating diamond. NCD is further characterised by sub-50 nm grain size, and the average grain size in this material was measured to be ~50 nm.

Cavity ring-down spectroscopy (CRDS) and optical emission spectroscopy (OES) were used to measure the number density of species in the gas phase. The carbon dimer, C_2, is often identified as the species responsible for the formation of NCD [1]. However, CRDS and OES measurements performed simultaneously with NCD growth demonstrated that NCD forms in both C_2 rich and C_2 depleted environments. With Ar addition to the gas mixture, C_2 was present in abundance (4×10^{12} molecules cm^{-3}) whereas with He addition, C_2 was below the detection threshold of the CRD spectrometer. This evidence suggests that C_2 is not the growth species for NCD.

The smooth morphology of the Ar grown films versus rough He grown films may indicate a link with the heavier Ar-ions as compared to lighter He-ions. Surface roughness measurements revealed consistently smooth Ar grown NCD (~30 nm RMS) and a gradually decreasing surface roughness for He grown NCD (600 to 60 nm RMS).

[1] D. Zhou, T.G. McCauley, L.C. Qin, A.R. Krauss and D.M. Gruen, *J. Appl. Phys.* **64**, 1502 (1994).

*corresponding author present address: *Micro Analytical Research Center, School of Physics, University of Melbourne, Melbourne, Australia,* jrabeau@physics.unimelb.edu.au

WP13

Nucleation and Optical Properties of Gold Nano-Hemispheres on Plate Glass

X. Xu, M.B. Cortie and M. Stevens

Institute for Nanoscale Technology, University of Technology Sydney,
PO Box 123, Broadway NSW 2007, Australia

Semi-transparent gold films on plate glass have applications in the architectural industry, especially in hot climates. Such films can block most of the solar heat in the near-infrared region while retaining a degree of transparency. However, current methods of applying such coatings, such as sputtering, are expensive, due primarily to the need to amortize the cost of the very expensive vacuum equipment required. In the present research, the properties of gold nano-films applied by an economic process of wet chemical deposition was studied.

It is found that gold nano-films with a neutral grey-blue colour can be deposited When deposited at pH 8.0, there is initially a plasmon resonance peak at 520 nm from isolated particles. However, the peak is later swamped by the development of the resonance due to particle-particle interactions, which manifests as a broad absorption peak around 700 nm. In all cases the 700 nm peak could be broadened and red-shifted by increasing deposition time. It is also found there is a quite a big difference for the T_{Vis}/T_{IR} between the gold nano-films deposited by wet chemical deposition and by sputtering [1]. The gold nano-film deposited by the wet chemical process was less spectrally selective between visible and IR wavelengths than that produced by sputtering. Further study found that pre-treatment of the glass and nature of the nucleation process of the gold nanoparticles both greatly influence the morphology of the coatings, which affects their optical properties significantly [2]. It is found the glass pretreated with sulfuric acid tended to form a gold nano-coating with dual peaks at around 540 nm and 700 nm, while the surface pretreated with buffered HF tended to form a gold nano-coatings with a single broad peak at around the 700 nm. The trend may be explained and simulated by classic heterogeneous nucleation theory.

1 S. Chaudhuri, D. Bhattacharyya et al Materials Science Forum, **246**, (1997), 181-206

2 H. K. Jang, Y. D. Chung, J. Vac. Sci. Technol. A **18**, (2000), 401-404

WP14

Electrochemical Capacitors Based on Self-Assembled Gold Nanoparticle Films Cross-Linked with Thiols

Burkhard Raguse, Wenrong Yang , G. Stockton

CSIRO Telecommunications and Industrial Physics, Lindfield, NSW 2070, Australia

A new type of nanocomposite electrode fabricated from gold nanoparticle films were examined as novel electrochemical capacitors. The gold nanoparticle film electrodes were characterized by cyclic voltammetry and electrochemical impedance spectroscopy. The electrochemical studies were performed by connecting each of the two films in a standard two-electrode measurement in 1M NaCl solution. The nanoparticle films were found to be highly porous with a relatively large ion-accessible surface area and a gravimetric capacitance of approximately 2.6 to 3.2 F/g.

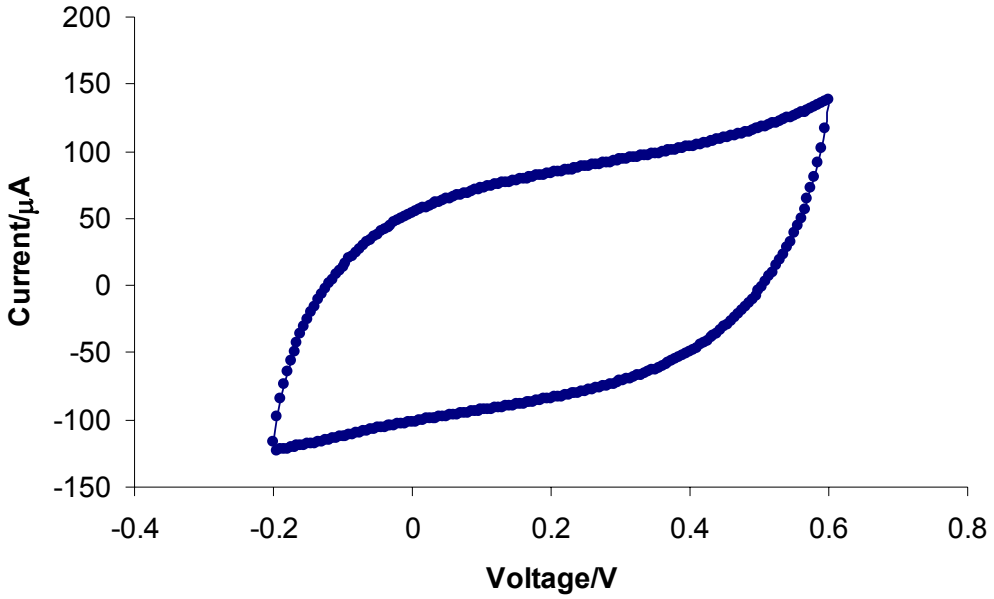

Cyclic voltammograms of a capacitor consisting of two gold nanoparticle film electrodes in 1M NaCl electrolyte solution. (Films were made from 16 nm Au nanoparticles functionalised with cystamine hydrochloride as crosslinker. Film thickness was approximately 210 nm. Scan rate: 200mV/s.

Reference

1. B. Raguse, J. Herrmann, G. Stevens, J. Myers, G. Baxter, K-H. Müller, T. Reda, A. Molodyk, V.Braach-Maksvytis (2002) "Hybrid Nanoparticle Film Material" *J. Nanoparticle Res.*, **4**, 137-143.

WP15

Synthesis and Characterization of RF Magnetron Sputtered Carbon Nanostructures

D.M. Zhu, S. Goh, G. Jakovidis and L. Bourgeois

School of Physics and Materials Engineering, Monash University, Victoria 3800, Australia.

Carbon nanostructures are an intriguing field for fundamental and practical research due to their low dimensionality and their interesting chemical, mechanical and electrical properties. To date, various methods have been used to synthesize carbon nanotubes and related structures, such as arc discharge, laser ablation, ion beam radiation and chemical vapour deposition. However, there are have been only few reports on their synthesis using sputtering, which has a great advantage in obtaining an excellent film uniformity over a large area.

A new method for graphitic nanostructure growth by thermal annealing of precursor carbon thin film deposited by magnetron sputtering is reported here. This is a two-step method, involving magnetron sputtering of carbon at ≤ 450 ^{o}C followed by an annealing step at an elevated temperature. The films were first deposited on Mo substrates, with a 99.999% pure graphite target operated at an RF power of 200 W and a discharge argon gas pressure of 4.2 Pa (~ 30 milli-Torr). In order to activate nanostructure growth, the as-deposited films were then annealed in situ by heating the substrates over the range 800 – 950 ^{o}C under argon gas pressures of 26.6 – 101 kPa (~200 –760 Torr). The morphology and microstructure of the as-deposited and post-annealed films were investigated by high resolution transmission electron microscopy (HRTEM), and energy dispersive X-ray spectroscopy (EDXS). A precursor film which possesses regions of a disordered, turbostratic and defective graphitic structure was obtained when the substrate temperature during deposition is ≤ 450 ^{o}C. It was found that the higher thermal annealing temperature quoted above is essential for the transformation from the precursors to well-graphitised polyhedral nanoparticles, including some carbon nanotubes, as evident in the HRTEM images. EDXS has confirmed that these polyhedral nanoparticles are high-purity carbon. Therefore, this study suggests a straightforward, convenient and cost-effective method to grow high-purity and high-quality carbon nanostructures.

WP16

Muon Spin Relaxation in Spin-Peierls Phase of NaV_2O_5

M. Aïn[a,b], J. Lord[c], J. Jegoudez[d] and A. Revcolevschi[d]

[a] *Bragg Institute, ANSTO PMB1 Menai NSW 2234. Australia.*

[b] *Laboratoire Léon Brillouin (CEA-CNRS) CE-Saclay. 91191 Gif/Yvette Cédex France.*

[c] *ISIS Facility, Rutherford Appleton Laboratory, Chilton Didcot, Oxfordshire OX11 0QX UK.*

[d] *Laboratoire de Chimie des Solides (Bat 414)-UMR 8648 Universite de Paris-Sud. 91405 Orsay Cedex FRANCE.*

Ground states of one-dimensional antiferromagnets are topical subjects in regard of their quantum mechanical nature. Spin-Peierls (sP) systems and even-legged ladders systems, have a fundamental non magnetic state which is a singlet. It is separated by a gap, from the triplet magnetic excitations. The sP transition occurs at low temperature (T_{sP}), in several quasi-one-dimensional antiferromagnetic compounds which do not undergo a transition to long range magnetic order. Coupling with phonons leads to a crystalline distortion and the chain dimerises. $CuGeO_3$ (T_{sP} = 14.2 K) [1] is the first inorganic sP compound to have been discovered, NaV_2O_5 which is the subject of the present study, does not appear to be a conventional sP system. The sP transition is accompanied here, by charge ordering, in the sense that above T_{sP}, one electron is orbiting around a V^{4+} - O^{2-} - V^{4+} group, then settling on one specific vanadium ion below T_{sP}.

Depolarisation of muons have been carried out on NaV_2O_5, between 6 and 150 K, through the transition at T_{sP} = 33 K. Surprisingly the transition is well fitted throughout to a stretched exponential, $\exp-[\lambda(T).t]^{\beta(T)}$. While λ rises dramatically below T_{sP}, the exponent β is greater than 1 above T_{sP} but falls to below 1/3 at 6 K as is the case in frustrated systems?

1. Aïn *et al,* PRL **78** 1560 (1997).

WP17

Magnetic Properties of $Dy_{1-x}Sr_xCoO_{3-\delta}$ (x = 0.67 to 0.95)

D.J. Goossens[a], K.F. Wilson[b,c] and M. James[d]

[a] *Research School of Chemistry, Australian National University, Canberra Australia.*

[b] *Department of Physics, Australian National University, Canberra Australia.*

[c] *School of Physics, University of New South Wales, Sydney, Australia.*

[d] *Bragg Institute, Australian Nuclear Science and technology Organisation, Sydney, Australia*

The AC magnetic susceptibility of $Dy_{1-x}Sr_xCoO_{3-\delta}$ has been measured from 17 to 320 K for a range of samples, x = 0.67 to 0.95. These results have shown that for x = 0.95 the systems enters a spinglass state at approximately 131K on cooling. This is demonstrated by a large cusp in the imaginary susceptibility, indicating the onset of time-dependent effects. For smaller x, the system enters a magnetically ordered state at approximately 300K. This state shows evidence for a spin state transition in the Co ions at around 120K [1], but no evidence of a spin-glass phase.

Structurally, the system is tetragonal, I4/mmm, becoming closer to cubic as x increases, until at x = 0.95 the system is metrically cubic. Further, as x increases the fraction of Co^{4+} in the system also increases, as shown by TGA. At x = 0.95 over 50% of the Co sites are 4+, and the mixture of exchange interactions resulting is thought to give rise to the spinglass state. At smaller x the system appears weakly ferromagnetic, probably due to local ferromagnetic clusters [2], with the Dy moments remaining paramagnetic to temperatures below the instrumental limit.

1. C. Zobel, M. Kriener, D. Bruns, J. Baier, M. Grüninger and T. Lorenz, *Phys. Rev. B* **66**, 020402(R) (2002)
2. J. Wu and C. Leighton, *Phys. Rev. B* **67**, 174408 (2003)

WP18

Magnetic Structures and Valence States of $YbMn_2Si_xGe_{2-x}$

D. Grimm[a], M. Hofmann[b], S. J. Campbell[a], A. V. J. Edge[a] and A. Studer[c]

[a]*School of Physical, Environmental and Mathematical Sciences, The University of New South Wales, ADFA, Canberra*

[b]*FRM-II, Technische Universität München, Germany*

[c]*Bragg Institute, Australian Nuclear Science and Technology Organisation, Sydney*

Rare-earth intermetallic compounds containing ytterbium exhibit a wide range of interesting and unusual physical and magnetic properties. This occurs mainly as a result of their mixed valence states (II/III) or changes from one valence state to the other.

Here we present a set of results for the $YbMn_2Si_xGe_{2-x}$ series (8 samples from x = 0 to 2), focusing on the magnetic structure and valence state of these compounds as investigated by neutron powder diffraction (2-530 K). We have found that the valence state of the Yb ion changes from the trivalent state of $YbMn_2Si_2$ to a divalent-like behaviour for $YbMn_2Ge_2$ with increasing Ge concentration x, with significant changes in the magnetic structure taking place around $1.5<x<1.9$ [1]. An overview of the structural and magnetic changes that occur around this critical concentration region will be presented. Emphasis will be placed on current research that focuses on the compound $YbMn_2Si_{0.3}Ge_{1.7}$ in an attempt to characterise the transition.

[1] M. Hofmann, S. J. Campbell and A. V. J. Edge, J Magn Magn Mater (Proc ICM2003, in press, 2004)

WP19

Soft Magnetic Properties of Nanocrystalline $Fe_{89-x}Zr_7B_3Cu_1Co_x$ (x = 0 to 70) Alloys

N. Ito

School of Physics and Materials Engineering, Monash University, Victoria 3800, Australia.

Nanocrystalline Fe-Zr-B alloys prepared by crystallization of amorphous precursors exhibit excellent magnetic softness as well as high saturation magnetization (B_s). It has been widely known that the magnetic moments of Fe-rich Fe-Co alloys exceed the values of pure-Fe or –Co [1] and hence, the addition of Co to Fe-based magnetic alloys has been a standard approach for enhancing B_s in Fe-based alloys. In this work we have investigated the technical magnetization behaviors of nanocrystalline $Fe_{89-x}Zr_7B_3Cu_1Co_x$ (x = 0 to 70) alloys in order to clarify the effect of Co on the soft magnetic properties of nanocrystalline Fe-Zr-B alloys.

Rapidly-solidified ribbons of $Fe_{89-x}Zr_7B_3Cu_1Co_x$ (x = 0, 5, 10, 20, 30, 50 and 70) were produced by the single roller method. The ribbon samples were annealed at 898 K for 600 s or at 873 K for 3.6 ks. The coercivity (H_c) of the samples was measured with a DC B-H tracer.

The coercivity of nanocrystalline $Fe_{89-x}Zr_7B_3Cu_1Co_x$ (x = 0 to 70) showed a tendency to increase with the amount of Co, indicating that the magnetic anisotropy is enhanced by Co. Since the annealing temperatures of this study are below the Curie temperature of the nanocrystallites, the annealing-induced anisotropy due to Fe-Co atomic pair ordering is likely to be the mechanism of this Co-induced magnetic hardening effect in the Fe-Zr-B-Co alloys.

1. S. Chikazumi, *Physics of Magnetism* (John Wiley & Sons, Inc, 1964) p 73.

WP20

The Magnetic Properties of $GdNiAl_4$

G.A. Stewart[a], W.D. Hutchison[a], A.V.J. Edge[a], K. Rupprecht[b], G. Wortmann[b], K. Nishimura[c] and Y. Ishikawa[d]

[a] *School of Physical, Environmental and Mathematical Sciences, The University of New South Wales at ADFA, Canberra, ACT 2600, Australia.*

[b] *Department of Physics, Faculty of Science, University of Paderborn, 4790 PaderbornGermany.*

[c] *Faculty of Engineering, Toyama University, Toyama 930-8555, Japan.*

[d] *Department of Physics, Toyama University, Toyama 930-8555, Japan.*

Several members (R = $Nd_{1-x}Pr_x$, Tb) of the orthorhombic $RNiAl_4$ series of intermetallic compounds have been observed to exhibit intriguing magnetic behaviour. The compounds order antiferromagnetically. However, there are typically two magnetic transition temperatures and there is evidence for metamagnetic behaviour. The nature of the intermediate phases is unknown, and it is uncertain as to how universal this behaviour is across the series. Furthermore, the magnetic anisotropy varies from one compound to another. We report here ^{155}Gd Mössbauer spectroscopy, d.c. magnetisation, a.c. susceptibility, electrical resistivity, and specific heat results for a polycrystalline specimen of $GdNiAl_4$. The data are consistent with low temperature antiferromagnetism and, again, there are two distinct transition temperatures (in this case at 25 K and 21 K). The specific heat and paramagnetic susceptibility measurements confirm that the rare earth sub-lattice is the sole contributor to the compound's magnetisation. Given that Gd^{3+} is an S-state ion, the 85 keV ^{155}Gd Mössbauer resonance probes the alignment of the magnetic hyperfine field with the principal axes of the lattice electric field gradient. When combined with simple point charge model calculations, these data imply that the bulk magnetisation is directed along either the crystallographic b- or c-axis.

WP21

Magnetic and Crystal Field Properties of Thulium Calcium Manganite

G.A. Stewart[a], A.V.J. Edge[a] A. Studer[b], M. Elcombe[b], J. Horvat[c] and R. Lewis[c]

[a] *School of Physical, Environmental and Mathematical Sciences, The University of New South Wales at ADFA, Canberra, ACT 2600, Australia.*

[b] *Bragg Institute, ANSTO, Lucas Heights, NSW 2234, Australia.*

[c] *School of Engineering Physics, University of Wollongong, NSW 2522, Australia*

For sufficiently large average Ln/A radii, the hole-doped manganites $Ln_{2/3}A_{1/3}MnO_3$ (Ln = lanthanide, A = divalent metal) exhibit "colossal" magneto-resistance (CMR), which is associated with a transition from paramagnetic insulator to a low temperature ferromagnetic metal phase. However, with decreasing radius, the transition temperature is lowered and the ordered phase eventually reverts to that of a magnetic insulator. In this work, ^{169}Tm Mössbauer spectroscopy has been used to investigate $Tm_{2/3}Ca_{1/3}MnO_3$, which falls into the latter category. From the temperature of the onset of line broadening, the magnetic ordering temperature is determined as $T_{order} \approx 40$ K (compared with ≈ 32 K from a.c. and d.c. susceptibility). The local Tm^{3+} magnetisation is almost certainly that of an isolated pseudo-doublet ground state driven by a weak (compared with the crystal field) Mn-Tm exchange interaction. To a good approximation, the low temperature ^{169}Tm spectrum is the superposition of a relaxation-broadened sextet and a paramagnetic doublet. This is consistent with regions of large slowly fluctuating magnetic clusters and regions of smaller rapidly fluctuating clusters, as has been observed for the generic CMR manganite, $La_{2/3}Ca_{1/3}MnO_3$.

However, recent neutron diffraction measurements performed on the Bragg Institute's HRPD facility are insensitive to this weak magnetism, suggesting a complex (perhaps spin-glass in nature) Mn sub-lattice magnetisation. The refinement of the position parameters for the near-neighbour oxygen atoms has assisted with the interpretation of the temperature-dependent ^{169}Tm quadrupole interaction data in terms of a crystal field scheme for the Tm^{3+} ion. The appropriateness of this scheme will be considered in terms of the above observations.

This work was supported by separate grants for source irradiation and neutron diffraction from the Australian Institute of Nuclear Science and Engineering.

WP22

Structural and Magnetic Properties of $DyFe_{12-x}Nb_x$ Compounds

J.L. Wang, S.J. Campbell, S. James, A.V.J. Edge and D. Grimm

School of Physical, Environmental and Mathematical Sciences,
The University of New South Wales at ADFA, Canberra ACT 2600 Australia

We have investigated spin reorientation effects in $DyFe_{12-x}Nb_x$ compounds with x=0.6, 0.7 and 0.8 over the temperature range 4.2-300 K using standard ac magnetic susceptibility techniques. AC magnetic susceptibility measurements are a basic and effective experimental technique in studying the magnetic properties of materials, particularly magnetic transitions. The temperature dependence of the ac susceptibility was measured using a standard helium cryostat and a computer controlled Lakeshore Cryogenics temperature controller. $DyFe_{12-x}Nb_x$ compounds crystallize in the tetragonal $ThMn_{12}$-type structure and exhibit ferrimagnetic ordering [1]. With decreasing temperature the magnetic moment has been found to tilt from the easy c-axis to an easy cone configuration at T_{sr2}, with further decrease in temperature producing a reorientation of spins to the easy plane at T_{sr1} [2]. With increasing Nb content both T_{sr1} and T_{sr2} decrease monotonically (T_{sr1} from 155 K for x=0.6 to 94 K for x=0.8 and T_{sr2} from 244 K for x=0.6 to 204 K for x=0.8) while the ordering temperature is found to be almost independent of the Nb content (T_C~518 K). The total anisotropy in rare earth (R) transition metal (T) compounds is determined by the interaction between the anisotropy of the R- and T-sublattices. In these $DyFe_{12-x}Nb_x$ compounds, the spin reorientation occurs because the iron sublattices favour a uniaxial magnetic anisotropy parallel to the c-axis, whereas, because of the negative second-order Stevens coefficient for Dy, the Dy sublattice favours a basal anisotropy. From refinements of x-ray diffraction patterns it is concluded that the lattice parameters increase slightly with increasing Nb content (for x=0.7 a= 0.8505 nm, c= 0.4789 nm and V= 0. 3465 nm^3) and that the Nb atoms preferentially occupy the 8i sites. In order to further study the individual site anisotropy from the three inequivalent crystallographic 8f, 8i and 8j sites, Mössbauer spectra at various temperatures are currently being measured and analyzed.

[1] B.P. Hu, K.Y. Wang, Y.Z. Wang et al. Phys. Rev. B **51**, 2905 (1995).

[2] K.Y. Wang, Y.Z. Wang, B.P. Hu and W.Y. Lai, IEEE Trans Magn **30**, 4963 (1994).

WP23

Exchange Bias in a Model System

R. L. Stamps[a], W. Pang[a], Z. Celinski[b]

[a] *School of Physics, University of Western Australia, Australia.*

[b] *Department of Physics, University of Colorado at Colorado Springs, USA.*

Good lattice match between Fe, Ni and Co ferromagnetic films and potassium (Fe,Ni,Co) flouride antiferromagnetic films make this an excellent model system for studies of exchange bias . The interfaces are expected to be fully compensated for this particular growth orientation, and the good lattice match between the ferromagnetic and antiferromagnetic layers preserve the cubic structure of both. Exchange bias shifts are observed with enhanced coercivities at temperatures well below the Neel temperature. Features associated with training are exhibited and clear evidence of thermally-activated processes for single crystal films were obtained in a thermal pulse experiment. The existence of training and its correlation with thermal activation processes suggest that exchange bias in this mainly compensated system is controlled by magnetization processes in the antiferromagnet. Spin-flop coupling is very likely in this system, and it is suggested that pinning of antiferromagnet spins near the interface is responsible for the exchange bias shifts. A rotatable anisotropy is observed in some systems using FMR. A mechanism and model for the rotatable anisotropy is presented.

This project is a systematic examination of an excellent model system for studies of exchange bias and coercive field formation in well characterized, near ideal single crystal structures. Magnetic characterization includes SQUID magnetometry and low temperature ferromagnetic resonance. Correlations between these two techniques for observed training effects and rotatable anisotropies have provided a reasonably clear picture of many of the essential processes governing bias shifts and enhanced coercivities in these compensated interface systems.

WP24

Analysis of an Ideal Amorphous Solid

L. Th. To[a], and Z. H. Stachurski[b]

[a] *School of Electrical Engineering, ADFA, Canberra, Australia.*

[b] *Department of Engineering, ANU, Canberra, Australia.*

In geometrical terms, amorphous solids are fundamentally different from crystalline solids in that they can not be constructed by the crystallographic method of translation of the basis along a lattice. Therefore, to study amorphous structures we must invoke concepts and use measures different to those used for ordered structures. Nevertheless, an ideal amorphous solid must share together with the ideal crystalline solid in the same definition of the term "ideal". In both cases it must be a perfect body, in which perfection is carried through in every detail to an unlimited (infinite) size without fault or defect. The latest results on this research will be presented.

To qualify for a solid, rigid body, close packing of the spheres is required. For an ideal amorphous solids composed of hard spheres of identical size, we impose a stricter condition for the packing, namely, to be such that all spheres are in fixed positions (no loose spheres). To define the ideal solid, we must define what we mean by a perfect amorphous structure. Here, perfection is defined by, first the definition of imperfections, and next by the requirement of absence of imperfections of any kind. We envisage two types of defects: (i) geometrical, and (ii) statistical. Geometrical defects are: a sphere of different size, a loose sphere, and a vacancy. A statistical defect is defined with respect to two statistical functions: $\Psi(N_C)$, and $\Phi(s_\beta)$. The former describes the probability of a given sphere having N_C number of touching contacts, and the latter describes the disposition of the contacts on the surface of the sphere. Defects relating to the two functions will be described.

The results for the functions, $\Psi(N_C)$, and $\Phi(s_\beta)$, for the corresponding radial distribution function, and so called blocking number will be presented from simulations of an ideal amorphous solid.

WP25

A Comparison of the Influence of Different Dopants on the Radar-absorbing Properties of Barium Hexaferrite

M. Jones[a], M. M. Suder[a], A. Amiet[b], A. V. J. Edge[a], G. A. Stewart[a], W. D. Hutchison[a], and P. Jewsbury[b]

[a] *School of Physical, Environmental and Mathematical Sciences, UNSW at ADFA, Canberra, Australia 2600.*

[b] *Maritime Platforms Division, DSTO, Maribyrnong, Australia 3032.*

The ferromagnetic resonance of barium hexaferrite is at approximately 48 GHz, which sits well above the frequency bands employed by most radar systems. However, certain elements (or combinations of elements), when doped into the iron sub-lattice, have been observed to weaken the system's uniaxial magnetocrystalline anisotropy and thereby lower the ferromagnetic resonance frequency. This contribution presents a survey of ferromagnetic resonance frequencies published in the literature, as well as resonance frequencies that we have converted from published magnetic characterisations of the magnetic anisotropy.
In several cases we have confirmed the reliability of such converted values, and new data will be presented for ($Co_{1/2}Zr_{1/2}$)- and ($Co_{1/2}Mo_{1/2}$)-doped barium hexaferrite.

Our specimen materials were prepared by solid state reaction, and characterised using x-ray powder diffraction and ^{57}Fe Mössbauer spectroscopy. The electromagnetic response characteristics were recorded with a microwave network analyser, using either a co-axial specimen (0 - 18 GHz) or a larger, planar tile specimen (0 - 40 GHz).

An ideal radar absorbing material would require just a small concentration of an inexpensive dopant to lower the ferromagnetic resonance frequency into the 0 - 2 GHz band that is typical of long-range radars. The likelihood of finding such a doped barium hexaferrite system will be discussed.

WP26

Analysis of Hydrogenated Amorphous Carbon Films Deposited using an Open Plasma Generator under Various Bias Voltages

M. Rybachuk, J.M. Bell

School of Mechanical, Manufacturing and Medical Engineering, Queensland University of Technology, Gardens Point, Brisbane, QLD 4001, Australia

Over the years extensive research work has been conducted to identify suitable techniques to characterise the structural composition of amorphous hydrogenated carbon (a-C:H) films. One of the core aspects in analysis of a-C:H is the value ratio of the diamond-like/graphite-like (sp^3/sp^2) bonding. It is known that changing the negative substrate bias can modify the ratio of sp^3/sp^2 bonding, consequently changing the film properties. However similar deposition methods may yield contradictory results.

X-ray photoelectron spectroscopy (XPS) is frequently used to determine bonding structure of a-C:H films. However, it is still an open question whether the sp^3/sp^2 obtained ratio is reliable and whether current models for XPS analysis are correct. The majority of published work on XPS analysis deals with considerable C_{1s} spectral shifts between the sp^2 and sp^3 peaks, however to date, there were no reports providing an analysis of minor spectral shift in the order of 0.01 eV and it consecutive reflection to film morphology.

In this paper we examine XPS C_{1s} spectra of a-C:H films with total peak shift of 0.07 eV corresponding to the change in deposition conditions. Multiple function fitting of C_{1s} spectra have been used to obtain sp^3/sp^2 ratio value. Visible Raman was also employed to study film disorder using conventional D and G modes separately and in combination with additional bands at 1150 cm^{-1} and 1500 cm^{-1}, which reflect changes in the hydrogenation level. The results show that the sp^3/sp^2 ratio derived by XPS C_{1s} is valid and that visible Raman spectra can be used to monitor the complexity of a-C:H structural transitions by using suitable analysis models. XPS together with Raman and the band gap can be used together to estimate the sp^3/sp^2 ratio, and all techniques give similar results. Mechanical hardness and Young's elastic modulus data were used to support the above results. We note that minor XPS C_{1s} spectral shift corresponds to significant changes in a-C:H film structure. The changes in a-C:H under an increased substrate bias is also examined further.

WP27

The Electric Field Gradient of $FePS_3$: A Comparison Between Calculated and Measured Values

A. E. Smith, K.C. Rule, J.D. Cashion and T.J. Hicks

School of Physics and Materials Engineering, Monash University, Victoria 3800, Australia.

Iron thiophosphate, a member of the transition metal thiophosphate family, is frequently considered as quasi-two dimensional in both crystallographic and magnetic structure. It is an antiferromagnetic with previously reported magnetic and Mössbauer spectra structure [1,2,3]. These allow comparisons to be made with the results of electric field gradient (EFG) computations using the WIEN2k program suite at VPAC [4], thus providing information on the electronic charge distribution. Owing to the monoclinic nature of the crystal, particular care must be taken in interpreting the computed directions of the principle axes of the EFG. However, they can be understood by considering the underlying quasi-close packed structure of the sulphur atoms and the relative positions of the iron and phosphor atoms. Good agreement is also obtained with experimental measurements for the EFG asymmetry parameter and magnitude.

[1] K.C. Rule, S.J. Kennedy, D.J. Goosens, A.M. Mulders, T.J. Hicks, Appl. Phys A **74**, S811 (2002).

[2] K.C. Rule, T. Ersez, S.J. Kennedy and T.J. Hicks, Physica B **335**, 6 (2003).

[3] K.C. Rule, J.D. Cashion, A.M. Mulders and T.J. Hicks, Hyperfine Interactions **141/142**, 219 (2002).

[4] P. Blaha et al., *WIEN2K, An Augmented Plane Wave + Local Orbitals Program for Calculating Crystal Properties* (Karlheinz Schwarz, Techn. Universität Wien, Austria, 2001).

WP28

Mapping Disorder-Order Induced Changes to the Fermi Surface of Cu_3Au using a new Toroidal Electron Energy Analyser

A. Tadich[a], L. Broekman[a], J.Riley[a], R.Leckey[a] ,T. Seyller[b], K.Emtsev[b] L Ley[b]

[a]*School Of Physics, Latrobe University ,Bundoora Campus, Victoria 3083, Australia.*

[b]*Institut fur Technische Physik II, Universitat Erlangen Nurnberg, 91058 Erlangen, Germany.*

Many physical properties of a crystalline material (transport, optical properties, magnetic properties) depend critically on the topology of the Fermi Surface (FS). The compositionally random Cu-Au system displays a variety of unusual phases which, together with other properties such as the incommensurate long-period superlattice in CuAu, are believed to be related to FS topology[1, 2]. Thus knowledge of the FS of these materials is of fundamental importance in explaining these phenomena.

The FS of Cu_3Au has previously been studied by Angle resolved Photoemission (ARPES) in the Constant Initial State mode[3], using a previous generation toroidal-type angle resolving analyzer[4]. However the introduction of new Brillioun Zone boundaries in the ordered phase of Cu_3Au causes band back-folding to occur. This results in the predicted FS of the ordered structure possessing a much more intricate topology than the disordered phase. Thus for investigation using ARPES, one requires high angle and energy resolution of the electron spectrometer. A new generation toroidal angle resolving electron energy analyzer, developed at Latrobe University, has been used to map the changes that occur to the disordered state Fermi Surface across the disorder-order transition using the so-called Azimuthal Scan technique. This method maps the distribution of electrons from the Fermi level over the entire photoemission hemisphere, allowing an overview of transitions across a wide area in k-space. In addition to unusual 3-fold structures that are not believed to originate from the Fermi surface we observe distinct changes to the FS across the transition, which are believed to be the new FS contours of the ordered state.

1. Deimel, P.P., *Fermi Surface And Electronic Structure Of Ordered Cu_3Au.* Physical Review B., 1981. **24**(10): p. 6197.
2. Kevan, S.D., *Fermi Surface Studies Using Angle Resolved Photoemission.* Journal Of Electron Spectroscopy And Related Phenomena, 1995. **75**: p. 175-186.
3. Con Foo, J.A., et al., *The Fermi Surface Dimensions Of Disordered Cu3Au As Determined By Angle Resolved Photoemission Spectroscopy.* Solid State Communications, 1998. **107**(8): p. 385-390.
4. Leckey, R.C.G. and J.D. Riley, Appl. Surf. Sci., 1985. **22/23**: p. 196.

WP29

High Resolution Angle Resolving Toroidal Electron Spectrometer

A Tadich [a], L Broekman [a], E Huwald [a], R Leckey [a], J Riley [a], T Seyller [b] and L Ley [b]

[a] *Department of Physics, La Trobe University, Victoria 3086, Australia.*

[b] *Institut fur Technische Physik,Universitat Erlangen/Nurnberg, Erlangen, Germany.*

This paper describes the design characteristics of a second generation Toroidal Electron Spectrometer for use in the determination of electronic states in crystalline solids and in the observation photoelectron electron diffraction. The spectrometer is designed for use on a high resolution beam of a synchrotron. It is currently installed at the Berlin Synchrotron BESSY.

The design features which ensure that the foci in the sagital and meridinal planes are coincident to obtain maximum resolution in both angle and energy, are explained. Simulations showing electron trajectories and the resulting resolving powers in both angle and energy are given. The energy resolution with respect to the electron kinetic energy is ~5000 and the angle resolution is $< 0.1^{\circ}$.

Preliminary results showing Fermi surfaces of Cu and Cu_3Au and the electronic bands in SiC are included to show the capability of the analyzer even when used on a low resolution beam line, TGM4.

WP30

Whisky: Further EPR and Antioxidant Efficiency Studies

Irwin Cheah[a], Steven J.Langford[a], Jim Kelly[b], and Gordon Troup[c]

[a]*School of Chemistry, and* [c]*School of Physics and Materials Engineering,*

Monash University, *Victoria, Clayton 3800*

[b]*Angoves Pty.Ltd.*

A further selection of high standard, internationally recognised whiskies, (Irish, Canadian, Japanese for example) have been put to the same tests as described in the work of these authors in Abstract WP2, Wagga Conference '03. In each case, the EPR spectra are unique to the whisky, as regards Cu^{2+}, Fe^{3+}, and free radical features, and the antioxidant efficiencies are comparable with those of vitamins C and E, as determined by the test used, described in: *I. Cheah et al*.,(2003), *AIM-digest* **12** (1) 14-15.

The importance of this work to the Industry is currently being assessed.

WP31

An EPR and Antioxidant Efficiency Study of the Pinebark Phenolic Extracts Pycnogenol (R) and Endogenol.

Irwin Cheah[a], Steven J. Langford[a], and Gordon Troup[b]

[a]School of Chemistry, and [b]School of Physics and Materials Engineering, Monash University, Victoria, Clayton 3800

Pycnogenol (R) is a phenolic extract of French Maritime Pine bark: the name was invented by Jack Masquelier, a noted researcher into phenolic antioxidant activity, but is now owned by the Company Horphag. Endogenol is a New Zealand phenolic extract of Pinus Radiata bark: both products are sold as dietary supplements.

EPR and antioxidant efficiency measurements were made on both. The EPR signal from Endogenol was stronger than that from Pycnogenol (R), but the antioxidant efficiencies were almost the same, at slightly more than 50% that of vitamin C as measured by the technique used, already described by these same authors in: I. Cheah *et al.*, (2003), *AIM-digest* **12**,(1) 14-15.

It is not only useful, but necessary to check such dietary supplements for their claimed contents and actions.

Samples were kindly supplied by the manufacturers.

WP32

Theory of the Variable Quantum Yield of Bilirubin-IX Photoisomers: the End of a Chapter

G.J.Troup[a], Marina Mazzoni[b], G. Agati[b] and R. Pratesi[b]

[a] *School of Physics and Materials Engineering, Monash University, Clayton Victoria3800.*

[b] *Istituto di Fisica Applicata del C.N. R., Area di Ricerca, Sesto Fiorentino, Italy.*

Bilirubin-IX (BR-IX), responsible for neonatal jaundice, has two slightly different chromophores which undergo the Davidoff (exciton) interaction. Because of this, BR-IX in certain solvents, e.g. human serum albumin (but not Me/OH) exhibits magnetic circular dichroism (MCD), due to the exciton lines only. The absoption spectrum of BR-IX in the exciton line region is best fitted by two gaussian lines of equal width, but the MCD spectrum best fit requires two gassians of unequal width: the gaussian assumption is made for ease of calculation. The difference between the fitted spectra shows up as a single broad line of maximum smaller than that of the gaussian lines, and in the region of the central portion of the gaussians'overlap. The origin of this line is as yet unknown, so that much further work needs to be done on the structure of the excited state of BR-IX giving rise to the exciton interaction. This is currently being undertaken. However, the variation of the exciton interaction energy with wavelength as deduced from present theory seems reasonably certain though its origin may not be.

WP33

High-Power Ultrasonic Treatment of Contaminated Soils and Sediments

A.F. Collings[a], P.B. Gwan[a] and A.P. Sosa Pintos[b]

[a] *CSIRO, Telecommunications & Industrial Physics, Lindfield, NSW 2070, Australia.*

[b] *University of Western Sydney, Penrith Campus, NSW 2750, Australia .*

The propagation of high-power ultrasound through a liquid can initiate the phenomenon of cavitation. This occurs with the collapse of gas bubbles formed during the rarefaction phase of the ultrasonic wave either from the dissolution of air or vaporisation of the liquid. Bubble collapse can generate localised temperatures up to 5,000 K and pressures up to 1,000 atmospheres. Solid particles in slurry have been shown to act as foci for the nucleation and collapse of bubbles. Theory and experiment have confirmed that the rupture of a bubble on a solid surface generates a high speed jet directed towards the surface. In this case, the extreme conditions generated by the non-linear shock wave produced by bubble collapse are localised on the solid surface.

Since Persistent Organic Pollutants (POPs) are hydrophobic and are also readily absorbed on the surface of soil particles, the energy released by cavitation in a soil or sediment slurry is selectively directed towards them. The temperatures are sufficient to decompose these molecules. However, the extreme conditions are highly localised and the bulk solution temperature is essentially unaffected. Any decomposition products are immediately quenched and recombination reactions are avoided.

Recent advances in ultrasound technology have produced commercial equipment capable of high power which has enabled us to remediate soils and sediments containing Organochlorine Pesticides (OCPs), Polyaromatic Hydrocarbons (PAHs) and Polychlorinated Biphenyls (PCBs). With reductions greater than 80% within minutes, this technique shows great promise with advantages of on-site treatment and reduced operating and capital costs compared with conventional methods.

WP34

Phase Transformations in the $Ca_{1-x}Sr_xTiO_3$ Perovskite System

J.E. Daniels[a], M.M. Elcombe[b], T.R. Finlayson[a] and E.R. Vance[c]

[a] *School of Physics and Materials Engineering, Monash University, Victoria 3800, Australia.*

[b] *Bragg Institute, ANSTO, Lucas Heights, NSW 2234, Australia.*

[c] *Materials and Engineering Sciences, ANSTO, Lucas Heights, NSW 2234, Australia.*

The mixed perovskite $Ca_{1-x}Sr_xTiO_3$ is one of the major constituent phases of SYNROC, a synthetic rock form proposed for the long term immobilisation of high-level nuclear waste [1]. A complete understanding of the crystal structures formed, and transitions within, each of the constituent phases is of vital importance to gaining a complete knowledge of the overall structural stability of SYNROC. This study investigated the transition temperatures and the space group symmetry of several samples between the composition values of x = 0.6 to 0.85.

Previous studies of this compound have produced many conflicting results. It is believed that the reason for this is the sample preparation technique coupled with the form of the sample during experimentation, i.e., powder vs. polycrystalline solid. This study has attempted to produce samples using techniques closely related to those used in bulk SYNROC manufacture and to analyse these samples in their polycrystalline form as they would exist in SYNROC.

Transition temperatures were determined by observing the dynamic Young's modulus and internal friction of the samples between 4K and 420K using the Piezoelectric Ultrasonic Composite Oscillator Technique [2]. Classifications of the crystal structures formed were carried out using the High Resolution Powder Diffractometer at the Lucas Heights Research Reactor within the temperature range of 8K to 300K. Space group symmetries for each phase were then determined by Rietveld refinement.

[1] A.E. Ringwood, S.E. Kesson, N.G. Ware, W. Hibberson, and A. Major, *Nature* **278**, 219 (1979).

[2] S.L. Quimby, *Phys. Rev.* 1925. **25**, 558 (1925).

WP35

High-temperature Viscoelastic Relaxation: in Search of the Creep Function

Ian Jackson[a], and Ulrich H. Faul [a]

[a] *Research School of Earth Sciences, Australian National University, Canberra ACT 0200*

Most materials tested at high temperature undergo a progressive transition from elastic, through anelastic, to viscous behaviour with decreasing frequency. Such viscoelastic relaxation is manifest in strain-energy dissipation (Q^{-1}) and an associated frequency dependence (dispersion) of the shear modulus G – both of which can be determined with torsional forced oscillation/microcreep techniques. The application of such methods is well illustrated by recent results from our laboratory on fine-grained polycrystalline olivine $(Mg,Fe)_2SiO_4$ isostatically hot-pressed with and without added basaltic melt glass. The primary feature of the dissipation in melt-free materials is the existence of a broad, largely anelastic absorption band within which Q^{-1} varies mildly with period and average grain size, and displays an Arrhenian dependence upon temperature. For melt-bearing materials the behaviour is qualitatively different: a broad peak superimposed upon a monotonically frequency- and temperature-dependent background is consistently observed. Linear viscoelastic relaxation is best modelled by specifying the creep function giving the time-dependent strain caused by unit step-function stress. The complex compliance, being the response to harmonically time-varying stress, is essentially the Laplace transform of the creep function. The shear modulus and strain energy dissipation are simple functions of the real and imaginary parts of the complex compliance. In modelling the viscoelastic relaxation in our melt-free olivine polycrystals we have employed a creep function of the Burgers (spring and dashpot) type, with a suitable distribution $D(t) \sim t^{a-1}$ $(0 < a < 0.5)$ of anelastic relaxation times. The upper and lower bounds for this distribution are both grain-size and temperature dependent, as is the Maxwell relaxation time used in parameterising the viscous part of the deformation. A Burgers creep function of this type satisfactorily describes the variation of both G and Q^{-1} with period, temperature and average grain size for our suite of melt-free olivine polycrystals – allowing interpolation amongst the experimental data and providing a secure internally consistent basis for extrapolation beyond the observational window. Progress in modifying the distribution of anelastic relaxation times to account quantitatively for the dissipation peak for the melt-bearing materials will also be described.

WP36

Proximity Effect in Low-resistivity Yttria-stabilized Zirconia Thin Films

S. K. H. Lam and S. Gnanarajan

CSIRO Telecommunications and Industrial Physics, PO Box 218, NSW 2070, Australia

Abstract – Most of the applications of Josephson junctions in superconducting electronics require a non-hysteretic current-voltage characteristic (IVC), which gives one value of voltage for each bias current (overdamped). The critical parameters of the junction are the critical current density, J_c, and the critical current - normal resistance product, I_cR_n. The device performance would improve for junctions with a higher J_c and higher I_cR_n values. Nb/Yttria-stabilized Zirconia (YSZ)/Nb junctions with three different geometries (ramp edge, trilayer and planar types) have been fabricated and characterised. The junctions were non-hysteretic with very high I_cR_n, ~ 1 mV. The junction critical current has an exponential relationship with both temperature and interlayer length, analogous to a superconducting proximity effect through a metal interlayer. The coherence length of the YSZ interlayer was estimated to be ~ 3 nm. The resistivity of the YSZ interlayer has a range of 0.4 - 116 mΩ–m, which depends on the crystallinity of the interlayer.

WP37

A New Thin Film Deposition Process by Cathodic Plasma Electrolysis

Thierry Paulmier[a], Emad Kiriakos[a], John Bell[a], Peter Fredericks[b]

[a] *Built Environment and Engineering Research Centre, School of Mechanical, Manufacturing and Medical Engineering, Queensland University of Technology, GPO Box 2434, Brisbane, QLD 4001, Australia*

b Science Research Centre, School of Physical and Chemical Science, Queensland University of Technology, GPO Box 2434, Brisbane, QLD 4001, Australia

A new technique, called atmospheric pressure plasma deposition (APPD), has been developed since a few years for the deposition of carbon and DLC, Titanium or Silicon films on metal and metal alloys substrates. A high voltage (2kV) is applied in a liquid electrolytic solution between an anode and a cathode, both electrodes being cylindrical: a glow discharge is then produced and confined at the vicinity of the cathode. The physic of the plasma in the electrolytic solution near the cathode is very different form the other techniques of plasma deposition since the pressure is here close to the atmospheric pressure.

We describe here the different physico-chemical processes occurring during the process. In this cathodic process, the anodic area is significantly larger than the cathode area. In a first step, the electrolytic solution is heated by Joule effect induced by the high voltage between the electrodes. Due to the high current density, the vaporization of the solution occurs near the cathode: a large amount of bubbles are produced which are stabilized at the electrode by hydrodynamic and electromagnetic forces, forming a vapour sheath. The electric field and voltage drop are then concentrated in this gas envelope, inducing the ionization of the gas and the ignition of a glow discharge at the surface of the material. This plasma induces the formation of ionized and reactive species which diffuse and are accelerated toward the cathode. These excited species are the precursors for the formation of the deposition material. At the same time, the glow discharge interacts with the electrolyte solution inducing also ionization, convection and polymerization processes in the liquid: the solution is therefore a second source of the deposition material.

A wide range of films have been deposited with a thickness up to 10 micrometers. These films have been analyzed by SEM and Raman spectroscopy. The electrolytic solution has been characterized by GC-MS and the formed precipitates by IR and Raman spectroscopy.

WP38

The Storage of Nuclear Waste in Concrete

T M Sabine
Department Of Applied Physics, University Of Technology, Sydney, Australia

This project was undertaken to investigate the setting of cement with a view to using concrete as a medium for the “dilution and dispersion” of low-level nuclear waste. This is the preferred option for this category of waste chosen in 1981 by the International Atomic Agency (IAEA), which is a standing committee of the United Nations.

This method has never been used because of the "nimby (Not In My Back Yard)" syndrome. This syndrome, which is not logical, as shown by the Chernobyl accident in 1989, never the less is very popular. In this country we apply a weighting factor based on money. Imagine if we chose Vaucluse as a site to deposit waste. The backyards of the wealthy have high fences. In contrast the backyards of the residents of remote areas in South Australia have a low, or non-existent, fence. This is the criterion we used for the British bomb tests in the 50's and are using for waste now. Dilution in concrete is much fairer. The social equity is provided by the fact that the social groups consuming more energy will use more concrete, and will be more exposed to any slight hazards resulting from this use.

It should be remembered that, while Australia does not use nuclear power for the generation of electricity, we produce and sell about 20 percent of the world's uranium. Uranium is not an uncommon element. Earth. It is about as common as nickel. The total amount of low-level nuclear waste accumulated in Australia after 40 years is 3,500 cubic metres. The dilution factor in the amounts of concrete we producewould easily satisfy IAEA standards.

The starting point for the concrete project is the work of two eminent French chemists. Their interest probably arose from the very long lifetime of the Roman fortifications in the south of France, which have lasted for thousands of years.

Lavoisier, in 1765, suggested that during hydration, very small crystals are produced which are “so entangled with each other that a very hard mass results”.
Le Chatelier proposed in 1887 that “A very weak adhesion, per unit of surface, multiplied by a considerable extent of surface, will give a very great force of adhesion”.

Because cement is essentially amorphous the only suitable diffraction technique is high-resolution small angle scattering, UltraSANS, which examines the zeroth order reflection. Neutrons were chosen since, being electrically uncharged, they interact relatively weakly with matter and can be used to examine macroscopically sized specimens. For these measurements we used instruments at the Hahn-Meitner Institute, Berlin, the Ustav Jademe Fyziky, Prague and the Oak Ridge National Laboratory, Tennessee. These were the only ones available. It has been established that particles of approximately 2 microns in radius are formed as cement hydrates and that about one-half of the available water is in the particles.

The next step is to determine if the addition of nuclear waste modifies the hydration process and, if this does occur, what is the safe level of dilution. With the inevitable increase in electricity consumption, and the increase in global warming with increased fossil fuel burning, this is a field of research that will become more important.

WP39

Fermi Surface Comparisons for Materials Susceptible to Phase Transitions

A. E. Smith[a], T.R. Finlayson[a], Robert Leckey[b] and J. Riley[b]

[a] *School of Physics and Materials Engineering, Monash University, Victoria 3800, Australia.*

[b] *Department of Physics, LaTrobe University, Bundoora, Victoria 3086. Australia.*

The noble-metal binary alloy Cu_3Au and the Heusler alloy Ni_2MnGa are studied by means of band structure computations together with calculations of their Fermi surfaces. The first of these materials is a simple alloy with a classical order-disorder phase transition at 663K. The second is a shape memory compound with a series of reversible transitions, including both martensitic and ferromagnetic transitions. Comparisons are made between results obtained for different structures using the WIEN2k program suite at VPAC. Based on experimental lattice structures [2], calculations identify dominant atom and angular momentum type states close to the Fermi level [3]. Results are shown for bulk electronic band structures, densities of states (DOS) for individual atoms and cuts across the Fermi surface. In particular the Fermi surface structure calculations allow direct comparison with novel direct Fermi mapping high resolution photoemission experiments employing synchrotron radiation [4].

[1] P. Blaha et al., *WIEN2K, An Augmented Plane Wave + Local Orbitals Program for Calculating Crystal Properties* (Karlheinz Schwarz, Techn. Universität Wien, Austria, 2001).

[2] P.J. Webster, K.R.A. Ziebeck, S.L. Town and M.S. Peak, Phil. Mag. B 49, 295 (1984).

[3] O.I. Velikokhatnyi and I.I. Naumov, Phys. Solid State, 41, 617 (1999).

[4] J.A. Con Foo, A.P.J. Stampfl, B. Mattern, A. Ziegler, M. Hollering, L.Ley, J.D. Riley, and R.C.G. Leckey, Sol. Stat. Comm. 107, 385 (1998).

WP40

Formation of Ion Tracks in Single-Crystal Indium Phosphide Irradiated by Swift Heavy Ions

A. S. Khalil, A. M. Stewart, M. C. Ridgway, L. T. Chadderton, D. J. Llewellyn, A. P. Byrne

Research School of Physical Sciences and Engineering, Australian National University, Canberra, Australia 0200

Transmission Electron Microscopy has been used to study radiation damage in 200 MeV gold ion-irradiated Indium Phosphide. The observations reveal the presence of individual latent tracks of intermittent nature about 7-10 nm in diameter. Ultra-thin crystals of molybdenum trioxide (MoO_3), irradiated simultaneously, were used for the exact determination (microdosimetry) of the projectile ion fluence (total dose).

The effect of ion fluence upon the surface roughness of irradiated crystals was studied by Atomic Force Microscopy. The roughness increases slowly with irradiation dose but a rapid increase of roughness is observed at doses sufficient to result in the formation of an amorphous layer.

WP41

Fe and Mg Solubility in the Ca Site of Zirconolite, $CaZrTi_2O_7$

E.R.Vance, J.G. Cashion, J.V.Hanna, Z.Garrett and M. Bhati,

Materials Engineering and Science, ANSTO, Menai, NSW 2234, Australia,

The solid solubility of Fe in the Ca site of zirconolite appears to be approximately the same whether it is incorporated as the divalent or trivalent species. Divalent Fe was encouraged by using an argon firing atmosphere and direct substitution in the Ca site [$Ca_{(1-x)}Fe_xZrTi_2O_7$] and trivalent Fe by the use of an air atmosphere and Al compensation in the Ti site [$Ca_{(1-x)}Fe_xZrTi_{(2-x)}Al_xO_7$]. The anticipated valences were confirmed by X-ray near-edge, X-ray photoelectron and Mossbauer spectroscopies. Changing the firing atmosphere from argon to air and vice versa also changed the Fe valences, but scanning electron microscopy showed that small amounts of second phase, Fe-bearing materials were present. The possible reasons for the apparently similar solid solubilities of divalent and trivalent Fe in the Ca site are discussed.

Solid state magic-angle nuclear magnetic resonance was used to study Mg speciation in the Ca and Ti sites of zirconolite.

WP42

Thermal Expansion Studies of Ni_2MnGa Shape-Memory Material

X.D. Wu and T.R. Finlayson

School of Physics and Materials Engineering, Monash University, Victoria 3800, Australia.

The Heusler alloy Ni_2MnGa is a ferromagnetic shape memory alloy. It exhibits giant magnetic-field-induced strains at room temperature, resulting in its commercial application as a magnetically-driven actuator. Due to this technological application, Ni_2MnGa has received considerable attention recently.

A unique feature in the behaviour of Ni_2MnGa is that prior to the martensite transformation, a weak, first-order transition takes place. In order to study the pre-martensite transformation behaviour, and the influence of external stress (either applied mechanically or magneto-mechanically) on it, a Ni_2MnGa single crystal is being studied by high precision, capacitance dilatometry.

In this paper the results from these measurements will be discussed, in the light of the known static and dynamic structural behaviour for Ni_2MnGa, determined by neutron scattering techniques [1,2].

1 A. Zhludev, S.M. Shapiro, P. Wochner, A. Schwartz, M. Wall and L.E. Tanner, *Phys. Rev. B* **51**, 11310 (1995).

2 P.J. Brown, J. Crangle, T. Kanomata, M. Matsumoto, K-U. Neumann, B. Ouladdiaf and K.R.A. Ziebeck, *J. Phys.: Condens. Matter* **14**, 10159 (2002).

WP43

Characterization of Microstructural Evolution in Fe-C(-Mn) Alloys During Early Stages of Ageing using Atom Probe

X. Y. Xiong[a], P. Tran[a], S.P. Ringer[b] and E. Pereloma[a]

[a] *School of Physics and Materials Engineering, Monash University, Victoria 3800, Australia.*

[b] *Australian Key Centre for Microscopy & Microanalysis, The University of Sydney, NSW 2006, Australia.*

Extensive studies (e.g. [1]) on the effect of ageing treatment on the microstructure and mechanical properties of most commercial ferritic (α) Fe-C(-X) alloys reveal age-hardening characteristics that involve a monotonic increase towards a peak hardness after several hours of ageing. Peak hardness is always associated with the formation of precipitate particles (e.g: MnC_3). However, there is relatively little systematic work on the very early stages of ageing using direct nanostructural analysis and many questions remain on the potential for clustering of interstitial C atoms prior to the precipitation reaction. In this experimental work, we report a small but significant hardness peak within 300 sec during ageing at 550 °C. High resolution transmission electron microscopy (HRTEM) observations did not show any microstructural change during this early stage of ageing.

In order to understand the microstructural evolution in ultra-low carbon α-Fe-C(-Mn) alloys during these early stages of ageing, 3-dimensional atom probe (3DAP) has been used to examine the C atom distribution and possible segregation of C and Mn atoms in these alloys. In this report, the 3DAP analyses and HRTEM observations of Fe-C and Fe-C-Mn alloys are correlated with age hardening measurements and possible mechanisms of the initial hardening phenomenon will be discussed.

1 G. Lagerberg and B. S. Lement, *Transaction of American Society for Metals,* **50**, 141 (1958).

Poster Session
Abstracts

Thursday
5 February

TP1

Surface Electron Structure of Short-Period Semiconductor Superlattice.

I.Bartos[a,b], T. Strasser[c], W. Schattke[c]

[a]*School of Physics, University of New South Wales, Sydney, Australia*
[b]*Institute of Physics, Czech Acad. Sci., Prague, Czech Republic*
[c]*Institute of Theoretical Physics, Christian-Albrechts-University, Kiel, Germany*

Semiconductor superlattices represent man-made crystals with unique physical properties. By means of the directed layer-by-layer molecular epitaxy growth their electric properties can be tailored (band structure engineering). Longer translational periodicity in the growth direction is responsible for opening of new electron energy gaps (minigaps) with surface states and resonances localized at superlattice surfaces. Similarly as for the electron structure of the bulk, a procedure enabling to modify the surface electron structure of superlattices is desirable.

Short-period superlattice $(GaAs)_2(AlAs)_2$ with unreconstructed (100) surface is investigated in detail. Theoretical description in terms of full eigenfunctions of individual components has to be used. The changes of electron surface state energies governed by the termination of a periodic crystalline potential, predicted on simple models, are confirmed for this system. Large surface state shifts are found in the lowest minigap of the superlattice when this is terminated in four different topmost layer configurations.
The changes should be observable in angle resolved photoelectron spectroscopy as demonstrated in calculations based on the one step model of photoemission [1].
Surface state in the center of the two dimensional Brillouin zone moves from the bottom of the minigap (for the superlattice terminated by two bilayers of GaAs) to its top (for the superlattice terminated by two bilayers of AlAs) where it becomes a resonance. No surface state/resonance is found for a termination with one bilayer of AlAs. The surface state bands behave similarly in the corresponding gaps of the k-resolved section of the electron band structure.

The molecular beam epitaxy, which enables to terminate the superlattice growth with atomic layer precision, provides a way of tuning the superlattice surface electron structure by purely geometrical means.

The work was supported by the Grant Agency of the Academy of Sciences of the Czech Republic, grant no.1010108.

[1] I. Bartos, T. Strasser, W. Schattke, Surface Review and Letters **10** (2003) 195 and Progress in Surface Science, to be publ.

TP2

Quantum Pumping and Geometric Phases in Nanoscale Electronic Devices

Huan-Qiang Zhou[a], Sam Young Cho[b] , Urban Lundin[b], and Ross H. McKenzie[b]

[a] *Centre for Mathematical Physics, University of Queensland, Brisbane Qld 4072, Australia*

[b] *Department of Physics, University of Queensland, Brisbane Qld 4072, Australia*

Adiabatic quantum pumping produces a finite charge/spin transfer through a quantum device whose external parameters are changed slowly and brought back its initial state after a certain period. After a cycle of the adiabatic change of the external parameters one returns to the initial configuration, but the wave function have its phase changed with respect to the initial wave function. To observe the additional phase directly, a double-path type of electron interferometer is proposed. The interference due to the geometric phase results in the oscillation of current collected in the drain of the interferometer. In addition, the phase associated with time-reversed state corresponds to charge/spin that passes through the quantum device. It is shown that quantum pumping has a natural geometric representation in terms of gauge fields (both Abelian and non-Abelian) defined on the space of system parameters. Tunneling from a scanning tunneling microscope tip through a magnetic atom could be used to demonstrate the non-Abelian character of the gauge field responsible for spin pumping.

1 H.-Q. Zhou, S. Y. Cho, and R. H. McKenzie, *Phys. Rev. Lett*. **91**, 186803 (2003).

2 H.-Q. Zhou, U. Lundin, S. Y. Cho, and R. H. McKenzie, *cond-mat/0309096*.

TP3

High Resolution Lithography of PMMA with a Scanning Probe Microscope

A. Cimmino, D. Gassull, S. Prawer, D. Jamieson

Centre for Quantum Computer Technology and School of Physics,
TheUniversity of Melbourne

Lithography with 10nm resolution is necessary for the construction of the Kane Quantum Computer. PMMA is shown to be a good e-beam resist for the fabrication of nanometer scale components required for the implementation of a solid state qubit and at the same time ideal for stopping P+ ions intended to be implanted into the silicon at precisely specified positions (Top Down approach).

We have developed AFM lithographic techniques that enables us to directly strip the PMMA resist with nanometer resolution to locally expose the substrate for ion implantation. The advantage of such technique is the high positioning precision without alignment markers and the simplicity of use.

We also show the use of conductive canilevers to perform contact e-beam lithography, followed by conventional resist development and etching. We present results on the electrical behavior of nanowires and nanostructures fabricated with these techniques.

.

TP4

Towards a Quantum-Limited Charge Detector

N.A. Court, D.J.Reilly, T.M. Buehler, R.P.Starrett, R.G. Clark and
A.R. Hamilton.
Centre for Quantum Computer Technology, School of Physics,
University of New South Wales, Sydney 2052, Australia

The radio frequency single electron transistor (rf-SET) is a near quantum-limited electrometer, capable of sensing sub-electron charge signals on microsecond timescales [1]. In addition to applications in radio astronomy and nuclear magnetic resonance, this device holds promise as a read-out detector for solid state quantum computing [2]. At present the sensitivity of the rf-SET is limited by the noise contribution of the post amplifier, which is typically a cryogenic transistor (HFET). In an effort to overcome this limitation we propose to exploit the dc-SQUID (superconducting quantum interference device) as a near-quantum limited post amplifier of radio frequency signals [3]. This hybrid configuration, consisting of a near quantum-limited electrometer (rf-SET) coupled to a near quantum-limited post amplifier (dc-SQUID) opens the prospect of studying sub-electron charge motion in condensed matter systems with unheralded sensitivity.

In this poster we present results to date in our effort to optimize the sensitivity of the rf-SET and its integration with a SQUID amplifier. We include numerical simulations of the microwave circuits and compare these results to data taken with the rf-SET at mK temperatures.

1 R.J. Schoelkopf et al, Science **280**, 1238 (1998)
2 T.M. Buehler et al, arXiv:cond-mat/0302085
3 M. Andre et al, Appl. Phys. Lett. **75**, 698 (1999)

TP5

Influence of N_2 Background Pressure on the Incorporation of Arsenic During MBE Growth of GaAs

T. Dieing[1] and B.F. Usher

Department of Electronic Engineering, La Trobe University, Victoria, 3086, Australia.

MBE growth of the dilute nitride III-V compound semiconductor GaAsN on GaAs(100) substrates typically uses RF or microwave plasmas as sources of nitrogen [1-3]. The N_2 background pressure in the growth chamber during normal operation of our Tectra™ nitrogen plasma source is in the range of 1-6x10^{-5} Torr since only a small fraction of the beam emitted from the source is in the form of atomic nitrogen.

The influence of this high N_2 background pressure on the minimum necessary As_4 pressure for stoichiometric homoepitaxial growth of GaAs has been investigated at various substrate temperatures in the absence of a significant N_2 background pressure as well as in the presence of 6x10^{-5} Torr N_2 in the chamber.

The experiments revealed firstly, that the minimum necessary As_4 pressure decreased with decreasing substrate temperature, which is expected due to the reduced loss of Arsenic from the substrate at lower temperatures. Secondly, the As_4 pressures required in cases when a high nitrogen background was present lay systematically above the values measured without the nitrogen background. This effect becomes more pronounced as the substrate temperature is reduced towards 400°C. To explain this behavior, the GaAs growth process has been modelled using kinetic rate equations and by including surface site blocking terms the model accounts for the data. The model also agrees well with GaAs growth kinetic data published by several other authors [4-6].

[1] S. G. Spruytte, C. W. Coldren, A. F. Marshall, et al., *MRS Internet Journal of Nitride Semiconductor Research* **5**, W8.4 (2000)
[2] H. C. Alt, A. Y. Egorov, H. Riechert, et al., *Physica B* **302**, 282 (2001).
[3] S. A. Lourenco, I. F. L. Dias, L. C. Pocas, et al., *J. Appl. Phys.* **93**, 4475 (2003).
[4] Brennan T.M., Tsao J.Y., et al, *J.Vac.Sci.Technol. A* **10**, 33 (1992).
[5] SpringThorpe A. J. and Mandeville P., *J.Vac.Sci.Technol. B* **6**, 754 (1988).
[6] SpringThorpe A. J. and Arent D. J., *J.Vac.Sci.Technol. B* **11**, 783 (1993).

[1] Electronic address: t.dieing@ee.latrobe.edu.au

TP6

Comparison of Hydrogen Resist Removal Techniques for STM-Fabricated Nanoscale Devices

T. Hallam, L. Oberbeck, F.J. Ruess, N.J. Curson, M.Y. Simmons and R. G. Clark

Center for Quantum Computer Technology, School of Physics, University of New South Wales, NSW 2052, Australia

High resolution Scanning Tunnelling Microscopy (STM) is used to compare thermal desorption, STM tip-induced desorption and electron beam desorption of hydrogen resist layers used for STM based nanolithography on the Si(100)2×1 surface.

The use of STM lithography for nanoscale device fabrication was first proposed in 1998 [1]. In STM based nanolithography the STM tip is used to locally remove hydrogen atoms from a hydrogen terminated Si(100) surface to create structured regions of reactive silicon [2]. Exposure to phosphine gas (PH_3) and a subsequent low temperature annealing at 350°C, incorporates phosphorus dopant atoms from the PH_3 in the nanolithographically exposed regions creating surface dopant structures [3]. It is then necessary to completely remove the monolayer of hydrogen to achieve high quality epitaxial silicon overgrowth for device encapsulation [4].

We demonstrate that complete hydrogen desorption is possible using thermal desorption or STM tip-based desorption. Thermal hydrogen desorption allows complete removal of hydrogen but suffers from dopant diffusion out of structured regions making it only suitable for larger feature sizes only. STM tip-based desorption is limited to small areas of several μm^2, but avoids dopant rearrangement, allowing atomic scale features to be preserved. Electron beam desorption is not suitable for completely removing hydrogen but has good prospects as a hydrogen resist compatible lithographic technique for large scale features complimentary to nanoscale STM tip lithography.

[1] J. R. Tucker *et al.*, Solid-State Electron. **42,** 1061 (1998).

[2] J. W. Lyding *et al.*, Appl. Phys. Lett. **64,** 2010 (1994).

[3] S. R. Schofield *et al.*, Phys. Rev. Lett. **91,** 136104 (2003).

[4] L. Oberbeck *et al.*, Appl. Surf. Sci. **212-213,** 319 (2003).

TP7

Measurement and Simulation of the Effects of Ion-Induced Defects on Ion Beam-Induced Charge (IBIC) Measurements in Si Schottky Diodes

S.M.Hearne *, M. D. H. Lay, and D.N. Jamieson.

Mircoanalytical Research Centre, School of Physics, University of Melbourne, Victoria 3010, Australia.

The Ion Beam Induced Charge (IBIC) technique is a very sensitive tool for investigating the electronic properties of semiconductor materials and devices[1,2]. However, obtaining quantitative information from IBIC experiments requires an accurate model of the materials properties.

The interaction of high energy ions with crystalline materials is known to create point defects within the crystal[3]. A significant proportion of defects introduced by the interaction of the ion with the crystal are electrically active and are therefore an important consideration when undertaking an IBIC experiment. The goal of this work is to investigate the possibility of including the relevant defect parameters in computer simulations of the IBIC experiment implemented using Technology Computer Aided Design (TCAD) software.

We will present the results from an IBIC study on Si Schottky diodes using 1 MeV alphas. A reduction of greater than 50% in the detected IBIC signal was observed for fluences greater than $5x10^{10}$ He^{+}/cm^{2}. The trap parameters following ion irradiation were determined experimentally using DLTS. Comparisons between the experimental IBIC results and TCAD simulations will be discussed.

1. M.B.H.Breese, P.J.C.King, G.W.Grime and F.Watt, *J.Appl.Phys* **72** 2097 (1992)
2. E.Vittone, C.Manfredotti, F.Fizzotti, A.Lo Guidice, A.Lorenzi, S. Galassini, M.Jaksic, *Nucl. Instr. And Meth. In Phys. Res. A* **476** 607 (2002).
3. K.Gill, G.Hall, B. MacEvoy, *J. Appl. Phys.,* **82** 126 (1997)

TP8

Magnetic Resonance and P:Si Qubits

W.D. Hutchison[a], D. Tempelaars[a], R. Bramley[b], A.R. Hamilton[c], E. Gauja[c] and R.G. Clark[c]

[a] *Centre for Quantum Computer Technology, School of PEMS, The University of New South Wales @ ADFA, Canberra ACT 2600*

[b] *Research School of Chemistry, Australian National University, Canberra ACT 0200*

[c] *Centre for Quantum Computer Technology, The University of New South Wales, Sydney NSW 2052.*

Much work has been done recently in the field of quantum computation, including demonstration of simple quantum operations in a range of physical systems, at least for a few quantum bits (qubits). However the challenge remains to scale such devices to a usefully large number of **identical** qubits and overcome the difficulties of stability and error correction. A solid state quantum computer based on silicon still has potential in terms of scalability and compatibility with existing electronic fabrications. The Kane [1] model for a silicon based quantum computer proposes that the nuclear spins of individual phosphorus dopant atoms be the qubits. An external voltage applied to so-called 'A gates' would be used to control the phosphorus hyperfine field and hence the nuclear magnetic resonance (NMR) frequency of the qubits. In this paper we present current measurements, using electron spin resonance (ESR), on bulk P:Si as a function of externally applied voltage.

The specified operating conditions for the Kane model are ~100mK and ~2 T, producing full spin polarisation of the P electronic spins. We also discuss preliminary measurements on the P:Si system in the millikelvin regime.

1 B. Kane, *Nature* **393**, 133 (1998).

TP9

Electron Transport in Multi-layer Thermionic Cooling Structures

S.P. Lee[a], B.C.C. Lough[a], X.Z. Shang[b], Q. Wang[c], R. A. Lewis[a] and C. Zhang[a]

[a] *Institute for Superconducting and Electronic Materials, University of Wollongong, Wollongong NSW 2522, Australia.*

[b] *Institute of Physics, Chinese Academy of Science, Beijing, China.*

[c] *Department of Physics, Xinjiang University, Urumqi, Xinjiang, China.*

There has been much interest in the use of semiconductor multi-layer structures for applications in thermionic cooling and power generation since the publication of Mahan and Woods' seminal paper [1]. The basic principle involves ballistic transport of electrons/holes across a barrier driving thermal transport. The use of a multi-layer structure allows simultaneous (1) ballistic transport, which is achieved in practice across a small layer, and (2) adequate thermal resistance to control heat backflow, which is achieved in practice by the barrier-electrode interfaces. More recent studies have included the effects of various non-idealities in practical structures.

We report on the electrical characterisation of two types of structures grown by molecular-beam epitaxy: (1) GaAs/AlGaAs heterostructures, and (2) *n*-GaAs homostructures, in which the barriers and electrodes are created by varying the electron doping. *I-V* characteristics now have been measured over a wide temperature range (10 - 300 K) for both types of structure, greatly extending our previous work [2]. The calculated *I-V* characteristics reveal the importance of taking into account space-charge effects between the electrodes.

1 G.D. Mahan and L. M. Woods, *Phys. Rev. Lett.* **80**, 4016 (1998).

2 B.C.C. Lough, S.P. Lee, Z. Dou, R.A. Lewis and C. Zhang, *Physica E* **17**, 651 (2003).

TP10

Characterization of Si-SiO_2 Trap Density due to Ion Implantation

D.R. McCamey[a,b], M.J. Francis[b], J.C. McCallum[a,c], A.R. Hamilton[a,b], A.D. Greentree[a,b], and R.G. Clark[a,b]

[a]*Australian Research Council Centre of Excellence for Quantum Computer Technology*

[b]*School of Physics, University of New South Wales, Sydney, NSW 2052, Australia.*

[c]*School of Physics, University of Melbourne, Victoria 3010, Australia.*

Ion implantation of dopant atoms is widely used in electronic device fabrication, with applications ranging from advanced nanoscale MOSFETs [1,2] to quantum cellular automata and quantum computation [3]. As these devices are made smaller, the detrimental effect of traps, such as their ability to localise or scatter electrons, becomes more pronounced. Here we study the number of traps created due to ion implantation, using a novel DC measurement technique to determine the number of electrically active traps at low temperatures, where capacitance based methods become unusable.

Hall-bar MOSFETs are fabricated and implanted with 15keV phosphorus ions. After a rapid thermal anneal to activate dopants and repair damage, Hall measurements are performed at 4.2K and the mobility as a function of carrier density determined. The critical density is obtained by extrapolating the mobility to zero, from which we estimate the density of traps that are localising the electrons. Studies are also underway on silicon implanted devices, aimed at separating the effect of interface traps due to implantation from charged P traps in the bulk.

Studies of more than 30 devices show that the trap density increases linearly with the density of implanted ions: $\Delta n_{trap} = 0.08\ (\pm\ 0.01)\ n_{implanted}$. We also find the interface trap density of unimplanted devices, $n_{trap} = 2.06\ (\pm\ 0.32) \times 10^{11}\ cm^{-2}$. This shows that the major source of traps is the oxide, with low density implantation having a minimal effect.

[1] T. Shinada, *Appl. Surf. Sci.* **162**, 499 (2000).
[2] P. A. Stolk, *Nucl. Instr. and Meth. in Phys. Res. B,* **148**, 242 (1999).
[3] R.G. Clark et al, *Philos. Trans. R. Soc. Lond. A.* **361**, 1451 (2003).

TP11

Nanofabrication of Charge-based Si:P Quantum Computer Devices using Single-ion Implantation

M.Mitic[a], T.M. Buehler[a], A.J. Ferguson[a], V. Chan[a], E. Gauja[a], F.E. Stanley[a], S.J. Angus[a], K.H. Lee[a], A.D. Greentree[a], D.J. Reilly[a], A.R. Hamilton[a], A.S. Dzurak[a], R.G. Clark[a], C.I. Pakes[b], C. Yang[b], D.N. Jamieson[b] and S.Prawer[b]

[a] *Centre for Quantum Computer Technology, University of New South Wales, NSW 2052*

[b] *Centre for Quantum Computer Technology, University of Melbourne*, VIC 3010

Quantum computing offers computational speed-up by using the inherent power of quantum mechanical systems, such as superposition and entanglement. Many different schemes for the realisation of quantum computers have been proposed, of which solid state quantum computing is the most promising for scale-up to multi-qubit processors.

Here we report on progress in one such scheme [1] using phosphorus atoms implanted in a silicon substrate. Prototype devices have been fabricated using standard lithographic techniques and a new method of controlled single phosphorus ion implantation using on-chip detector electrodes. Positional accuracy of the implanted ions was achieved using a nanoaperture mask defined using electron beam lithography. The two implanted phosphorus atoms, positioned 50 nm apart, are the qubits in this scheme [1] and the two lowest energy states of the electron remaining after ionisation of one phosphorus atom form the logical states. A series of process steps have been developed to repair the damage in the silicon substrate created by the implantation process, to define surface gates to control the electrostatic potential around the qubit and to define single electron transistors used for qubit readout via the detection of sub-electron charge transfer signals.

Preliminary electrical measurements on these devices have been performed and single charge transfer events, resilient to thermal cycling, have been observed. Additional experiments are underway to fully characterise these devices and eventually, to determine the quantum coherence time for the Si:P qubit system.

[1] L.C.L Hollenberg et. al., "Charge-based quantum computing using single donors in semiconductors", to appear in Physical Review B; cond-mat/0306235.

TP12

The Diffusion Mechanism of Mn in GaAs.

D. James[a], J. Riley[a], R. Leckey[a], Yvegen Biltosky[a] and Kathryn Prince[b]

[a] *Department of Physics, La Trobe University, Bundoora VIC Australia.*
[b] *ANSTO, Lucas Heights Research Laboratories, Private Mail Bag 1, Menai NSW 2234*

Studying the diffusion of dopant impurities in the semiconductors is important for the design and fabrication of devices as migration of dopants can destroy quantum well structures[1]. Ferromagnetic semiconductors are distinctive as they have the capability of using the flow of electrical charge and spin to give an extra degree of freedom for information transport. Until recently Mn was rarely used as a p-type dopant in GaAs. Some observations of diffusion profiles have been made but the diffusion profiles varied considerably depending on the conditions of its incorporation[2].

The diffusion of zinc in GaAs has been widely studied and as the Zn diffusion profiles are very similar to those of Mn the process of diffusion is similar. It has been found that Zn diffuses via the 'kick out' reaction where the singly charged Zn ion displaces a host Ga atom and the Ga becomes the interstitial having both a 2+ and 3+ charge state[3, 4]. In the case of manganese, the ion travels interstitially as a doubly charged deep donor [5, 6].

This paper investigates a theoretical model of diffusion in order to simulate experimental SIMS profiles of the diffusion of an evaporated Mn layer into a GaAs substrate. The samples were prepared by MBE and SIMS profiles were obtained using the Cameca Sims 5f which is part of the Environment division of the Australian Nuclear Science and Technology Organisation (ANSTO) in Lucas Heights, Sydney[7].

1. Tan, T.Y. and U. Gosele, *Destruction mechanism of III-V compound quantum well structures due to impurity diffusion.* J. Appl. Phys., 1987. **61**(5): p. 1841-1845.
2. Wu, C.H. and K.C. Hsieh, *The effects of As overpressure and diffusion source on the diffusion of Mn in GaAs.* J. Appl. Phys., 1992. **72**(12): p. 5642.
3. Gosele, U., *Fast diffusion in semiconductor.* Annual Review of Material Science, 1988. **18**.
4. Bosker, G., et al., *Use of zinc diffusion into GaAs for determining properties of gallium interstitials.* Phys. Rev. B, 1995. **52**: p. 11927-31.
5. Jungwirth, T., J. Sinova, and A.H. MacDonald, *Magnetic and transport properties of (III,Mn)V ferromagnetic semiconductors.* Acta Physica Polonica A, 2003. **(in press)**.
6. Edmonds, K.W., et al., *Mn Interstitial diffusion in GaMnAs.* Phys. Rev. Lett., 2003.
7. http://www.ansto.gov.au/ansto/environment1/capabilities/sims01.html, *ANSTO Environment Division - SIMS: Secondary Ion Mass Spectrometry*. 2001.

TP13

Atomic structure of the hydrogen saturated a-planes of 4H-SiC

Th. Seyller[1], N. Sieber[1], A. Taddich[2], D. James[2], J.D. Riley[2], R.G.C. Leckey[2], and L. Ley[1]

[1] *Institut für Technische Physik, Universität Erlangen-Nürnberg, Erwin-Rommel-Strasse 1, D-91058 Erlangen, Germany*

[2] *Department of Physics, La Trobe University, Bundoora, Victoria 3083, Australia*
Phone: ++49-9131-8528335; FAX: ++49-9131-8527889
Email: thomas.seyller@physik.uni-erlangen.de

We have investigated the hydrogenation of the non-polar 4H-SiC$(11\bar{2}0)$ and $(1\bar{1}00)$ surfaces. Surface hydrogenation was carried out by thermal treatment in ultra-pure hydrogen. The surfaces were characterized by low-energy electron diffraction (LEED), surface sensitive photoelectron spectroscopy using synchrotron radiation (SXPS) and Fourier-transform infrared absorption spectroscopy (FTIR) in attenuated total reflection mode (ATR). The hydrogen saturated surfaces exhibit a (1×1) periodicity and are stoichiometric. C1s core level spectra taken using synchrotron radiation show a hydrogen induced chemically shifted (0.42 eV) surface component in good agreement with 6H-SiC$(000\bar{1})$-(1×1):H surface indicating the presence of Si_3C-H entities at the surface. Corresponding Si2p spectra indicate a chemically shifted surface component due to hydrogen-silicon bonds. On 4H-SiC$(1\bar{1}00)$ C_3Si-H entities were also dentified by absorption bands due to Si-H stretch modes. Structural models for the hydrogen saturated a-planes of 4H-SiC are derived from the spectroscopic observations.

TP14

Spin Structure of Small Quantum Dots

C. Sloggett and O. P. Sushkov

School of Physics, University of New South Wales, Sydney NSW 2052, Australia.

Evidence of atom-like shell structure in small, symmetric quantum dots was first observed by Tarucha *et al* in 1996.[1] This has led to much interest and further work in the area. We have performed unrestricted Hartree-Fock simulations of round and elliptical parabolic quantum dots at various values of the effective interaction parameter r_s. In round dots, the addition spectra and spin behaviour clearly reflect the 2D parabolic shell structure, while this breaks down quite quickly under elliptical deformation. Unrestricted Hartree-Fock suggests that in round dots Hund's rule is obeyed for a large range of r_s.

As r_s is increased, it is known that Hartree-Fock becomes less accurate. Specifically in this case, when the spin is zero unrestricted Hartree-Fock can artificially break the symmetry of the dot, leading to an incorrect spin result. We have modelled true zero and non-zero spin and included the terms given by second-order correlation diagrams as a correction to the Hartree-Fock energy. We find that the correlations give qualitatively different energies and spin structure for the dot when compared to values obtained using unrestricted Hartree-Fock or the Local Density Approximation.

1 S. Tarucha, D. G. Austing, T. Honda, R. J. van der Hage and L. P. Kouwenhoven, *Phys. Rev. Lett.* **77**, 3613 (1996).

TP15

Local Bonding Environment of Low-Temperature Silicon Nitride Thin Films Produced by Plasma-Enhanced Chemical Vapour Deposition

M.T.K. Soh[a], N.Savvides[b], C.A. Musca[a] and L. Faraone[a]

[a]School of Electrical, Electronic & Computer Engineering, The University of Western Australia, Crawley 6009, Australia

[b]CSIRO Telecommunications and Industrial Physics, West Lindfield 2070, Australia

In practice, plasma deposited silicon nitride are amorphous alloys containing Si, N and H, Its apparent electronic and mechanical flexibility has led to new and novel applications in microelectronic devices, in particular micro-electro-mechanical-systems (MEMS). Although the high temperature processing of such films is not a significant issue in silicon-based semiconductor technology, there is a pertinent requirement to gain a clearer appreciation of its deposition chemistry at low temperatures (<150^{o}C) in order to evaluate the feasibility of monolithic integration with emerging II-VI semiconductor technological platforms, This study reports on detailed infrared transmission measurements (400-4000 cm^{-1}) of approximately 0.5μm thick NH_3/SiH_4 plasma-deposited silicon nitride alloys prepared at temperatures between 80 and 300°C using fixed process parameters. We establish from a thorough oscillator parametric analysis of the transmission spectra that the ‘condensation' mechanism is not thermally activated as previously reported [1], but is an entropic process required to stabilise the film structure, with the final structure resembling silicon diimide for films deposited at ~80°C [2]. Parametric fitting of the absorption bands leads to the proposition that thermally activated 'condensation' (networking) is really the formation of $N(-Si=)_3$ bonds from the reaction between silazane bridges. Evidence that the absorption feature around 640cm^{-1}, usually attributed to Si-H (bending), is N-H related is also discussed.

[l] D. L. Smith, A. S. Alimonda, C. Chen, S. E. Ready and B. Wacker. *J. Electrochem. Soc. (USA)* **137**, 614 (1990).

[2] D. V. Tsu, G. Lucovsky and M. J. Mantini. *Phys. Rev. B.. Condens. Matter (USA)* **33**, 7069 (1986).

TP16

Variations in the Apparent Optical Band-gap of RPE-CVD Grown Indium Nitride Thin Films

K. S. A. Butcher[a], M. Wintrebert-Fouquet[a], P. P.-T. Chen[a], T. L. Tansley[a] and K. E. Prince[b]

[a]*Physics Department, Macquarie University, Sydney N. S. W. 2109, Australia.*

[b]*Australian Nuclear Science and Technology Organisation, Private Mail Bag 1, Menai NSW 2234, Australia.*

Indium nitride is a semiconducting material with a band-gap which is in current dispute. Although a ~ 0.75 eV band-gap was announced by some international groups in 2002 [1,2], it has since been shown that all the evidence for a ~ 0.75 eV band-gap is due to deep level defects [3, 4]. Despite this there still appears to be anomolous variations in the apparent band-gap for this material. The Macquarie University Low Temperature Nitride Film Growth Facility has recently grown some very high quality indium nitride thin films by remote plasma enhanced chemical vapour deposition (RPE-CVD). This material shows a variation in the apparent band-gap, as measured by optical absorption techniques, of 1.2 eV to 1.8 eV, dependent on the growth temperature and time. SIMS results measured by the ANSTO SIMS group show that the oxygen content of the films is low and that the variation in the apparent band-gap is not correlated to oxygen content. Other film properties will be described.

[1] J. Wu, W. Waluklewicz, K. M. Yu, J. W. Ager III, E. E. Haller, H. Lu, W. Schaff, Y. Saito and Y. Nanishi, Appl. Phys. Lett., **80**, 3967 (2002).

[2] V. Tu Davydov, A. A. Klochikhin, V. V. Emtsev, D. A. Kurdyukov, S. V. Ivanov, V. A. Vekshin, F. Bechstedt, J. Furthmuller, J. Aderhold, J. Graul , A. V. Mudryi, H. Harima, A. Hashimoto, A. Yamamoto, and E. E. Haller, Phys. Stat. Sol. B **234,** 787 (2002).

[3] "Mie-resonances, infrared emission and band gap of InN" T. V. Shubina, S. V. Ivanov, V. N. Jmerik, D. D. Solnyshkov, V. A. Vekshin, P. S. Kop'ev, A. Vasson, J. Leymarie, A. Kavokin, H. Amano, K. Shimono, A. Kasic and B. Monemar, accepted for publication in Physical Review Letters.

[4] "Detailed analysis of absorption data for indium nitride" K. S. A. Butcher, M. Wintrebert-Fouquet, P. P. -T. Chen, H. Timmers and S. K. Shrestha, accepted for publication Materials Science in Semiconductor Processing.

TP17

TP18

TP19

Electronic Structure of Single Crystal Copper Measured by Electron Momentum Spectroscopy

C. Bowles, C. Chen, A. Kheifets, M. Vos and E. Weigold

Atomic and Molecular Physics Laboratories, Research School of Physical Sciences and Engineering, Australian National University, Canberra ACT 0200 Australia.

The electronic structure of solids can be measured directly in the form of the spectral function using Electron Momentum Spectroscopy (EMS), which is a kinematically complete electron scattering experiment that is resolved in both energy and momentum. The spectrometer's high operating energies gives low multiple scattering contributions to the observed intensity, which results in high-contrast measurements.

EMS was used to measure single crystal copper, which provides a very good reference for calibrating the spectrometer due to its well known band structure and Fermi surface. The measurements were performed along three symmetry directions (<100>, <110> and <111>). As these measurements are resolved in both energy and momentum and the measured intensity is directly proportional to the momentum density they provide a comprehensive comparison for current solid state calculations.

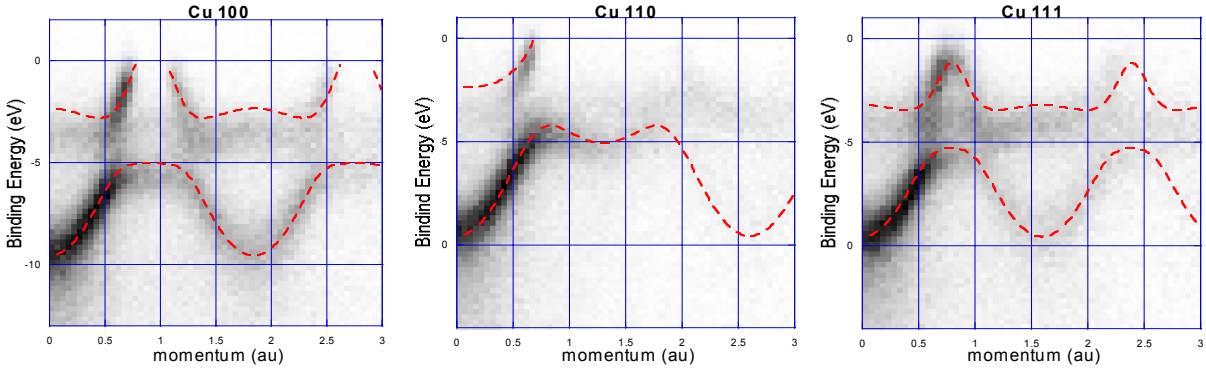

The data are compared to the full-potential linear muffin-tin orbital (FP-LMTO) method within the framework of density functional theory, which is a *first-principles* band structure method [1]. EMS gives a very complete description of the electronic structure of copper that includes peak intensities, peak shapes (width and asymmetries) as well as dispersion, and satellite intensities, which provide detailed tests of electronic structure theories.

[1] A. S. Kheifets, D. R. Lun, S. Yu. Savrasov, J.:Phys Condens. Matter, **11**, 6779 (1999)

TP20

Fast Simulation of a Quantum Phase Transition in an Ion-trap Realisable Unitary Map

J P Barjakatevic [a], G Milburn [a], R H McKenzie [a]

[a] *University of Queensland*

We demonstrate a method of exploring the quantum critical point of the Ising universality class using unitary maps that have recently been demonstrated in ion trap quantum gates. We reverse the idea with which Feynman conceived quantum computing, and ask whether a realisable simulation corresponds to a physical system. We proceed to show that a specific simulation (a unitary map) is physically equivalent to a Hamiltonian that belongs to the same universality class as the transverse Ising Hamiltonian. We present experimental signatures, and numerical simulation for these in the six-qubit case.

TP21

Magnetic Materials for Hyperthermic Cancer Treatment

K.M. Spiers, J.D. Cashion, K.A. Gross and S.J. Harker

School of Physics and Materials Engineering, Monash University, Victoria 3800, Australia.

One method of hyperthermic treatment of tumours is by hysteresis heating of a magnetic implant. This project aims at developing a suitable combination of magnetic material and AC magnetic field which could provide a means of treating deep-seated cancers such as liver cancer. The first part is the production of a smooth-shelled magnetic powder, of micrometre dimensions, which can be introduced by injection into a suitable artery. Magnetite, Fe_3O_4, and maghemite, γ-Fe_2O_3, are the prime candidates. Since the heating power is proportional to the frequency, the second part is to develop an AC magnet with sufficient strength and which is capable of operating at suitable frequencies. Most work to date has used air-cored solenoids, but we are trialling a pole-piece electromagnet system which will provide a more focussed magnetic field and hence reduce the resistive heating of nearby tissue.

Samples of magnetite were produced from a solution of $FeSO_4.7H_2O$ by adding KOH/KNO_3. The washed and dried precipitate was heated in flowing air to convert the magnetite to maghemite. XRD analysis confirmed the structures. Squid measurements were taken at 40^oC in fields of ±24 kA/m (±300 Oe) to determine the hysteresis loop area. Maghemite produced the larger hysteresis area. Mössbauer spectra of the maghemite showed a quite symmetrical sextet structure for which a left and right sextet gave a better fit than did an inner and outer sextet. However, some other workers [e.g. 1,2] have obtained distinctively asymmetrical sextets. There is disagreement in the literature regarding the extent to which ordering of the iron vacancies occurs and it probably preparation dependent. Further fitting and modelling of the spectra are being undertaken to try and determine how much information can be obtained about vacancy ordering in the maghemite structure.

[1] R.J. Pollard, Hyperfine Interact. **41**, 509 (1988)

[2] G.M. da Costa, E. De Grave, L.H. Bowen, R.E. Vandenberghe and P.M.A. de Bakker, Clays and Clay Min. **42** 628 (1994).

TP22

Mixed-Spin S=(½,1) Quantum Ferrimagnet at Zero Temperature

Weihong Zheng and J. Oitmaa

School of Physics, The University of New South Wales, Sydney NSW 2052, Australia.

Ferrimagnets are materials where ions on different sublattices have opposing magnetic moments which do not cancel in the ordered phase [1]. There is growing interest in such systems, both from fundamental physics and through their technological potential. Arguably the simplest such structures are bipartite (A,B) lattices structures with $S_A \neq S_B$. Realizations include bimetallic chains, rare-earth nickelates R_2BaNiO_5 and an Fe-Ni cyanide bridged network [2].

In this work [3] we investigate bipartite AB systems with $S_A = 1/2$, $S_B = 1$ in 1-dimension, 2-dimensions (square lattice) and 3-dimensions (simple cubic lattice). The model used is the Heisenberg antiferromagnet with nearest neighbour exchange, including exchange anisotropy

$$H = J\sum_{<ij>}[S_i^z S_j^z + \gamma\,(S_i^x S_j^x + S_i^y S_j^y)]$$

We use a combination of high-order linked cluster expansions and second-order spin wave theory to calculate the ground state energy, sublattice magnetizations and magnon energies. At the isotropic point $\gamma = 1$ one of the two magnon branches becomes gapless, with quadratic dispersion while the other remains gapped. Agreement between series results and second-order spin wave theory is found to be excellent.

1 W.P. Wolf, *Rep. Prog. Phys.* **24**, 212 (1961).

2 P.J. Koningsbruggen, *et al. Inorg. Chem*. **29**, 3325(1990), A. Zheludev *et al. Phys. Rev. Lett*. **80,** 3630(1998), J.W. Park *et al. cond-mat/0206319.*

3 W. Zheng & J. Oitmaa, *Phys. Rev.* B**67**, 224421(2003).

TP23

Phase Diagram of the BCC S=½ Heisenberg Antiferromagnet with First and Second Neighbour Exchange

J. Oitmaa and Weihong Zheng

School of Physics, The University of New South Wales, Sydney, NSW 2052, Australia.

The occurrence of competing exchange interactions in magnetic materials can give rise to a rich variety of magnetic ordered states, and of phase transitions between them. Studies of such phenomena, within the classical "molecular-field" approximation go back half a century [1] or more. It is perhaps surprising that open questions remain, but, at least for quantum models, this is the case.

In this work [2] we use linked-cluster series expansions, both at T=0 and at high temperature, to analyse the phase structure of the spin-1/2 Heisenberg antiferromagnet on the body-centred-cubic lattice with first and second-neighbor exchange

$$H = J_1 \sum_{<ij>} \mathbf{S}_i \cdot \mathbf{S}_j + J_2 \sum_{[kl]} \mathbf{S}_k \cdot \mathbf{S}_l$$

At zero temperature we find a first-order quantum phase transition at $J_2 / J_1 = 0.705 \pm 0.005$ between AF_1 (Néel) and AF_2 ordered phases. The high temperature series yield quite precise estimates of the critical line separating the AF_1 and paramagnetic phases, and an apparent critical line for the AF_2 phase, with a bicritical point at $J_2 / J_1 = 0.71,\ k_B T / J_1 = 0.34$. The possibility that this latter transition is first-order cannot be excluded.

1 J.S. Smart, *Effective Field Theories of Magnetism*, (Saunders, Philadelphia, 1966).

2 J. Oitmaa & W. Zheng, submitted to *Phys. Rev.* B.

TP24

Comparative Numerical Study of Localization in Disordered Electron Systems

G. Schubert[a], A. Weisse[b] and H. Fehske[a]

[a] *Institut für Physik, Ernst-Moritz-Arndt Universität Greifswald, Greifswald, Germany.*

[b] *School of Physics, The University of New South Wales, Sydney, Australia.*

Taking into account that a proper description of disordered systems should focus on distribution functions, the authors develop a powerful numerical scheme for the determination of the probability distribution of the local density of states (LDOS), which is based on a Chebyshev expansion with kernel polynomial refinement and allows the study of large finite clusters (up to 100^3). For the three-dimensional Anderson model it is demonstrated that the distribution of the LDOS shows a significant change at the disorder induced delocalization-localization transition. Consequently, the so-called typical density of states, defined as the geometric mean of the LDOS, emerges as a natural order parameter. The calculation of the phase diagram of the Anderson model proves the efficiency and reliability of the proposed approach in comparison to other localization criteria, which rely, e.g., on the decay of the wavefunction, the inverse participation number or the conductance. In addition the method is successfully applied to the study of the metal-insulator transition in one dimensional systems with correlated disorder and to the quantum percolation problem on a simple cubic lattice.

G. Schubert, A. Weisse, and H. Fehske, cond-mat/0309015

TP25

Structure Factors for the Alternating Heisenberg Chain

C.J. Hamer and Weihong Zheng
University of New South Wales

and R.R.P. Singh
UC Davis

We develop a linked cluster method to calculate the spectral weights of many-particle excitations at zero temperature. The dynamical structure factor, which is measured in neutron scattering experiments, is expressed as a sum of "exclusive" structure factors, each representing the contribution of a specific excited state. We apply these methods to the alternating Heisenberg chain, where complete wave-vector and frequency dependent spectral weights for one- and two-particle excitations (continuum and bound states) are calculated near the dimerized limit ($\lambda = 0$). We also examine the variation of the spectral weights as the uniform chain ($\lambda = 1$) is approached. In agreement with Schmidt and Uhrig, we find that the spectral weight is dominated by 2-triplet states, even at $\lambda = 1$, which implies that a description in terms of triplet-pair excitations remains a good quantitative description even for the uniform, undimerized chain.

TP26

Superconducting Correlations and Model System Design

Y. Hancock and D.M. Paganin

School of Physics and Materials Engineering, Monash University, Victoria 3800, Australia.

The mechanism which leads to Cooper pair formation in high T_C superconducting systems is a point of intense controversy and remains a "hot topic" in current condensed matter research [1]. Recently the trend has been to move away from conventional BCS theory and to use a range of minimal models, which assume very little about the pair formation mechanism [2]. In this case pair formation arises as an emergent phenomenon, thereby giving greater freedom for uncovering new microscopic effects.

In this work the superconducting (s-wave) pair correlation functions are calculated for small ring cluster systems of up to 12 atoms. The results are determined by exact diagonalization of various single band Hubbard-type Hamiltonians, namely, the Hirsch (correlated hopping) model [2], the t-t′-U Hubbard model (with next nearest neighbour hopping) [3] and the anisotropic extended Hubbard model [4]. Combinations of these systems and the role of inhomogeneity are studied with the Hubbard model [5] used as the base comparison. The pair correlation is found to be strongly influenced by variations in model energetics. The underlying microscopic mechanisms for these trends are explained together with predictions for new cluster designs that exhibit enhanced pairing effects.

1. A.A. Aligia and L. Arrachea, Phys. Rev. B **64**, 214518 (2001).
2. J.E. Hirsch, Phys. Rev. B **48**, 3327 (1993); http://physics,ucsd.edu/~jorge/jh.html.
3. M.E. Torio, A.A. Aligia and H.A. Ceccatto, Phys. Rev. B **67**, 165102 (2003).
4. H. Otsuka, Phys. Rev. Lett. **84**, 5572 (2000).
5. J. Hubbard, Proc. Roy. Soc. London A **276**, 238 (1963).

TP27

Low-lying Excitations in Odd-legged Spin-½ Tubes with Strong Rung Coupling

A. Lüscher[a], R. Noack[b], G. Misguich[c], V. Kotov[d], F. Mila[d]

[a] *School of Physics, University of New South Wales, Sydney 2052, Australia*

[b] *Institut für Theoretische Physik III, Universität Stuttgart, Pfaffenwaldring 57, D-70550 Stuttgart, Germany*

[c] *Service de Physique Théorique, CEA Saclay, 91191 Gif-sur-Yvette Cedex, France*

[d] *Institut de théorie des phénomènes physiques, École Polytechnique Fédérale de Lausanne BSP, CH-1015 Lausanne, Switzerland*

We study the low-lying excitations of odd-legged spin-½ tubes with nearest-neighbour Heisenberg interactions $\mathbf{S}_i \cdot \mathbf{S}_j$ in the limit of strong rung coupling. The periodic boundary conditions applied in the rung direction give rise to an effective model with spin and chirality degrees of freedom, interacting with one another by a geometry dependent coupling constant. By means of DMRG calculations, we show that spin and chirality excitations are gapped. These gaps exhibit a power-law dependence on the coupling strength, which is derived in a mean-field approach and compared to numerical results. The nature of excitations is revealed using Wang's variational approach [1] and the DMRG calculations. Bound soliton states (magnon-like excitations), the deconfinement and the onset of the unbound two-soliton states (spinon-like excitations) are observed in the chirality channel for increasing coupling between spin and chirality degrees of freedom.

1 H.-T. Wang, Phys. Rev. B **64**, 174410 (2001).

TP28

Photoconductivity in Disordered GaN

A. Koo[a], B. J.Ruck[a], H. J. Trodahl[a], F. Budde[a] and A. Bittar [b]

[a] *MacDiarmid Institute and School of Chemical and Physical Sciences, Victoria University of Wellington, Wellington, New Zealand*

[b] *Industrial Research Limited, Lower Hutt, New Zealand*

Disordered semiconductors and their optoelectronic behaviour are of interest for their potentially exploitable characteristics. Moreover the relationship between the ordering of the sample, the presence of oxygen and hydrogen and the optoelectronic behaviour presents an interesting and complex problem. In the case of gallium nitride with a band gap of 3.4 eV, various degrees of order are able to be produced when depositing thin films by Ion Assisted Deposition (IAD). The introduction of water vapour into the vacuum chamber during deposition induces amorphisation and a significant change in the band edge photoconductive response. More disordered samples exhibit much slower response times, on the scale of hours, and a much stronger response, by several orders of magnitude as shown in the figure below. The difference in recombination characteristics displayed by these results correlates well with the Rose exponents extracted from the intensity dependence of the photoconductivity.

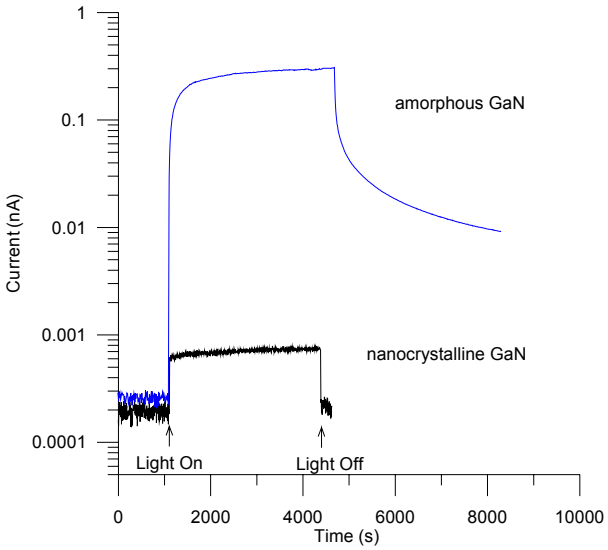

Figure 1. Time dependence of photoconductivity for two GaN films.

TP29

TP30

Quantum Interference with Heisenberg Spin Chains

D. J. Miller

[a] *Centre for Time, University of Sydney, NSW 2006.*

Spins coupled via the Heisenberg interaction on lattices of various dimensions have been of interest in condensed matter physics for many years. Recently it has been shown that systems of that type can be used for quantum computation and quantum communication [1,2].

Modern advances in experimental condensed matter physics have broadened the range of physical objects whose mutual interactions can be described in terms of the simple Heisenberg interaction which was previously associated mainly with the spins of atoms or nuclei. A notable example is the interaction between spins on quantum dots [3]. Consequently, it has become possible to fabricate structures of interacting Heisenberg "spins" which are different from the conventionally studied lattice.

The purpose of the present work is to investigate the consequences of using configurations of Heisenberg spins to emulate quantum interference devices equivakent to the 2-slit experiment and the Mach-Zehnder interferometer.

As one might expect, it is found that the interference effects are sensitive to the interaction between the spins and this means the effects could lead to practical applications which are discussed.

[1] D. P. DiVincenzo, D. Bacon, J. Kempe, G. Buckard and K. B. Whaley, Nature **408**, 339 (2000); quant-ph/0005116.

[2] S. Bose, Phys. Rev. Lett. **91**, 207901 (2003); quant-ph/0212041.

[3] G. Buckard, D. Loss and D. P. DiVincenzo, Phys. Rev. B **59**, 2070 (1999).

TP31

Shockley and Rydberg Surface States and Quantum Wells on the Cu(111) Surface

M. N. Read

School of Physics, University of New South Wales, NSW 2052, Australia.

Adsorbed alkali metals such as Na on (111) noble (and near-noble) metal surfaces form quantum well systems where the electron is trapped between the surface barrier and crystal substrate forming a quasi-2-dimensional electron gas. Such systems can be used as metal-based nanostructured quantum electronic devices.

As a preliminary to the study of the surface states of these systems we have calculated the band structure of surface states for the clean Cu(111) surface from just below the Fermi level to 30 eV above it. An advantage for this surface is that the Shockley state is so accurately known from photoemission (PE) data because it occurs in a bulk band gap: the energy is –0.39(1) eV with respect to the Fermi level at $\overline{\Gamma}$ with an effective mass of 0.46(1). This is precisely the energy at which saturation occurs from the image barrier. Also the unoccupied Rydberg resonances have been measured using STM.

We have used our layer-by-layer-KKR method to theoretically reproduce these states and resonances. Because we have reproduced bulk band edges with respect to the Fermi level we have been able to determine the vacuum energy level for Fermi energy electrons at $\overline{\Gamma}$, which fixes the barrier height for electrons in this energy region for our theoretical bulk potential.

An exponentially saturated image barrier with truncation in the region of the jellium discontinuity is found to reproduce experimental results. This is a different form of saturation from that earlier estimated by an approximation method by other investigators. We have found excited surface features which could elicit the variation of the self-energy of the electron with energy and momentum as well as higher energy variation of the image potential. These higher energy features should be observable in inverse photoemission (IPE) and very low energy electron diffraction (VLEED) and other surface spectroscopies.

TP32

Searches for the Electron Electric Dipole Moment and Nuclear Anapole Moments in Solids

T.N. Mukhamedjanov, O.P. Sushkov, J.M. Cadogan, V.A. Dzuba

School of Physics, University of New South Wales, Sydney 2052, Australia.

We consider effects caused by the electron electric dipole moment (EDM) in gadolinium garnets. Our estimates show that the experimental studies of these effects could improve the current upper limit on the electron EDM by several orders of magnitude. We suggest a consistent theoretical model and perform calculations of observable effects in gadolinium gallium garnet and gadolinium iron garnet.

It is also possible to probe for nuclear anapole moments in a solid state experiment. We suggest such NMR-type experiment and perform estimates of the expected results.

TP33

Apparent Sizes of Solute Atoms and Vacancies in Aluminium from First Principles

A. E. Smith and S. Homolya

School of Physics and Materials Engineering, Monash University, Victoria 3800, Australia.

First-principles methods, including the full potential augmented plane wave method within the the density functional theory scheme [1] and employing the Perdew-Burke-Ernzerhof GGA exchange correlation functional [2], are used to investigate substitutional defects in fcc aluminium. Defects considered include copper, silver and tin atoms, as well as vacancies. Results of ground state calculations are presented for supercells containing one solute atom or vacancy and up to 63 aluminium atoms. The distortion of the fcc lattice by the defect is calculated for each system by minimising ground state energy with respect to supercell lattice parameters and all atomic positions. The optimised supercell geometry is used to calculate the apparent sizes of solute atoms and vacancies, defined either in terms of microscopic or in terms of bulk properties properties of the system. Significant discrepancy between microscopic and macroscopic definitions of apparent defect size is attributable to the long-range nature of the strain in the fcc lattice near defects, which extends well beyond nearest neighbour sites. However, for copper and silver solute atoms the apparent sizes of defects defined in terms of the density of the bulk material show good quantitative agreement with previously reported experimental results. The results also show that the formation of isolated substitutional tin defects is energetically highly unfavourable, as would be expected from experiment [3,4].

1. P. Blaha et al.,*WIEN2K, An Augmented Plane Wave + Local Orbitals Program for Calculating Crystal Properties* (Karlheinz Schwarz, Techn. Universität Wien, Austria, 2001).
2. J.P. Perdew, K. Burke, and M. Ernzerhof, Phys.Rev. Lett. 77, 3865 (1996).
3. D. A. Porter and K.E. Easterling, *Phase transformations in metals and alloys*, Chapman & Hall, (1992).
4. I.J. Polmear, *Light Alloys*, Butterworth Heinemann, (2000).

TP34

Superconducting Spiral Phases in the Two-Dimensional t-J model.

Oleg P. Sushkov [a] and Valeri N. Kotov [b]

[a] *School of Physics, University of New South Wales, Sydney 2052, Australia.*

[b] *Institute of Theoretical Physics, University of Lausanne, CH-1015 Lausanne, Switzerland*

The t-J model has been suggested in 1987 by P. W. Anderson and V. J. Emery to describe the essential low-energy physics of the high-Tc cuprates. Formation of spirals in the doped t-J model was proposed by Shraiman and Siggia in 1989. The idea that the spiral state is the ground state of a cuprate attracted a lot of attention in 90s, however the question of stability of the state remained unresolved. Recently the interest in the spiral state was renewed because of the strong experimental indications that at small doping the cuprates behave as spin glasses or even exhibit some kind of magnetic ordering. The data also shows that magnetic ordering and superconductivity coexist. The spin glass behavior is consistent with the spiral scenario: since doping is not uniform the pitch of the spiral is varying from point to point and hence on large scales it leads to spin glass behavior .

In the present work we analyse the t-t'-t''-J model. By using chiral perturbation theory we have determined the ground state to be a spiral for small doping $\delta << 1$ near half filling. In this limit our solution does not contain any uncontrolled approximations. We evaluate the spin-wave Green's functions and address the issue of stability of the spiral state, leading to the phase diagram of the model. At t'=t''=0 the spiral state is unstable towards a local enhancement of the spiral pitch, and the nature of the true ground state remains unclear. However, for values of t' and t'' corresponding to real cuprates the spiral state is stable. We show that at $\delta = 0.119$ the spiral is commensurate with the lattice with a period of 8 lattice spacings in agreement with experimental data.

Even more important, we have demonstrated that the magnetic spiral and superconductivity coexist. Even though one cannot classify the superconducting gap symmetry according to the lattice representations (s,p,d,...) since the symmetry of the lattice is spontaneously broken by the spiral, the gap always has lines of nodes along (1,1) and (1,-1) directions.

TP35

Corrosion Resistance of Organic Layers on GaAs via X-Ray Reflectometry Characterization

J.D.Smith, T.R. Finlayson, C. Kirchner and U. Klemradt
School of Physics and Materials Engineering, Monash University, Victoria 3800, Australia.

Two different solutions of (3-mercaptopropyl) trimethoxysilane (MPT) were deposited on GaAs surfaces to provide passivation against corrosion by oxygen and to prevent AsO_3^{3-} escape into the surrounding environment. The solutions were compared to each other for their relative corrosion resistance by determining the resultant buried oxide layer and MPT layer thicknesses and densities. All samples were scanned using grazing incidence X-ray reflectometry at DESY, Hamburg, Germany. The samples were prepared under Argon during HCl etching and deposition. It was hoped that the corrosion of the surface and thus the relative thickness of the buried oxide layer could be reduced by changing from ethanol to methanol since ethanol is known to by hydrophilic. Even small quantities of moisture at the GaAs interface can lead to oxidation and corrosion. It was found from the models fitted that all samples had buried oxide layers due to surface corrosion. Further study is required regarding the effectiveness of thiol overlayers against arsenic and oxygen diffusion on the GaAs surface.

TP36

New Tools for the Numerical Calculation of Dynamical Correlation Functions at Finite Temperature

Alexander Weisse

School of Physics, The University of New South Wales, Sydney, Australia.

The calculation of dynamical correlation functions, like optical conductivities, spin structure factors and other (linear) response functions, is one of the typical problems in condensed matter physics. In many cases real materials are in a parameter regime where analytical methods are not applicable and therefore the use and development of numerical methods is indispensable. At zero temperature Chebyshev expansion and the Kernel Polynomial Method [1] proved to be a valuable tool for this kind of problems, for both interacting and non-interacting quantum systems. In this contribution we present a non-trivial extension of these methods to finite temperature. To demonstrate the power of the approach we calculate the optical conductivity of non-interacting electrons in a random potential (Anderson model), and transport properties of interacting (1D) quantum models

[1] Silver, Roeder, Phys. Rev. E 56, 4822 (1997)
[2] cond-mat/0309015

TP37

Does the Probability Density Imply the Equation of Motion?

Rotha P. Yu, David M. Paganin and Michael J. Morgan

School of Physics and Materials Engineering, Monash University, Victoria 3800, Australia.

The laws of physics dictate the evolution of matter and radiation. Quantum mechanics postulates that the matter or radiation is associated with a field whose magnitude is interpreted as the probability density, which is the only observable quantity. In general this field is either a single-component or multi-component complex scalar field, whose laws of evolution may be expressed in the form of partial differential equations. One may ask does the probability density of the complex scalar field imply the evolution of the field? Here we answer this fundamental question by examining a means for measuring the equation of motion of a single-component complex scalar field associated with a non-dissipative and nonlinear system, given measurements of the probability density. Applications of this formalism, to a number of systems in condensed matter physics, will be discussed.

TP38

Reactive Ion Etching of Microphotonic Structures

J. Du, J. Glasscock, J. Vanajek and N. Savvides

CSIRO Telecommunications & Industrial Physics, Lindfield, NSW 2070, Australia

Fabrication of microphotonic structures such as planar waveguides and other periodic structures based on silicon technology has become increasingly important due to the potential for integration of planar optical devices. We have fabricated various periodic microstructures on silicon wafers using standard optical lithography and reactive ion etching (RIE). For optical applications the surface roughness and the sidewall angle or steepness of microstructures are the most critical factors. In particular, sidewall roughness of the etched waveguide core accounts for most of the optical propagation loss. We show that by varying the main RIE parameters such as gas pressure, RF power and $CF_4/Ar/O_2$ gas composition it is possible to produce microstructures with near-vertical sidewalls and very smooth surfaces. In addition to plasma etching conditions, poor edge quality of the mask often causes sidewall roughness. We employed Ni/Cr metal masks in these experiments for deep etching, and used Ar^+ ion milling instead of wet chemical etching to open the mask. This improves the edge quality of the mask and ultimately results in smooth sidewalls.

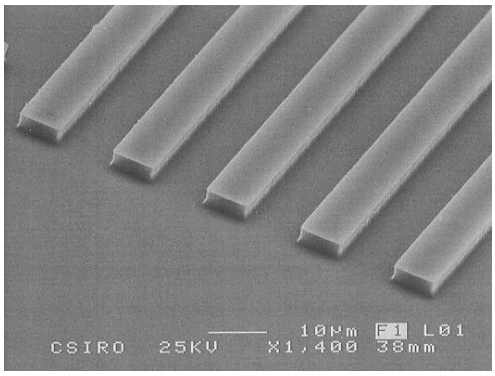

Figure 1. Waveguides etched in silicon using CF_4/Ar at 50 W RF power.

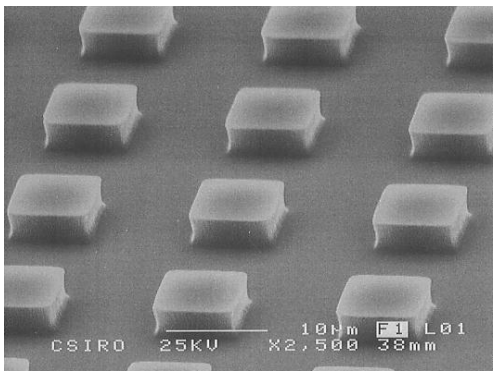

Figure 2. Square array etched in silicon using CF_4/Ar at 50 W RF power.

TP39

An Apparent Shift in Optical Constants in Nanostructured Metal Films Overcoated with Insulator: a New class of Multilayer Thin Film Systems

A.I. Maaroof and G.B. Smith

Department of Applied Physics

University of Technology, Sydney

PO BOX 123 BROADWAY NSW 2007

email g.smith@uts.edu.au

Thin metal films which contain arrays of nano-size voids have interesting optical responses, including higher than expected transmittance and larger than expected delays in electromagnetic energy transport over certain wavelength bands, mainly in the near infra red (NIR). As scattering is not observed an effective homogeneous complex refractive index applies. The result is a strongly elevated real part (from the delays) and strongly reduced imaginary part (from enhanced transmittance) relative to both a void free metal, and a "classical" metal with voids. This far field response depends on void nanostructure, grain size and plasmon frequency of the metal. It is shown that these indices cannot be explained by classical effective medium models which utilise quasi-static electric polarisation. Instead films have their NIR properties dictated by the special surface plasmons that form in the presence of nano-holes. Photon resonance with these excitations enhances delay times and effective response requires a dynamic field treatment at all size scales, since localised surface plasmon currents and associated magnetic fields are present.

Sensitivity to surface plasmons is dramatically illustrated when an insulating layer is present on such films. The apparent indices of the metal layer change, in some cases substantially. Classical multilayer thin film models in which each layer's refractive indices are independent of the neighbouring medium, cannot then be used. Results on two distinct nano-void systems are included, for which super high resolution SEM images from a new LEO SEM will be shown. Measured refractive indices will be used to demonstrate how thin metal layers containing nano-voids depart from the expected response of a metal with voids, to a degree dictated by the refractive index of the neighbouring medium.

TP40

Silicon Microphotonic Waveguides

V. Ta'eed[a], M. J. Steel[a], C. Grillet[a], B. Eggleton[a], J. Du[b], J. Glasscock[b] and N. Savvides[b]

[a] CUDOS, *School of Physics, The University of Sydney, NSW 2006, Australia.*

[b] CSIRO *Telecommunications & Industrial Physics, Lindfield NSW 2070, Australia.*

Silicon microphotonic devices have been drawing increasing attention in the past few years. The high index-difference between silicon and its oxide ($\Delta n = 2$) suggests a potential for high-density integration of optical functions on to a photonic chip. Additionally, it has been shown that silicon exhibits strong Raman nonlinearity [1], a necessary property as light interaction can occur only by means of nonlinearities in the propagation medium.

The small dimensions of silicon waveguides require the design of efficient tapers to couple light to them. We have used the beam propagation method (RSoft BeamPROP) to understand the principles and design of an inverse-taper mode-converter as implemented in several recent papers [2-3].

We report on progress in the design and fabrication of silicon-based waveguides. Preliminary work has been conducted by patterning silicon-on-insulator (SOI) wafers using optical lithography and reactive ion etching. Thus far, only rib waveguides have been designed [4], as single-mode ridge-waveguides are beyond the capabilities of conventional optical lithography. We have recently moved to electron beam lithography as the higher resolutions permitted will provide the flexibility to begin fabricating sub-micron waveguides.

1. Ricardo Claps et al., "*Observation of Raman emission in silicon waveguides at 1.54um*", Opt. Express, 10(22) 1305-1313, (2002)
2. T. Shoji et al., "*Low loss mode size converter from 0.3μm square Si wire waveguides to singlemode fibres*", Electron. Letters, 38 (25), (2002)
3. Laurent Vivien et al., "*2-D Taper for low-loss coupling between polarization-insensitive microwaveguides and single-mode optical fibers*", J. Light. Tech., Dec, 2002
4. Olly Powell, "*Single-mode condition for silicon rib waveguides*", J. Light. Tech., 20(10), 1851-1855, (2002)

Participants

PARTICIPANTS

Ahmad	Akhlaq	UET,Lahore, Pakistan	aamalik87@hotmail.com	TA6
Ain	Michael	ANSTO	mai@ansto.gov.au	WP16
Allan	Rodney	UTS	Rodney.S.Allan@uts.edu.au	
Angus	Susan	UNSW	susan.angus@student.unsw.edu.au	TP11, FM2
Armstrong	Kevin	AVT Services		Exhibitor
Armstrong	Nicholas	UTS	nicholas.armstrong@uts.edu.au	WA5
Asgari	Nasim Sabbah	UWA	asgari@ee.uwa.edu.au	
Asgari	Asghar	UWA	asgari@ee.uwa.edu.au	TM4
Barjaktarevic	John Paul	UQ	jpb@physics.uq.edu.au	TP20
Bartos	Igor	UNSW	ibartos@phys.unsw.edu.au	TP1
Baxter	Geoff	CSIRO	geoff.baxter@csiro.au	WP9
Bertram	Bill	ANSTO	wkb@ansto.gov.au	WP1
Bigelow	Roberta	Monash	roberta.bigelow@spme.monash.edu.au	
Bowles	Cameron	ANU	cameron.bowles@anu.edu.au	TP19

Broekman	Leonard	Latrobe	L.Broekman@latrobe.edu.au	WP28, WP29
Bryant	Gary	RMIT	gary.bryant@rmit.edu.au	WP2, WP7
Cahen	David	Weizmann Inst Israel	david.cahen@weizmann.ac.il	WM2
Cashion	John Paul	Monash	John.Cashion@spme.monash.edu.au	WP27, WP41, TM6, TA2, TP21
Chai	Roger	CSIRO	roger.chai@csiro.au	
Chen	Cheng	ANU	chc107@rsphysse.anu.edu.au	TP19
Cho	Sam	QUT	sycho@physics.uq.edu.au	TP2, TP7
Cimmino	Alberto	Melbourne	a.cimmino@physics.unimelb.edu.au	TP3
Collocott	Stephen	CSIRO	stephen collocott@csiro.au	
Court	Nadia	UNSW	ncourt@phys.unsw.edu.au	TP4
Crew	David	UWA	dcrew@physics.uwa.edu.au	TA3, TA5
Daivis	Peter	RMIT	peter.daivis@rmit.edu.au	TM8
Dieing	Thomas	Latrobe	t.dieing@ee.latrobe.edu.au	TP5
Downes	James	VUW, NZ	james.downes@vuw.ac.nz	TA1
Dunbar	Alan	Canterbury, NZ	alan.dunbar@canterbury.ac.nz	WM3

Dunlop	John	CSIRO	john.dunlop@csiro.au	
Edge	Vernon	UNSW, ADFA	v.edge@adfa.edu.au	WP18, WP20, WP21, WP22, WP25
Eggleton	Ben	Sydney U	egg@Physics.usyd.edu.au	TM1, TP38, TP40
Fehske	Holger	Uni Greifswald, DE	fehske@physik.uni-greifswald.de	TP24, FM6
Finlayson	Trevor	Monash	Trevor.Finlayson@spme.monash.edu.au	WP3, WP34, WP39, WP42, TP35
Fleming	Robert	Monash	Robert.Fleming@spme.monash.edu.au	
Fletcher	Neville	ANU	neville.fletcher@anu.edu.au	
Foley	Cathy	CSIRO	Cathy.Foley@csiro.au	WA1
Ford	Mike	UTS	mike.ford@uts.edu.au	WM4
Gassull	Daniel	Melbourne	dgassull@ph.unimelb.edu.au	TP3
Glasscock	Julie	CSIRO	julie.glasscock@csiro.au	TM9, TP38, TP40
Goossens	Darren	ANU	goossens@rsc.anu.edu.au	WM6, WA3, WP6, WP17
Gorham	Nicole	UWA	gorham@physics.uwa.edu.au	TA4
Greaves	Tam	Monash	tamar.greaves@spme.monash.edu.au	TA2
Greentree	Andy	UNSW	a.d.greentree@unsw.edu.au	TP10, TP11

Grillet	Christian	Sydney U	grillet@Physics.usyd.edu.au	TM2, TP38, TP40
Grimm	Douglas	UNSW, ADFA	dbg@ph.adfa.edu.au	WP18, WP22
Gwan	Paul	CSIRO	paul.gwan@csiro.au	WP33
Hagen	Mark	ANSTO	mhz@ansto.gov.au	WP4, WP5
Hallam	Toby	UNSW	toby@phys.unsw.edu.au	FM1, TP6
Hamer	Chris	UNSW	cjh@phys.unsw.edu.au	TP25
Hancock	Yvette	Monash	Yvette.Hancock@spme.monash.edu.au	TP26
Harker	Stephen	Monash	Stephen.Harker@spme.monash.edu.au	WP6, TM6, TP21
Hearne	Sean	Melbourne	smh@physics.unimelb.edu.au	TP7
Hutchison	Wayne	UNSW, ADFA	w.hutchison@adfa.edu.au	WP20, WP25, TP8
Ito	Naoki	Monash	Naoki.Ito@spme.monash.edu.au	WP19
Jakovidis	Greg	Monash	Greg.Jakovidis@sci.monash.edu.au	WP15, FM5
Jackson	Ian	ANU	Ian.Jackson@anu.edu.au	WP35
Jamieson	Ian	Monash	Ian.Jamieson@spme.monash.edu.au	TP7, FM5
Koo	Annette	VUW, NZ	a.koo@irl.cri.nz	FM4, TP28

Lam	Simon	CSIRO	simon.lam@csiro.au	WA1, WP36
Lamb	Belinda	NYST	belinda.lamb@nyst.edu.au	
Lang	Sidney	Ben Gurion U	lang@bgumail.bgu.ac.il	TM5
Lee	Sueping	UOW	sueping@uow.edu.au	TP9
Lenné	Thomas	RMIT	Thomas.lenne@rmit.edu.au	WP7
Lewis	Roger	UOW	roger@uow.edu.au	WP21, TP9
Lundin	Urban	UQ	ludin@physics.uq.edu.au	TP2, FM8
Luscher	Andreas	UNSW	andreas.luescher@a3.epfl.ch	TP27
Maaroof	Abbas	UTS	amaaroof@uts.edu.au	TP39
Madebo	Mebratu	Latrobe	m.mebratu@latrobe.edu.au	FM3
Marshall	Craig	Scitek Aust		Exhibitor
McCamey	Dane	UNSW	dane.mccamey@unsw.edu.au	TP10
Mezei	Ferenc	Hahn-Meitner Inst, DE	mezei@wanadoo.fr	WM5
Miller	David	Sydney U	davmille@arts.usyd.edu.au	TP30
Mitic	Mladen	UNSW	m_mitic2003@yahoo.com	TP11

Mukhamedjanov	Timur	UNSW	tmukham@phys.unsw.edu.au	TP32
Muller	Karl	CSIRO	karl.muller@csiro.au	WM1, WP9
Nakamura	Yuichi	Tokyo Uni, Japan	yuichi@iis.u-tokyo.ac.jp	WA6
Norris	Ray	ATNF	Ray.Norris@csiro.au	
Oitmaa	Jaan	UNSW	j.oitmaa@unsw.edu.au	WA4, TP22, TP23
Pardoe	Heath	UWA	hpardoe@physics.uwa.edu.au	WA2
Paulmier	Thierry	QUT	t.paulmier@qut.edu.au	WP37
Price	Don	CSIRO	don.price@csiro.au	
Ponomarenko	Olena	Newcastle	olena@engmail.newcastle.edu.au	WP10, WP11
Rabeau	James	Melbourne	jrabeau@physics.unimelb.edu.au	WP12
Read	Marlene	UNSW	m.read@unsw.edu.au	TP31
Riley	John Paul	Latrobe	j.riley@latrobe.edu.au	WP28, WP29, WP39, TP12, TP13, FM3
Roberts	Mark	CSIRO	mark.roberts@csiro.au	
Robinson	Robert	ANSTO	rro@ansto.gov.au	WA3
Rosse	Meg	Latrobe	M.Rosse@latrobe.edu.au	

Ruck	Benjamin	VUW, NZ	avekony@paradise.net.nz	FM4, TP28
Russo	Salvy	RMIT	salvy.russo@rmit.edu.au	FM9
Rybachuk	Maksym	QUT	m.rybachuk@qut.edu.au	WP26
Sabine	Terry	UTS	terencesabine@hotmail.com	WP38
Savvides	Nick	CSIRO	Nick.Savvides@csiro.au	TP15, TP38, TP40
Shadrivov	Ilya	ANU	ivs124@rsphysse.anu.edu.au	TM3
Schmid	Siggi	Sydney U	siegbert@chem.usyd.edu.au	WM7
Sirker	Jesko	UNSW	sirker@phys.unsw.edu.au	WM8
Sloggett	Clare	UNSW	clares@phys.unsw.edu.au	TP14
Smith	Andrew	Monash	Andrew.Smith@spme.monash.edu.au	WP27, WP39, TP33
Smith	Geoff	UTS	g.smith@uts.edu.au	TP39
Smith	Justin	Monash	Justin.Smith@spme.monash.edu.au	TP35
Simmons	Michelle	UNSW	Michelle.Simmons@unsw.edu.au	TP6, FM1
Soh	Martin	UWA	msoh@ee.uwa.edu.au	TP15
Sosa Pintos	Andreas	UWS	andreas.sosapintos@csiro.au	WP33

Soule de Bas	Benjamin	UTS	benjamin.souledebas@uts.edu.au	WM4
Spiers	Kathryn	Monash	kathryn.spiers@spme.monash.edu.au	TM6, TP21
Stamps	Robert	UWA	stamps@lps.u-psud.fr	WP8, WP23, TA3, TA4, TA5
Stanton	Bill	Stanton Scientific		Exhibitor
Stachurski	Zbigniew	ANU	zbigniew.stachurski@anu.edu.au	WP24
Stewart	Andrew	ANU	andrew.stewart@anu.edu.au	WP40
Stewart	Glen	UNSW, ADFA	g.stewart@adfa.edu.au	WP20, WP21, WP25
Studer	Andrew	ANSTO	ajs@ansto.gov.au	WP18, WP21, WP25
Sushkov	Oleg	UNSW	sushkov@phys.unsw.edu.au	TP14, TP32, TP34
Suwuntanasarn	Nakorn	UNSW, ADFA	n.suwantanasarn@student.adfa.edu.au	
Ta'eed	Vahid	Sydney U	vahid@Physics.usyd.edu.au	TP40
Tadich	Anton	Latrobe	a.tadich@latrobe.edu.au	WP28, WP29
Tansley	Trevor	Macquarie	Trevor.tansley@mq.edu.au	TP16
Tempelaars	Dave	UNSW, ADFA	d.tempelaars@student.adfa.edu.au	WP8
Tilbrook	David	CSIRO	david.tilbrook@csiro.au	WA1

Trodahl	Joe	VUW, NZ	Joe.Trodahl@vuw.ac.nz	FM4, FM7, TP28
Troup	Gordon	Monash	gordon.troup@spme.monash.edu.au	WP30, WP31, WP32
Usher	Brian	Latrobe	B.Usher@latrobe.edu.au	TP5, FM3
Vance	Lou	ANSTO	erv@ansto.gov.au	WP34, WP41
Von Brasch	Alexander	UNSW	alexvb@phys.unsw.edu.au	WA4
Wang	Jianli	UNSW, ADFA	jlw@ph.adfa.edu.au	WP22
Wang	Qian	UOW	qian@uow.edu.au	TP9
Warnes	Bill	Monash	bill.warnes@spme.monash.edu.au	
Weisse	Alexander	UNSW	aweisse@phys.unsw.edu.au	TP24, TP36, FM6
White	Guy	CSIRO	guy.white@csiro.au	
Woodward	Robert	UWA	woodward@physics.uwa.edu.au	TA4, TA5
Wu	XD	Monash	Xiaodong.wu@spme.monash.edu.au	WP3, WP42
Xiong	Xiangyuan	Monash	xiangyuan.xiong@spme.monash.edu.au	WP43
Xu	David	UTS	xiaoda.xu@uts.edu.au	WP13
Yang	Wenrong	CSIRO	wenrong.yang@csiro.au	WP14

Yu	Dehong	ANSTO	dyu@ansto.gov.au	WM9, WP6
Yu	Rotha	Monash	rotha.yu@spme.monash.edu.au	TP37
Zalich	Michael	UWA	mzalich@cyllene.uwa.edu.au	TM7
Zhu	DeMing	Monash	Deming.Zhu@spme.monash.edu.au	WP15